The use of light in cancer immunotherapy

Kleinovink, E.J.W.

The use of light in cancer immunotherapy

Jan Willem Kleinovink

The use of light in cancer immunotherapy
Jan Willem Kleinovink

The research described in this thesis was performed at the department of Immunohematology and Blood Transfusion of the Leiden University Medical Center in the Netherlands, in the context of the Cancer Vaccine Tracking project (#03O-302) of the Center for Translational Molecular Medicine (CTMM).

Layout: Jan Willem Kleinovink
Cover design: Jan Willem Kleinovink
Thesis printing: Off Page (Amsterdam)

ISBN: 978-94-6182-882-8

The use of light in cancer immunotherapy

Proefschrift

ter verkrijging van
de graad van Doctor aan de Universiteit Leiden,
op gezag van Rector Magnificus prof.mr. C.J.J.M. Stolker,
volgens besluit van het College voor Promoties
te verdedigen op

donderdag 19 april 2018 klokke 15:00 uur

door

Evert Jan Willem Kleinovink
geboren te Den Ham in 1986

PROMOTORES
Prof. Dr. F.A. Ossendorp
Prof. Dr. C.W.G.M. Löwik (Erasmus MC Rotterdam)

CO-PROMOTOR
Dr. M.F. Herbert-Fransen

LEDEN PROMOTIECOMMISSIE
Prof. Dr. M. Jager
Prof. Dr. W. Jiskoot
Dr. S. Oliveira (Universiteit Utrecht)

Table of Contents

Chapter 1 **7**
General Introduction

Chapter 2 **21**
Combination of Photodynamic Therapy and specific immunotherapy efficiently eradicates established tumors

Chapter 3 **43**
Photodynamic-immune checkpoint therapy eradicates local and distant tumors by CD8+ T cells

Chapter 4 **57**
Vaccine tracking by in vivo near-infrared fluorescence imaging of emulsified peptide antigen

Chapter 5 **71**
Near-infrared labeled, ovalbumin loaded polymeric nanoparticles based on a hydrophilic polyester as model vaccine: In vivo tracking and evaluation of antigen-specific CD8+ T cell immune response

Chapter 6 **93**
A dual-color bioluminescence reporter mouse for simultaneous in vivo imaging of T cell localization and activation

Chapter 7 **111**
Summary and General Discussion

Appendices
Nederlandse samenvatting **123**
Dankwoord **131**
Curriculum Vitae **133**
List of Publications **135**

Chapter 1

General Introduction

The use of light in cancer immunotherapy

The development of treatment options for advanced cancer forms a major challenge in medical oncology. The breakthrough of immunotherapy for cancer has introduced promising new options, but nonetheless only a minority of cancer patients show clinical benefit. This situation has inspired two avenues of research to find solutions to this problem: mechanistic studies to decipher the working mechanisms of immunotherapies and to investigate why many patients do not respond, and translational studies developing combination treatments to achieve clinical benefit in situations where immunotherapy alone is not sufficient. This thesis explores both these avenues by investigating applications of visible light in immunotherapy of cancer. The first aim of this thesis is to develop optical imaging platforms for visualization of immune cells and immunotherapies, which can shed light on the immunological events after administration of immunotherapy. The second aim is to develop novel therapies combining light-based tumor destruction and different types of immunotherapies. The following paragraphs will discuss how the immune system can recognize and attack tumors, how immunotherapy aims to boost immune attack of tumors, and how light-based technologies can be applied in this context.

The immune system

The immune system comprises a set of cells and molecules that forms a defense system against disease, and can be subdivided into an innate and an adaptive immune system. The innate immune system is the only immune system in plants and insects, and provides an immediate but non-specific layer of defense. Jawed vertebrates, including humans and most animals used in biomedical research, have additionally developed an adaptive immune system characterized by slower but target-specific effector mechanisms, which moreover can establish memory to protect against future challenges with the same pathogen (1). Despite their distinct evolutionary origins, the innate and adaptive immune system collaborate in both the formation and the regulation of immune responses. To ensure robust immune defense while avoiding auto-immune disease, the adaptive immune system is trained to recognize its targets based on the distinction between self and non-self, distinguishing the body's own tissue from invading pathogens. It has now become clear that cancer cells can also be recognized by the adaptive immune system, as mutations in cancer cells cause deviation from 'self', rendering them susceptible to immune attack. The following paragraphs will discuss how cancer cells are recognized and attacked by the adaptive immune system.

T cells

T cells, also called T lymphocytes, form the cellular effector arm of the adaptive immune system. T cells are small lymphoid cells that are named after the thymus, a lymphoid organ that trains developing T cells to distinguish foreign elements from the body's own healthy tissue in order to avoid auto-immunity. Target-specificity, a core principle of the adaptive immune system, is mediated by the T cell receptor (TCR) complex on the cell membrane of T cells that specifically recognizes a specific peptide antigen in the context of MHC molecules on the surface of target cells. T cells acquire their TCR by gene rearrangement processes in the thymus, and are then exposed to positive and negative selection procedures that assure the deletion of T cells expressing a TCR that either has insufficient affinity for MHC to serve as functional T cells, or binds so strongly to MHC molecules presenting self-peptides that auto-reactivity may occur. Traditionally, two T cell subsets are distinguished based on the expression of either the CD4 or the CD8 co-receptor as part of the TCR complex, which are known as CD4 T cells and CD8 T cells, respectively (2, 3). Naïve T cells express a TCR recognizing a specific peptide-MHC (pMHC) complex, but cannot exert their effector functions until they are properly activated. T cell activation is mediated by the same mechanisms as T cell target recognition,

involving TCR recognition of the specific pMHC complex, but only when this pMHC complex is presented by professional antigen-presenting cells (APCs) (4, 5). Dendritic cells (DCs) are innate immune cells that are the most efficient professional APCs capable of activating T cells. DCs can engulf extracellular material and present epitopes in MHC class II molecules to CD4 T cells, which do not directly engage extracellular pathogens but aid the effector mechanisms of other immune cells, including macrophages and antibody-producing B cells, mostly by cytokines or cell-cell interactions. Because of their importance in helping other immune cells, CD4 T cells are also called T-helper (T_H) cells. Several classes of CD4 T cells exist, including T_H1, T_H2, T_H17 and the immunosuppressive subset of regulatory T cells (Tregs), which are characterized by the expression of distinct transcription factors, membrane markers and cytokines and are involved in shaping several different types of immune responses. CD8 T cells on the other hand recognize epitope in MHC class I molecules, which are loaded with peptides derived from intracellular antigens. Importantly, DCs are able to cross antigens from the endocytosis pathway to the MHC I pathway in a process called cross-presentation, allowing the activation of CD8 T cells specific for extracellular antigens engulfed by DCs (6). DCs present various extracellular and intracellular receptors that sense the tissue for signs of infection (or more generally, danger) and only in that case present co-stimulatory molecules on their membrane. Co-stimulation is crucial for proper T cell activation, forming an additional layer of security against autoimmunity besides the deletion of auto-reactive T cells during thymic selection, the presence of Tregs and the expression of suppressive co-inhibitory molecules such as CTLA-4 and PD-1. This means that a naïve T cell can only be activated by a DC that has sensed danger and has (cross-)presented non-self epitopes in the correct MHC class. These strict requirements of T cell activation are necessary to guard the body from unrestrained T cell responses that may lead to auto-immune disease.

Immune recognition of cancer

So far, the immune system has been described as a defense mechanisms against pathogens, which throughout our evolutionary history have indeed posed a major threat to our survival from early age on. In contrast, cancer is a disease that typically becomes clinically apparent and relevant at higher age, suggesting that cancer has played no role in the evolution of the immune system (7). However, research in the last decades has confirmed century-old observations that the immune system is nonetheless capable of recognizing and attacking cancer cells (8, 9). Tumors arise from normal cells of the body in which genes regulating proliferation and survival have become dysfunctional by mutations, leading to unrestrained proliferation.

Fortunately, mutations do not only drive tumorigenesis but also facilitate immune recognition, as mutated genes may give rise to new T cell epitopes (neo-epitopes) in formerly self-proteins (10-12). As all nucleated cells of the body continuously present peptides from intracellular proteins in MHC class I, mutations in cancer cells may thus lead to recognition and attack by CD8 T cells. The aforementioned process of antigen cross-presentation by DCs is required for successful activation of tumor antigen-specific CD8 T cells, since healthy DCs themselves do not contain the required intracellular mutated self-proteins for the classical MHC class I pathway. Instead, DCs can take up cellular material from dying tumor cells and cross-present tumor antigens to the MHC class I pathway, allowing the activation of tumor antigen-specific CD8 T cells (13). It is now generally established that T cell immunity is the primary immune effector system against tumors. Cancers with a higher mutation rate, particularly those induced by exogenous mutagenic factors such as sunlight (melanoma) and tobacco smoke (lung and bladder cancer), have been shown to contain more T cell neo-epitopes and are indeed best recognized and infiltrated by T cells (10). However, tumors still manage to escape initial recognition and clearance by T cells and develop into clinically apparent cancer. Two prominent mechanisms of immune evasion by tumors are down-regulation of tumor-antigen presentation and suppression of T cell functionality by maintaining an immunosuppressive tumor microenvironment (14-16). The hypothesis of immune-surveillance and immune-editing tells the co-evolutionary story of the shared history of tumors and the immune system: newly formed malignant cells are most often immediately recognized by the surveilling immune system based on their non-self features, whereas the few variants that possess or acquire evasion mechanisms are able to escape immune attack and continue to grow and reshape the tumor. The success of modern cancer immunotherapies is based on the induction and/or enhancement of T cell responses against the tumor (17).

Cancer immunotherapy

Tumor elimination by T cell immunity is especially challenging in the case of advanced cancer, in which tumors have successfully evaded immune clearance by preventing the induction or the functionality of T cell responses. Cancer immunotherapy comprises various different strategies to increase the number and the effector function of tumor-specific T cells, as these have the exclusive ability to recognize intracellular mutations in malignant cells. Prominent forms of cancer immunotherapy include the administration of exogenous tumor antigen (vaccination) and the blockade of immunosuppressive molecules or activation of immune-stimulatory molecules by administration of immunomodulatory antibodies.

Therapeutic vaccination against cancer involves the administration of tumor epitopes in the form of protein or peptide antigens, or of DCs pre-loaded with such antigens (18). Antigen vaccines are typically administered together with adjuvants to deliver danger signals to the DC, resulting in the expression of co-stimulatory molecules and ensuring proper T cell activation. Alternative methods of vaccine administration include antigen encapsulation into biodegradable nanoparticles, which protect the antigen from premature degradation and may also enhance delivery to DCs with the optional co-delivery of DC-activating signals (19-22). To restrict MHC presentation to professional APCs only, the concept of synthetic long peptide (SLP) vaccines was designed (23-26). SLP vaccines contain extra amino acid sequences flanking the T cell epitope, rendering them too large to be directly bound by MHC molecules. Instead, only DCs can take up the SLP and (cross-) present it into MHC class I and II molecules. It was shown that SLP vaccination is most efficient when both CD8 and CD4 T cell epitopes are included in the vaccine (24). Moreover, SLP vaccines lead to better antigen uptake, processing and presentation than full protein vaccines (27). An SLP vaccine consisting of a set of overlapping peptides covering the E6 and E7 oncoproteins of human papillomavirus 16 (HPV16) has been successfully applied in patients with HPV16-induced pre-malignant lesions, but it was not clinically effective against advanced HVP16-induced cancer (28-30). Improved efficacy of SLP vaccination has been shown by combination with conventional cancer therapies and by conjugating Toll-like receptor (TLR) ligands to the peptide (31, 32). Importantly, therapeutic peptide vaccination is not limited to cancer types involving widely shared antigens as in the case of HPV-induced cancer, as shown by recent studies targeting neo-epitopes with individually designed peptide vaccines (33-37).

Unlike SLP vaccination, immunomodulatory antibodies (IMAbs) in cancer immunotherapy boost anti-tumor T cell immunity in a non-antigen-specific manner. IMAbs are directed against molecules that regulate T cell activation and/or effector function, and may be agonistic or blocking antibodies depending on the role of the targeted molecule in the immune response (38, 39). All currently FDA-approved IMAbs are blocking antibodies targeting the immune checkpoint molecules CTLA-4 and the receptor-ligand pair PD-1 and PD-L1. CTLA-4 is expressed on T cells and may regulate both T cell priming and effector function, and aid the suppressive function of a CD4 T cell subset called regulatory T cells (Treg) (40-42). Impressive results in metastatic melanoma patients treated with CTLA-4 blocking antibody established the prominent position of immune checkpoint blockade as a form of cancer immunotherapy (43). PD-1 is an inhibitory receptor expressed on activated T cells which upon ligation by PD-L1 induces T cell apoptosis (44, 45). PD-L1 can be expressed on various cell types including cancer cells and tumor-infiltrating myeloid

immune cells (46). Blockade of the PD-1/PD-L1 axis by antibodies was clinically effective in a range of cancer types including melanoma and non-small cell lung cancer (NSCLC) (47-49). Combinations of PD-1 and CTLA-4 blocking antibodies were shown to further improve clinical responses, supporting the hypothesis that tumors may evade single IMAb treatment by applying alternative immunosuppressive molecules (50-53). Agonistic IMAbs are currently in clinical trial following promising pre-clinical results targeting the DC-activating molecule CD40 or T cell co-stimulatory molecules such as CD137 (4-1BB), OX40, ICOS and CD27 (54, 55).

Optical imaging

Optical imaging has a wide range of applications in biomedical research, all comprising the measurement of optical signals from cells, tissues or living animals. Live *in vivo* optical imaging is of particular interest as a non-invasive strategy to follow physiological or experimentally-induced processes in time within an individual experimental animal. The source of the optical signals can be fluorescent molecules which emit light after being excited by an external light source (fluorescence imaging, FLI), or luciferase enzymes which produce light as a product of a chemical reaction converting an administered substrate (bioluminescence imaging, BLI) **(Figure 1)**. These two forms of optical imaging each have their advantages and disadvantages (56). For instance, FLI allows the administration of fluorescent dyes into living animals, either as such or conjugated to experimental reagents, after which the fate of the administered molecules can be tracked in real-time. Fluorescent molecules do not intrinsically produce photons, but need to be excited by an external light source, and then absorb the energy of the incoming photons and subsequently emit photons of a slightly lower energy (i.e. higher wavelength), which form the actual signal of fluorescence imaging. Since the source of optical signals in whole-body imaging may be relatively deep, photons may be absorbed by the tissue they have to pass during excitation and emission. As photons with higher wavelength are less likely to be absorbed, the most commonly used fluorescent dyes for *in vivo* FLI are near-infrared (NIR) dyes whose wavelength lies slightly above the human visible spectrum. In BLI, photons are produced intrinsically by luciferases, which therefore do not need external energy sources for excitation (57, 58). The most commonly used luciferases have been isolated from animals including the firefly (*Photinus pyralis*), which also produce the substrate to fuel the light-producing reaction. Instead, biomedical BLI systems require the introduction of the luciferase gene into cells or animals by transfection or transgenesis, and the administration of substrate prior to imaging. Besides the extra technical effort, this gives the advantage of placing luciferase gene expression under the control of a

promoter of interest, enabling protein-specific and cell type-specific analysis by BLI. The enzymatic reaction of luciferases requires ATP and oxygen, thus the context of a living cell, allowing the use of BLI for cell viability assays. Moreover, luciferases have a relatively photon quantum yield compared to fluorescent dyes, allowing the detection of low amounts of cells. However, the higher quantum yield of luciferases is counteracted by the fact that luciferases emit light within the human visible spectrum, which is more prone to absorption by tissue than NIR fluorescent dyes. The choice between FLI and BLI will therefore depend on the characteristics of the experimental model in which they are to be applied.

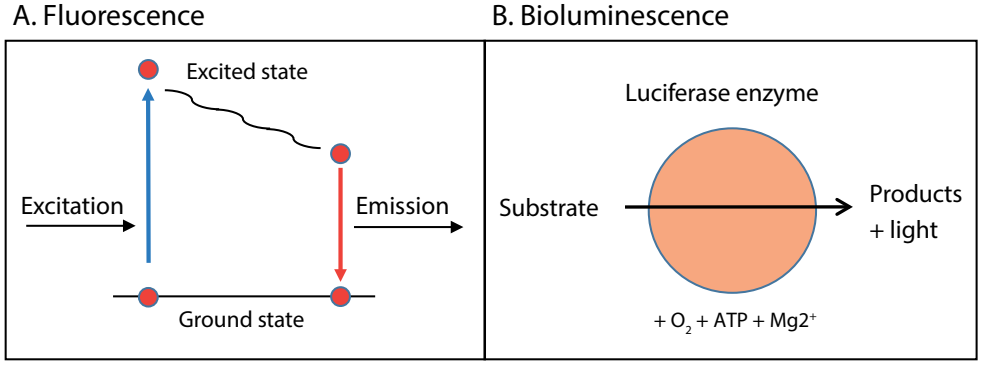

Figure 1. Optical imaging of fluorescent or bioluminescent molecules. (A) Fluorescence is the result of excitation of a fluorescent molecule, causing its electrons to reach the higher-energy excited state, after which they return to ground state, releasing the energy by the emission of light (emission) that can be measured by fluorescence imaging (FLI). Many fluorescent molecules exist in nature, but they do not produce light without a light source to excite them. **(B)** Bioluminescence is an enzymatic reaction of luciferase enzymes, fuelled by cellular ATP and co-factors, producing an oxidized product and visible light, which can be measured by bioluminescence imaging (BLI). Several animals produce luciferase enzymes that, as luciferase reactions are independent of external energy sources, can truly glow in the dark.

Photodynamic therapy

Besides measuring optical signals from biological samples, light can also be used to induce changes in cells and tissues. It is commonly known that exposure to light can directly influence the human body, such as skin pigmentation induced by the UV waves of sunlight, and regulation of the circadian rhythm by light exposure to the eyes. The ancient Indian and Chinese civilizations had already discovered that the application of certain plant extracts to the skin caused dramatic reactions to the skin following exposure to sunlight (59). In the early 20th century, the molecular basis of this 'photodynamic effect' was established. The photosensitive molecules could be isolated, but did not have any obvious effect on a protozoa culture unless exposed to a dose of light that by itself was also harmless. Moreover, oxygen was shown to be required for the photodynamic effect, and the mediators of the effect were extremely short-lived. Although the potential medical applications were realized

at the time, it took over 60 years until a cohort of patients with various types of cancer was treated with Photodynamic Therapy (PDT) showing generally positive results (60). Since then, several photosensitizers have been approved for a range of diseases including both cancer and benign skin conditions. In PDT of cancer, a photosensitizer is administered systemically or applied to the tumor topically, typically followed by a pause of several hours to allow photosensitizer distribution throughout the tumor, before the tumor is exposed to light. The light exposure excites the photosensitizer, which reacts with available oxygen to form the oxygen radicals that are the mediators of the cytotoxic effect of PDT (61). The resulting cancer cell death will alleviate tumor burden, but may also provide the tumor antigen and danger signals required to induce a tumor-specific T cell response (62, 63) **(Figure 2)**. This motivates combination therapies of PDT and immunotherapy to enable successful treatment of advanced tumors for which monotherapies are insufficient.

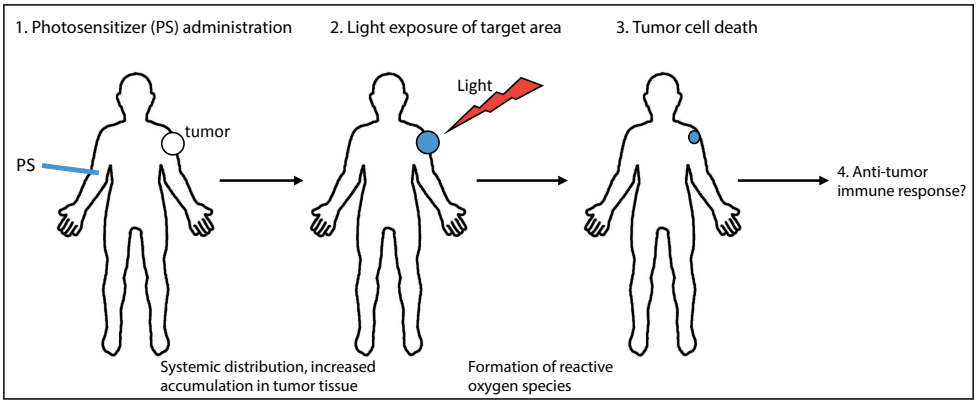

Figure 2. Photodynamic therapy of cancer involves several steps. Typical Photodynamic Therapy protocols involve the following steps. Step 1: systemic administration of a photosensitizer (PS), when then distributes through the body. Tumor cells may take up higher PS levels due to increased expression of lipid receptors on the membrane. Step 2: the PS is selectively activated in the tumor by exposing the tumor to visible light, which excites the PS and results in the formation of reactive oxygen species. Step 3: immediate and local damage to the plasma membrane and organelle membranes leads to tumor cell death. Step 4: massive tumor cell death may lead to the exposure of tumor (-associated) antigens and pro-inflammatory molecules to the immune system, which can induce and/or enhance anti-tumor immune responses.

Outline of this thesis

This thesis shows several different ways of using light in cancer immunotherapy. In **chapter 2**, we investigate combination therapy of PDT and therapeutic SLP vaccination in two aggressive mouse tumor models using an experimental setup in which neither monotherapy is able to eradicate the tumor. Besides following tumor outgrowth as the primary outcome parameter, we analyze the ability of single and combined therapy to induce CD8 T cell responses and the effect on distant identical

tumors. In **chapter 3**, we assess the efficacy of PDT in highly mutated tumor models that express several neo-epitopes that may be recognized by the immune system. We test whether T cells are involved in the effect of PDT and whether distant tumors are also affected. The effect of addition of CTLA-4 blocking antibody is investigated as a potent combination strategy without the need to know the neo-epitope profile of the individual tumor. In **chapter 4**, we test the feasibility of SLP vaccine tracking after vaccination by live *in vivo* fluorescence imaging using peptides labeled with a NIR fluorescent dye. We test whether NIR fluorescent dyes allow long-term vaccine visualization of the vaccination site and the vaccine-draining lymph nodes, and quantify the fluorescence signals at these sites to gather information on vaccine kinetics. In **chapter 5,** we use a similar approach to follow a model protein encapsulated in nanoparticles as a biodegradable delivery system for vaccines. Two fluorescent dyes are applied to independently visualize the nanoparticle carriers and the encapsulated protein vaccine, and the ability of encapsulated protein versus soluble administration to induce vaccine-specific CD8 T cell activation is assessed. In **chapter 6**, we show a T cell luciferase transgenic mouse that allows live *in vivo* visualization of T cells by bioluminescence imaging. We developed a dual-luciferase system where one luciferase is expressed constitutively and exclusively in T cells to report on the location of all T cells, while another luciferase is only expressed upon T cell activation to visualize T cell responses. Finally, **chapter 7** provides a general summary and discussion of the results reported in this thesis.

Reference List

1. Flajnik, M.F. and M. Kasahara, *Origin and evolution of the adaptive immune system: genetic events and selective pressures.* Nat Rev Genet, 2010. **11**(1): p. 47-59.
2. Germain, R.N., *T-cell development and the CD4-CD8 lineage decision.* Nat. Rev. Immunol, 2002. **2**(5): p. 309-322.
3. Klein, L., et al., *Positive and negative selection of the T cell repertoire: what thymocytes see (and don't see).* Nat. Rev. Immunol, 2014. **14**(6): p. 377-391.
4. Smith-Garvin, J.E., G.A. Koretzky, and M.S. Jordan, *T cell activation.* Annu. Rev. Immunol, 2009. **27**: p. 591-619.
5. Malissen, B., et al., *Integrative biology of T cell activation.* Nat. Immunol, 2014. **15**(9): p. 790-797.
6. Joffre, O.P., et al., *Cross-presentation by dendritic cells.* Nat. Rev. Immunol, 2012. **12**(8): p. 557-569.
7. de Magalhaes, J.P., *How ageing processes influence cancer.* Nat. Rev. Cancer, 2013. **13**(5): p. 357-365.
8. Parish, C.R., *Cancer immunotherapy: The past, the present and the future*.* Immunology and Cell Biology, 2003. **81**: p. 106-113.
9. Budhu, S., J. Wolchok, and T. Merghoub, *The importance of animal models in tumor immunity and immunotherapy.* Current Opinion in Genetics & Development, 2014. **24**: p. 46-51
10. Alexandrov, L.B., et al., *Signatures of mutational processes in human cancer.* Nature, 2013. **500**(7463): p. 415-421.

11. Lennerz, V., et al., *The response of autologous T cells to a human melanoma is dominated by mutated neoantigens.* Proceedings of the National Academy of Sciences, 2005. **102**: p. 16013-16018.
12. Linnemann, C., et al., *High-throughput epitope discovery reveals frequent recognition of neo-antigens by CD4+ T cells in human melanoma.* Nature medicine, 2015. **21**: p. 81-5.
13. McDonnell, A.M., B.W. Robinson, and A.J. Currie, *Tumor antigen cross-presentation and the dendritic cell: where it all begins?* Clin. Dev. Immunol, 2010. **2010**: p. 539519.
14. Rosenberg, S.A., et al., *Tumor progression can occur despite the induction of very high levels of self/tumor antigen-specific CD8+ T cells in patients with melanoma.* Journal of immunology (Baltimore, Md. : 1950), 2005. **175**: p. 6169-76.
15. Ahmadzadeh, M., et al., *FOXP3 expression accurately defines the population of intratumoral regulatory T cells that selectively accumulate in metastatic melanoma lesions.* Blood, 2008. **112**(13): p. 4953-4960.
16. Zarour, H.M., *Reversing T-cell Dysfunction and Exhaustion in Cancer.* Clinical Cancer Research, 2016. **22**: p. 1856-1864.
17. Couzin-Frankel, J., *Breakthrough of the year 2013. Cancer immunotherapy.* Science, 2013. **342**(6165): p. 1432-1433.
18. Guo, C., et al., *Therapeutic cancer vaccines: past, present, and future.* Adv. Cancer Res, 2013. **119**: p. 421-475.
19. Elamanchili, P., et al., *"Pathogen-mimicking" nanoparticles for vaccine delivery to dendritic cells.* J. Immunother, 2007. **30**(4): p. 378-395.
20. Pisal, D.S., M.P. Kosloski, and S.V. Balu-Iyer, *Delivery of therapeutic proteins.* J. Pharm. Sci, 2010. **99**(6): p. 2557-2575.
21. Hamdy, S., et al., *Co-delivery of cancer-associated antigen and Toll-like receptor 4 ligand in PLGA nanoparticles induces potent CD8+ T cell-mediated anti-tumor immunity.* Vaccine, 2008. **26**(39): p. 5046-5057.
22. Conniot, J., et al., *Cancer immunotherapy: nanodelivery approaches for immune cell targeting and tracking.* Front Chem, 2014. **2**: p. 105.
23. Corradin, G., A.V. Kajava, and A. Verdini, *Long synthetic peptides for the production of vaccines and drugs: a technological platform coming of age.* Sci Transl Med, 2010. **2**(50): p. 50rv3.
24. Melief, C.J.M. and S.H. van der Burg, *Immunotherapy of established (pre)malignant disease by synthetic long peptide vaccines.* Nature Reviews Cancer, 2008. **8**: p. 351-360.
25. Slingluff, C.L., *The present and future of peptide vaccines for cancer: single or multiple, long or short, alone or in combination?* Cancer journal (Sudbury, Mass.), 2011. **17**: p. 343-50.
26. Tomita, Y. and Y. Nishimura, *Long peptide-based cancer immunotherapy targeting tumor antigen-specific CD4+ and CD8+ T cells.* Oncoimmunology, 2013. **2**(9): p. e25801.
27. Rosalia, R.A., et al., *Dendritic cells process synthetic long peptides better than whole protein, improving antigen presentation and T-cell activation.* European Journal of Immunology, 2013. **43**: p. 2554-2565.
28. Kenter, G.G., et al., *Phase I immunotherapeutic trial with long peptides spanning the E6 and E7 sequences of high-risk human papillomavirus 16 in end-stage cervical cancer patients shows low toxicity and robust immunogenicity.* Clinical cancer research : an official journal of the American Association for Cancer Research, 2008. **14**: p. 169-77.
29. Kenter, G.G., et al., *Vaccination against HPV-16 oncoproteins for vulvar intraepithelial neoplasia.* The New England journal of medicine, 2009. **361**: p. 1838-47.
30. van Poelgeest, M.I.E., et al., *HPV16 synthetic long peptide (HPV16-SLP) vaccination therapy of patients with advanced or recurrent HPV16-induced gynecological carcinoma, a phase II trial.* Journal of translational medicine, 2013. **11**: p. 88.
31. van der Sluis, T.C., et al., *Vaccine-Induced Tumor Necrosis Factor-Producing T Cells Synergize with Cisplatin to Promote Tumor Cell Death.* Clinical Cancer Research, 2015. **21**: p. 781-794.
32. Zom, G.G., et al., *Efficient Induction of Antitumor Immunity by Synthetic Toll-like Receptor Ligand-*

Peptide Conjugates. Cancer Immunology Research, 2014. **2**: p. 756-764.
33. Yadav, M., et al., *Predicting immunogenic tumour mutations by combining mass spectrometry and exome sequencing.* Nature, 2014. **515**: p. 572-576.
34. Gubin, M.M., et al., *Checkpoint blockade cancer immunotherapy targets tumour-specific mutant antigens.* Nature, 2014. **515**(7528): p. 577-581.
35. Castle, J.C., et al., *Exploiting the mutanome for tumor vaccination.* Cancer Res, 2012. **72**(5): p. 1081-1091.
36. Sahin, U., et al., *Personalized RNA mutanome vaccines mobilize poly-specific therapeutic immunity against cancer.* Nature, 2017. **547**: p. 222-226.
37. Ott, P.A., et al., *An immunogenic personal neoantigen vaccine for patients with melanoma.* Nature, 2017. **547**: p. 217-221.
38. Pardoll, D.M., *The blockade of immune checkpoints in cancer immunotherapy.* Nature Reviews Cancer, 2012. **12**: p. 252-264.
39. Postow, M.A., M.K. Callahan, and J.D. Wolchok, *Immune Checkpoint Blockade in Cancer Therapy.* Journal of Clinical Oncology, 2015. **33**: p. 1974-1982.
40. Grosso, J.F. and M.N. Jure-Kunkel, *CTLA-4 blockade in tumor models: an overview of preclinical and translational research.* Cancer immunity, 2013. **13**: p. 5.
41. Selby, M.J., et al., *Anti-CTLA-4 antibodies of IgG2a isotype enhance antitumor activity through reduction of intratumoral regulatory T cells.* Cancer immunology research, 2013. **1**: p. 32-42.
42. Simpson, T.R., et al., *Fc-dependent depletion of tumor-infiltrating regulatory T cells co-defines the efficacy of anti?CTLA-4 therapy against melanoma.* The Journal of Experimental Medicine, 2013. **210**: p. 1695-1710.
43. Hodi, F.S., et al., *Improved survival with ipilimumab in patients with metastatic melanoma.* N. Engl. J. Med, 2010. **363**(8): p. 711-723.
44. Iwai, Y., et al., *Involvement of PD-L1 on tumor cells in the escape from host immune system and tumor immunotherapy by PD-L1 blockade.* Proc. Natl. Acad. Sci. U. S. A, 2002. **99**(19): p. 12293-12297.
45. Dong, H., et al., *Tumor-associated B7-H1 promotes T-cell apoptosis: a potential mechanism of immune evasion.* Nat. Med, 2002. **8**(8): p. 793-800.
46. Kleinovink, J.W., et al., *PD-L1 expression on malignant cells is no prerequisite for checkpoint therapy.* OncoImmunology, 2017. **6**: p. e1294299.
47. Topalian, S.L., et al., *Safety, Activity, and Immune Correlates of Anti–PD-1 Antibody in Cancer.* New England Journal of Medicine, 2012. **366**: p. 2443-2454.
48. Rosenberg, J.E., et al., *Atezolizumab in patients with locally advanced and metastatic urothelial carcinoma who have progressed following treatment with platinum-based chemotherapy: a single-arm, multicentre, phase 2 trial.* The Lancet, 2016. **387**: p. 1909-1920.
49. Fehrenbacher, L., et al., *Atezolizumab versus docetaxel for patients with previously treated non-small-cell lung cancer (POPLAR): a multicentre, open-label, phase 2 randomised controlled trial.* The Lancet, 2016. **387**: p. 1837-1846.
50. Wolchok, J.D., et al., *Nivolumab plus ipilimumab in advanced melanoma.* N. Engl. J. Med, 2013. **369**(2): p. 122-133.
51. Larkin, J., et al., *Combined Nivolumab and Ipilimumab or Monotherapy in Untreated Melanoma.* N. Engl. J. Med, 2015. **373**(1): p. 23-34.
52. Callahan, M.K., M.A. Postow, and J.D. Wolchok, *CTLA-4 and PD-1 Pathway Blockade: Combinations in the Clinic.* Frontiers in oncology, 2014. **4**: p. 385.
53. Koyama, S., et al., *Adaptive resistance to therapeutic PD-1 blockade is associated with upregulation of alternative immune checkpoints.* Nat. Commun, 2016. **7**: p. 10501.
54. Peggs, K.S., S.A. Quezada, and J.P. Allison, *Cancer immunotherapy: co-stimulatory agonists and co-inhibitory antagonists.* Clin. Exp. Immunol, 2009. **157**(1): p. 9-19.
55. Moran, A.E., M. Kovacsovics-Bankowski, and A.D. Weinberg, *The TNFRs OX40, 4-1BB, and CD40 as targets for cancer immunotherapy.* Curr. Opin. Immunol, 2013. **25**(2): p. 230-237.

56. Weissleder, R. and V. Ntziachristos, *Shedding light onto live molecular targets.* Nature Medicine, 2003. **9**: p. 123-128.
57. Roda, A., et al., *Biotechnological applications of bioluminescence and chemiluminescence.* Trends Biotechnol, 2004. **22**(6): p. 295-303.
58. Sato, A., B. Klaunberg, and R. Tolwani, *In vivo bioluminescence imaging.* Comp Med, 2004. **54**(6): p. 631-634.
59. Dolmans, D.E., D. Fukumura, and R.K. Jain, *Photodynamic therapy for cancer.* Nat. Rev. Cancer, 2003. **3**(5): p. 380-387.
60. Dougherty, T.J., et al., *Photoradiation therapy for the treatment of malignant tumors.* Cancer Res, 1978. **38**(8): p. 2628-2635.
61. Agostinis, P., et al., *Photodynamic therapy of cancer: an update.* CA Cancer J. Clin, 2011. **61**(4): p. 250-281.
62. Castano, A.P., P. Mroz, and M.R. Hamblin, *Photodynamic therapy and anti-tumour immunity.* Nat. Rev. Cancer, 2006. **6**(7): p. 535-545.
63. Mroz, P., et al., *Stimulation of anti-tumor immunity by photodynamic therapy.* Expert. Rev. Clin. Immunol, 2011. **7**(1): p. 75-91.

Chapter 2

Combination of Photodynamic Therapy and specific immunotherapy efficiently eradicates established tumors

Jan Willem Kleinovink, Pieter B. van Driel, Thomas J. Snoeks, Natasa Prokopi, Marieke F. Fransen, Luis J. Cruz, Laura Mezzanotte, Alan Chan, Clemens W. Löwik, Ferry Ossendorp

Clinical Cancer Research (2016) Mar 15;22(6):1459-68

Abstract

Purpose: The efficacy of immunotherapy against advanced cancer may be improved by combination strategies. Photodynamic therapy (PDT) is a local tumor ablation method based on localized activation of a photosensitizer, leading to oxygen radical-induced tumor cell death. PDT can enhance antitumor immune responses by release of antigen and danger signals, supporting combination protocols of PDT with immunotherapy.

Experimental Design: We investigated the local and systemic immune effects of PDT after treatment of established tumors. In two independent aggressive mouse tumor models, TC-1 and RMA, we combined PDT with therapeutic vaccination using synthetic long peptides (SLP) containing epitopes from tumor antigens.

Results: PDT of established tumors using the photosensitizer Bremachlorin resulted in significant delay of tumor outgrowth. Combination treatment of PDT with therapeutic SLP vaccination cured one third of mice. Importantly, all cured mice were fully protected against subsequent tumor rechallenge, and combination treatment of primary tumors led to eradication of distant secondary tumors, indicating the induction of a systemic antitumor immune response. Indeed, PDT by itself induced a significant CD8 T-cell response against the tumor, which was increased when combined with SLP vaccination and essential for the therapeutic effect of combination therapy.

Conclusions: We show that immunotherapy can be efficiently combined with PDT to eradicate established tumors, based on strong local tumor ablation and the induction of a robust systemic immune response. These results suggest combination of active immunotherapy with tumor ablation by PDT as a feasible novel treatment strategy for advanced cancer.

Translational relevance

Cancer immunotherapy has shown promising results although a significant proportion of patients respond poorly or relapse at a later stage, therefore more potent combination therapies are required. Tumor ablation by Photodynamic Therapy (PDT) can strongly reduce tumor mass and induce the release of tumor antigen and pro-inflammatory mediators, therefore being an attractive option for combination with immunotherapy. In this preclinical study, we show that tumor-specific immunotherapy by synthetic long peptide (SLP) vaccination can be efficiently combined with PDT, leading to eradication of established tumors based on strong local tumor ablation and the induction of a CD8 T cell response. PDT and SLP vaccination are independently already applied in the clinic, allowing a swift translation for potentially a large group of cancer patients.

Introduction

A major challenge in medical oncology is the development of efficient treatment options for advanced cancer, which currently are limited. The clinical situation of advanced primary tumors with possible metastases asks for therapeutic protocols that combine a strong anti-tumor effect to eradicate known tumors with the induction of a systemic anti-tumor immune response to eliminate distant metastases. As the immune system can strongly and specifically attack targets based on the principle of antigen-specificity, cancer immunotherapy aims to employ these characteristics of the immune system to attack and eradicate tumors.

A promising approach of cancer immunotherapy is therapeutic vaccination using synthetic long peptides (SLP) covering T cell epitopes of tumor antigens (1-4). Besides widely shared tumor antigens such as those expressed by virally induced tumors, this approach can also be applied to individual patient-specific neo-antigens (5, 6). Clinical studies using therapeutic SLP vaccination against cancer are ongoing based on encouraging results in preclinical tumor models (7-9). For instance, clinical Phase I/II studies using a set of overlapping peptides covering the E6 and E7 oncoproteins of Human Papillomavirus 16 (HPV16) have been successful in patients with HPV16-induced premalignant disease (10). This peptide vaccine formulation induced HPV16-specific T cell responses in all 20 patients and resulted in clinical responses in about 80% of patients and nearly 50% complete remissions correlating with robust effector T cell immunity. However, thus far this vaccine was not clinically effective against established HVP16+ cancer despite detectable vaccine-induced T cell responses (11, 12). This is one of the examples illustrating that successful treatment of advanced cancer requires combination protocols, as single-treatment modalities are insufficiently effective. Therapies causing immunogenic cell death are of particular interest for combination with immunotherapy, as the reduction of tumor burden and the immunogenic effects can enhance the efficacy of immunotherapy. Combinations of immunotherapy with conventional cancer therapies like chemotherapy or radiotherapy are already under investigation. In this study, we examine the use of Photodynamic Therapy (PDT), a tumor ablation method that is widely clinically applied for various premalignant and malignant lesions.

In PDT, an inactive light-sensitive molecule called photosensitizer is administered and subsequently activated by irradiation of the target area with visible light of a specific wavelength. The activated photosensitizer reacts with oxygen to form reactive oxygen species (ROS), which induce tumor cell death and vascular shutdown (13, 14). Besides direct cytotoxic effects on tumor cells, PDT has been shown to

cause the release of antigen and immunogenic factors such as damage-associated molecular patterns (DAMPs) from dying tumor cells (15-25). These immunological effects make PDT an attractive option for combinations with immunotherapy in the treatment of advanced tumors. Here, we use Bremachlorin, also known as Radachlorin, a novel photosensitizer that benefits from improved pharmacokinetics and high-wavelength irradiation reaching deeper tissue. Bremachlorin is currently being tested in clinical trials for basal cell carcinoma (BCC) and non-small-cell lung carcinoma (NSCLC) (26-31).

In this study, we investigated the combination of Bremachlorin-based PDT with therapeutic peptide vaccination in two mouse models of highly aggressive subcutaneous tumors. The tumor line TC-1 expresses the E6 and E7 oncoproteins of Human Papillomavirus 16 (HPV16) as a model for human HPV16-induced tumors, and has previously been shown to be sensitive for Bremachlorin-PDT (32, 33). RMA is an aggressive T cell lymphoma cell line induced by Rauscher murine leukemia virus (34). We show that PDT strongly ablated established fast-growing tumors, leading to a significantly longer survival and specific CD8+ T cell responses against the tumor. Combining PDT with therapeutic peptide vaccination efficiently eradicated established tumors, which was dependent on the presence of CD8 T cells. Importantly, combination treatment of primary tumors led to subsequent eradication of distant established secondary tumors and provided protection against repeated tumor challenge. Therefore, this successful combination of PDT and therapeutic vaccination, resulting in robust anti-tumor response and immunological memory, suggests a novel therapeutic combination strategy for advanced cancer.

Materials and Methods

Mice and cell lines

Wildtype C57BL/6 mice were obtained from Charles River Laboratories (France). Albino B6 mice (tyrosinase-deficient immunocompetent C57BL/6 mice) were bred in the animal breeding facility of the Leiden University Medical Center, the Netherlands. All experiments were approved by the animal experimental committee of the University of Leiden. The TC-1 mouse tumor cell line (a gift from T.C. Wu, John Hopkins University, Baltimore, MD) expressing HPV16 E6 and E7 oncoproteins was generated as previously described (32). RMA is a mutagenized derivative of RBL-5, a Rauscher Murine Leukemia Virus (MuLV)-induced T cell lymphoma line of C57BL/6 origin (34). Cell lines were assured to be free of rodent viruses and *Mycoplasma* by

regular PCR analysis. Authentication of the cell lines was done by antigen-specific T-cell recognition and the use of low passage number cells for all experiments. TC-1 cells were cultured as previously described (35). RMA cells were cultured in IMDM (Lonza) containing 8% Fetal Calf Serum (FCS, Greiner), 100 IU/mL penicillin/streptomycin (Gibco), 2 mM glutamin (Gibco) and 25 µM 2-mercaptoethanol. For tumor inoculation, 100,000 TC-1 or 1000 RMA tumor cells in 100 µL PBS were injected subcutaneously in the right flank of the mice. For tumor rechallenge, the identical injection was given in the left flank to distinguish possible outgrowth from regrowth of the original tumor. For double-tumor experiments, an identical TC-1 inoculation was given in the left flank 3 days after primary tumor inoculation. Tumors were measured 3 times per week with a caliper and the volume was calculated by multiplying the tumor diameters in three dimensions. Survival curves are based on the moment of sacrificing the mice upon reaching the maximally allowed tumor volume of 2000 mm^3.

Photosensitizer uptake and *in vitro* irradiation

In vitro Bremachlorin uptake by tumor cells was analyzed by incubating TC-1 tumor cells with Bremachlorin at the dose and time as indicated, washing the cells in PBS, and measuring the Bremachlorin fluorescence compared to control cells by flow cytometry (BD Calibur, emission channel FL4). In vivo Bremachlorin uptake by tumors was visualized using a Pearl Impulse imager (Li-cor). For photodynamic treatment *in vitro*, TC-1 tumor cells were incubated with 1 µg/mL Bremachlorin for 3 hours in 24 wells plates, then the cells were washed with PBS to remove all free photosensitizer, and fresh medium was added. Irradiation of the whole well followed immediately for 2 minutes at 116 mW/cm^2 (14 J/cm^2) using a 662 nm Milon Lakhta laser.

Photodynamic Therapy

Tumors were treated 9 days (TC-1) or 14 days (RMA) after inoculation, both at an average tumor diameter of 5 mm. First, 20 mg/kg Bremachlorin photosensitizer (RadaPharma International) was injected intravenously in the tail vein, followed by irradiation of the tumor 6 hours later using a 662 nm Milon Lakhta laser. A continuous irradiation protocol of 1000 seconds at 116 mW/cm^2 (116 J/cm^2) was used based on optimization experiments (data not shown). For irradiation, the skin in the tumor area was shaved and the mice were anaesthetized by inhalation of isoflurane and positioned horizontally on a heat mat. Precision irradiation of the tumor was ensured by using a fiber fixed vertically above the mouse, and the exposed area was precisely adjusted using a diaphragm.

Serum analysis for HMGB1

Serum was obtained from blood samples taken 1 hour after PDT treatment, or at the same time for untreated controls. The HMGB1 serum level was determined by a sandwich ELISA kit (IBL International) following the manufacturers protocol.

Ex vivo lymph node analysis

TC-1 tumor-bearing animals received the standard PDT treatment as described above, and were sacrificed after 6 days and the tumor-draining inguinal lymph node was obtained, together with the contralateral inguinal lymph node. The lymph nodes were incubated with 2.5 mg/mL Liberase TL (Roche) for 20 minutes at 37°C and single-cell suspensions were made using 70 μm cell strainers (BD Biosciences). The cells were then stained with fluorescently labeled antibodies against CD3ε, CD8α, CD11c and with 7-AAD and APC-labeled tetramer for flow cytometry analysis.

Flow cytometry

All flow cytometry analyses were performed by suspending cells in FACS buffer (PBS with 0.5% BSA and 0.02% sodium azide) and analysis on a BD FACS Calibur. Antibodies against CD3, CD8 or CD11c and the dyes Annexin V and 7-AAD were purchased from BD, eBioscience and BioLegend. The APC-labelled H-2Db RAHYNIVTF tetramer was own production.

Synthetic long peptide vaccination

The SLP vaccine for TC-1 (sequence GQAEPDRAHYNIVTFCCKCDSTLRLCVQSTHVDIR), including both a CD4 and a CD8 epitope from the HPV16 E7 oncoprotein, was given on day 7 and 21 after tumor inoculation by injecting 150 μg peptide subcutaneously in the left flank of the mouse (35). The peptide was dissolved in a 100 μL PBS and mixed 1:1 with Incomplete Freunds Adjuvant (IFA), which was then emulsified for 30 minutes on a vortex. The peptide vaccine for RMA tumors contains epitopes from Rauscher Murine Leukemia Virus (MuLV) and existed of a single vaccination on day 14 containing 20 nmole of the Env-encoded CD4 epitope EPLTSLTPRCNTAWNRLKL and 50 nmole of the Gag-encoded CD8 epitope CCLCLTVFL (36) complemented with 20 μg CpG (ODN 1826, Invivogen), in 100 μL PBS subcutaneously in the tail-base region.

Systemic blood analysis for specific CD8 T cell response

The systemic tumor-specific CD8 T cell response was determined by taking venous blood samples from the tail vein 8 days after peptide vaccination or on the same day for non-vaccinated animals. After erythrocyte lysis of the blood samples, the tumor-specific CD8 T cell response was determined by flow cytometry analysis

after staining of the cells with CD3ε, CD8β, and APC-conjugated tetramers for the relevant peptide-MHC complex on the CD8 T cell.

CD8+ T cell depletion

Hybridoma cells producing depleting CD8 mAb (clone 2.43) were cultured in Protein-Free Hybridoma Medium (Gibco), and mAbs were purified using a Protein G column. To deplete CD8 T cells, mice received an intraperitoneal (i.p.) injection of 150 µg anti-CD8 antibodies on day 8 after tumor inoculation, followed by periodical depletion of 50 µg antibodies every 5 days until day 30 after tumor inoculation. All control mice received in parallel similar amounts of isotype control rat immunoglobulin G. The effective T-cell depletion was assured by flow cytometry analysis of blood lymphocytes stained for cell surface expression of CD8.

Statistical analysis

Statistical analysis was performed using GraphPad Prism version 5.0 software. Data are shown as the mean ± SEM for each group, and comparison of groups was performed by two-tailed Student's t-test, with the exception of survival curves which were compared using the LogRank Mantel-Cox test. Statistical differences were considered significant at $p < 0.05$.

Results

Efficient photosensitizer uptake allows strong tumor ablation

For effective PDT, sufficient photosensitizer uptake by tumor cells is required to ensure irradiation-induced cell death. Both TC-1 and RMA tumor cells showed a dose-dependent uptake after incubation with Bremachlorin (**Supplementary Figure S1a**). Irradiation of Bremachlorin-treated TC-1 cells using visible light resulted in >98% cell death based on Annexin V and 7-AAD analysis, which was completely dependent on the presence of both the photosensitizer and the irradiation (**Supplementary Figure S1b**). Photosensitizer uptake in established tumors was shown by intravenously injecting mice bearing subcutaneous TC-1 or RMA tumors with Bremachlorin, which after 6 hours accumulated in the tumor area (**Supplementary Figure S2**). To analyze whether this photosensitizer accumulation is sufficient for photodynamic ablation, growing TC-1 tumors with a diameter of 5 mm were irradiated with a focused laser beam 6 hours after injection of Bremachlorin. After a clear inflammatory reaction in the treated area in the first days after PDT, a strongly flattened tumor lesion remained with a necrotic appearance. This resulted in a significant delay in tumor

growth of at least 7 days, after which tumor outgrowth resumed with a growth rate similar to untreated tumors (**Figure 1a**).

PDT induces an anti-tumor immune response

As we aimed to use Bremachlorin-based PDT in combination with immunotherapy, we analyzed the immunological effects of PDT in our model. It has previously been shown that PDT can contribute to anti-tumor immune responses through the release of DAMPs such as HMGB1 (17, 18). Serum analysis of TC-1 tumor-bearing mice 1 hour after PDT showed a significant increase in HMGB1 compared to untreated mice (**Figure 1b).**

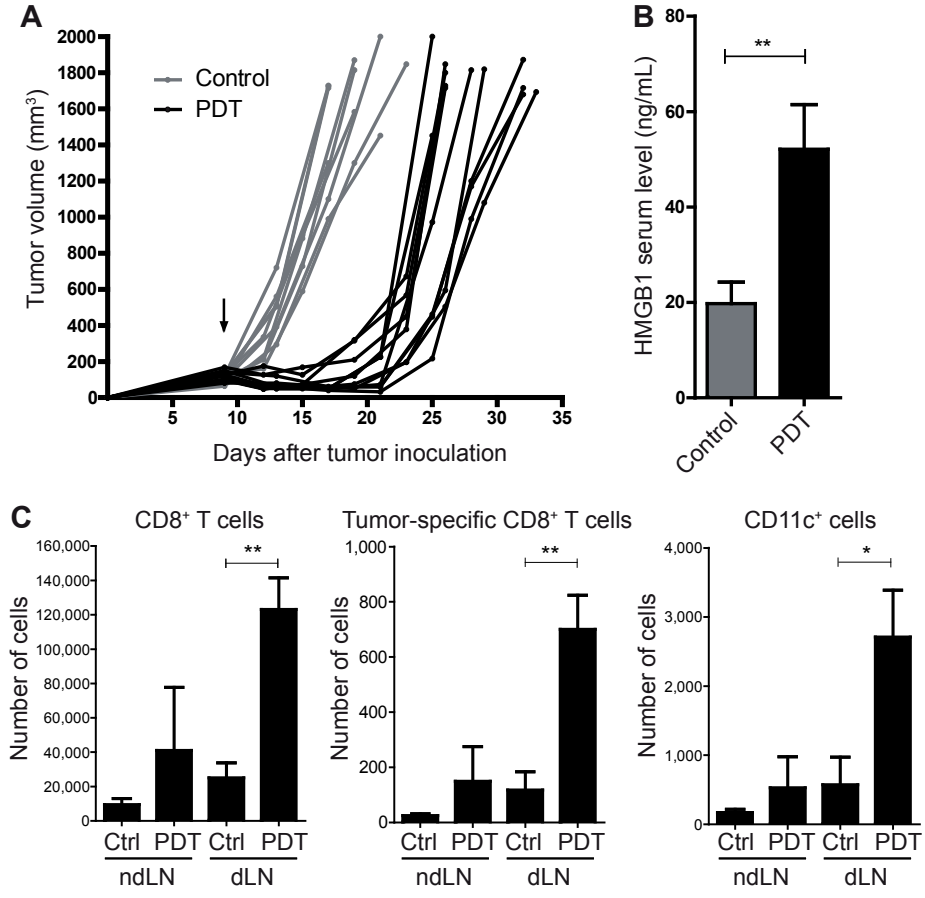

Figure 1. PDT strongly delays tumor outgrowth and induces an immune response against the tumor. (A) Tumor outgrowth curves of subcutaneous TC-1 tumors in BL/6 mice treated with PDT on day 9 (arrow) after tumor inoculation, compared to untreated control tumors. Pooled data of 2 independent experiments, n=10-12 mice. **(B)** ELISA serum analysis for HMGB1 in 9 mice at 1 hour after PDT versus untreated control mice. Pooled data of 2 independent experiments, n=9 mice. **(C)** Flow cytometry analysis of TC-1 tumor-draining lymph nodes (dLN) or contralateral non-draining lymph nodes (ndLN) of 4 mice at 6 days after PDT in comparison to untreated control mice (Ctrl). Single-cell suspensions from lymph nodes were stained for CD3ε, CD8α, CD11c and the Db-RAHYNIVTF Tetramer (Tm) for the tumor antigen-specific T cell receptor. Y-axes show absolute numbers of total CD8 T cells (CD3+ CD8+), tumor-antigen specific CD8 T cells (CD3+ CD8+ Tm+) or CD11c+ cells. Statistical analysis by Student's T test, significance is indicated by asterisks: * $p<0.05$, ** $p<0.01$.

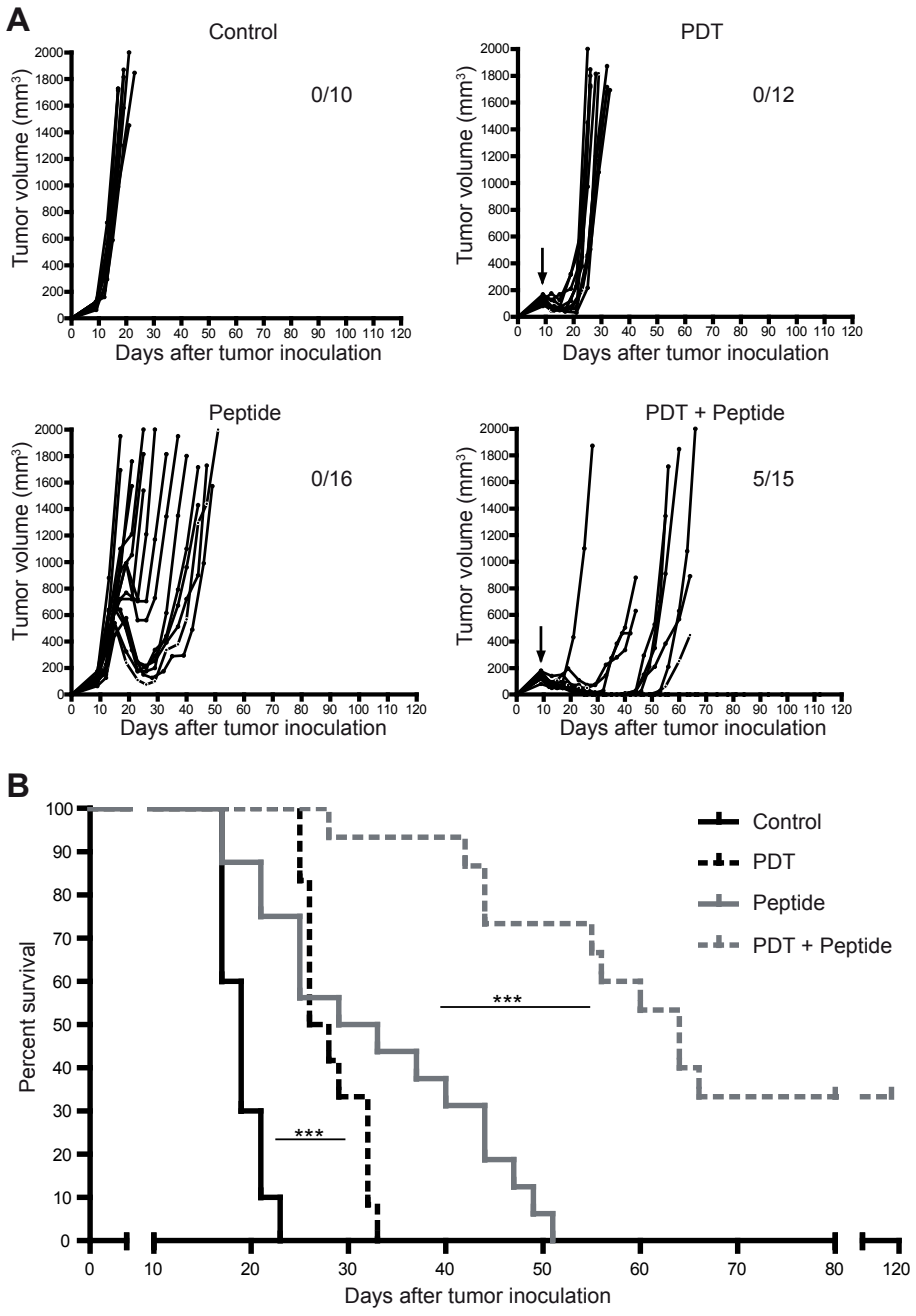

Figure 2. Curative combination treatment of established TC-1 tumors by PDT and synthetic long peptide vaccination. (A) Tumor outgrowth curves and **(B)** survival curves of TC-1 tumor-bearing mice treated with PDT, peptide vaccination or combined treatment, compared to untreated control tumors. PDT was done on day 9 after tumor inoculation (arrows), peptide was administered subcutaneously in IFA in the contralateral flank on day 7 and 21. Pooled data of 2 independent experiments, 10-16 mice. The fractions of mice that cleared the tumor are indicated. Survival curve statistics by LogRank X^2 test. Statistical significance is indicated by asterisks: *** $p<0.001$.

To investigate the immunological consequences of the massive tumor cell death induced by PDT, we analyzed the tumor-draining lymph nodes 6 days after PDT treatment of TC-1 tumors and compared them to contralateral lymph nodes not draining the irradiated tumor area. PDT induced a strong tumor antigen-specific CD8 T cell response in the tumor-draining lymph nodes, accompanied by a significant increase in the total number of CD8 T cells which was not increased in the non-draining nodes of the same animals (**Figure 1c).** Untreated tumor-bearing mice mounted only a minimal CD8 T cell response against the tumor, quantitatively similar to non-draining lymph nodes of PDT-treated mice. Strikingly, also the numbers of CD11c+ dendritic cells (DC) were strongly increased in the draining nodes of the PDT-treated tumor, suggesting that the DC facilitate cross-presentation of tumor-associated antigen to T cells in local lymphoid organs to stimulate anti-tumor responses.

Combination of PDT and therapeutic vaccination eradicates established tumors
Altogether, the strong tumor ablation and beneficial immunological effects of Bremachlorin-PDT make it an attractive candidate for combination with immunotherapy. As we have previously shown that the TC-1 tumor model is susceptible to therapeutic synthetic long peptide (SLP) vaccination (7), we combined Bremachlorin-PDT with SLP vaccination following the experimental setup depicted in **Supplementary Figure S3**. Single treatments of PDT or peptide vaccination of established TC-1 tumors each resulted in a significant delay in tumor outgrowth and increased survival, but neither treatment was curative**.** However, when PDT was combined with SLP vaccination, overall survival was strongly increased and over one third of mice were cured **(Figure 2)**.

Combination treatment protects against tumor rechallenge and eradicates established secondary tumors
All mice cured from their TC-1 tumor after combination therapy of PDT and SLP vaccination subsequently rejected TC-1 tumor cells injected at a distant location two to three months after primary curative treatment, indicating the induction of protective systemic immunity **(Supplementary Figure S4a)**. To investigate whether combination therapy can also eradicate existing established distant tumors, mice were inoculated with TC-1 tumors in both flanks followed by combination therapy where PDT was only applied on the primary tumor in the right flank, as depicted in **Supplementary Figure S4b.** The outgrowth of secondary tumors was not delayed by PDT of the contralateral primary tumor **(Figure 3a).** Mice treated by peptide vaccination showed an initial regression of both primary and secondary tumors, but none of the mice were cured from both tumors and all were eventually sacrificed due to tumor outgrowth. In contrast, combination treatment of PDT and peptide

vaccination caused definite cure from both primary and secondary tumors in almost 40% of mice, similar to the experimental model with a single TC-1 tumor. This can be appreciated when comparing the long-term survival between peptide vaccination and combination treatment from day 50 onwards **(Figure 3b).**

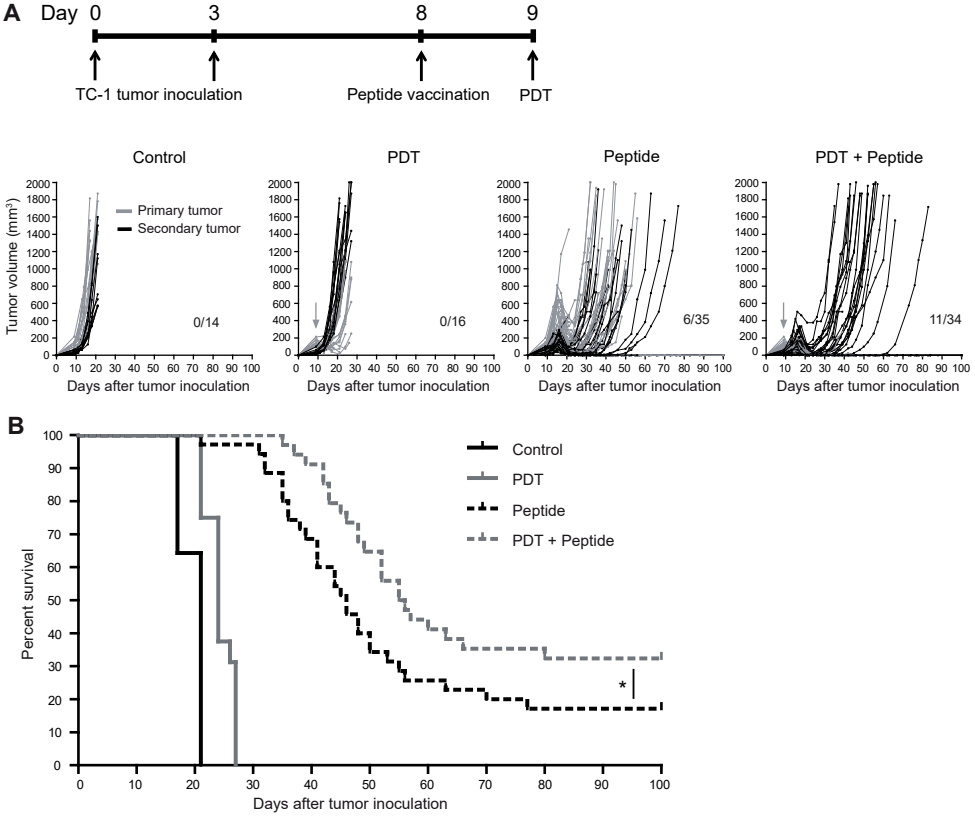

Figure 3. Combination treatment of primary tumors leads to durable eradication of distant tumors. (A) Tumor outgrowth curves of mice bearing established subcutaneous TC-1 tumors in both flanks, treated with systemic peptide vaccination on day 8 followed by PDT of only the primary tumor in the right flank on day 9 (arrows). Primary tumors (grey lines) were inoculated on day 0 in the right flank, secondary tumors (black lines) on day 3 in the left flank. The fractions of mice that cleared both tumors are indicated. **(B)** Corresponding survival curves, statistical analysis by LogRank X2 test. Statistical significance is indicated by asterisks: * $p<0.05$.

Treatment-induced anti-tumor CD8 T cells are essential for therapeutic efficacy

As we found that PDT induces a local immune response in lymph nodes and that combination therapy using local PDT is also able to cure distant secondary tumors, we analyzed the systemic CD8 T cell response against the tumor. Using specific MHC tetramer staining to identify tumor antigen-specific CD8 T cells, we could show that SLP vaccination raised the levels of CD8+ T cells specific for the HVP16 E7 epitope used for vaccination in circulating blood as we have reported previously (**Figure 4a)** (7)**.** Importantly, also PDT significantly increased percentage of tumor antigen-specific CD8+ T cells circulating in blood, supporting the immunogenic effects of

PDT described earlier. Moreover, PDT even further increased the SLP-induced CD8 T cell response, reflecting the efficacy of combination treatment in tumor control. To analyze whether these tumor-specific CD8 T cells are responsible for the observed tumor control, TC-1 tumor-bearing mice treated with PDT and SLP vaccination were depleted of all CD8+ cells using an anti-CD8 antibody. Periodical screening of systemic venous blood confirmed a persisting reduction in the number of CD8 T cells of over 98% during the experiment (data not shown). In the absence of CD8 T cells, the curative effect of PDT and SLP combination treatment was abrogated, suggesting a crucial role of CD8 T cells in this combination treatment protocol **(Figure 4b)**.

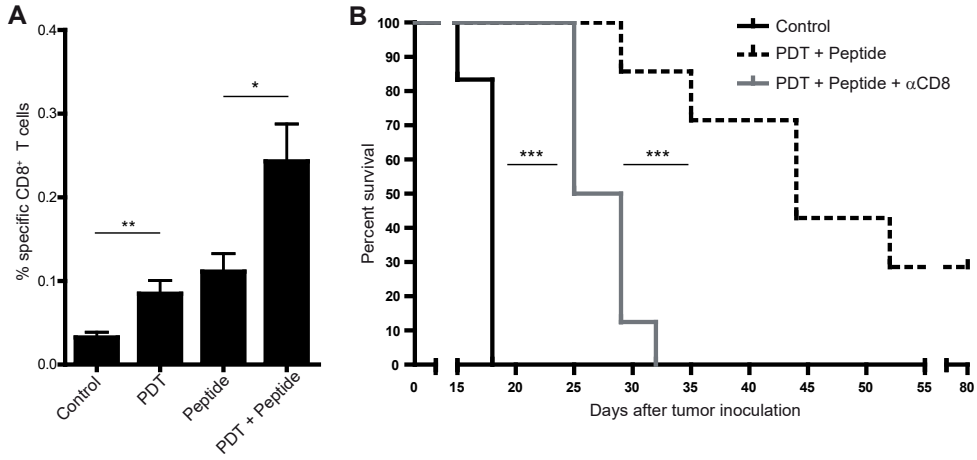

Figure 4. The strong effect of combination treatment is dependent on a treatment-induced systemic CD8 T cell response against the tumor. (A) Tetramer staining showing the percentage of CD8 T cells in tail vein blood that is specific for the HPV16 E7 epitope expressed by TC-1 tumor cells, 8 days after treatment. **(B)** Survival curves of TC-1 tumor-bearing mice treated with PDT and peptide vaccination during antibody-mediated depletion of CD8 T cells. PDT was performed on day 9 after tumor inoculation, peptide was administered subcutaneously in IFA in the contralateral flank on day 7 and 21. Depleting antibody was administered i.p. regularly from day 8 to day 45, resulting in >98% depletion of CD8+ cells in the blood within 24h after injection. Pooled data of individual experiments with in total 16-24 mice per group. Statistical analysis of Figure A by Student's T test and of Figure B by LogRank X^2 test. Statistical significance is indicated by asterisks: * $p<0.05$, ** $p<0.01$, *** $p<0.001$.

Efficient PDT-vaccination combination in virally-induced lymphoma tumors

Next, we applied PDT and peptide vaccination in another aggressive tumor system, the RMA lymphoma model for which we have previously described efficient prophylactic peptide vaccination, which prevented tumor outgrowth through the effects of both CD4 and CD8 T cells (36). Previous attempts in our group to treat established RMA tumors by therapeutic peptide vaccination have never been successful. Here, we show that combination of Bremachlorin-PDT and therapeutic peptide vaccination in mice bearing subcutaneous RMA tumors resulted in significantly prolonged survival compared to either single treatment alone, similar

to our observations in the TC-1 model **(Figure 5)**. All mice cured of their primary tumor were able to reject RMA tumor cells upon rechallenge at a distant location over two months after treatment (data not shown), suggesting that also in this model PDT and peptide vaccination induced systemic immunity against the tumor.

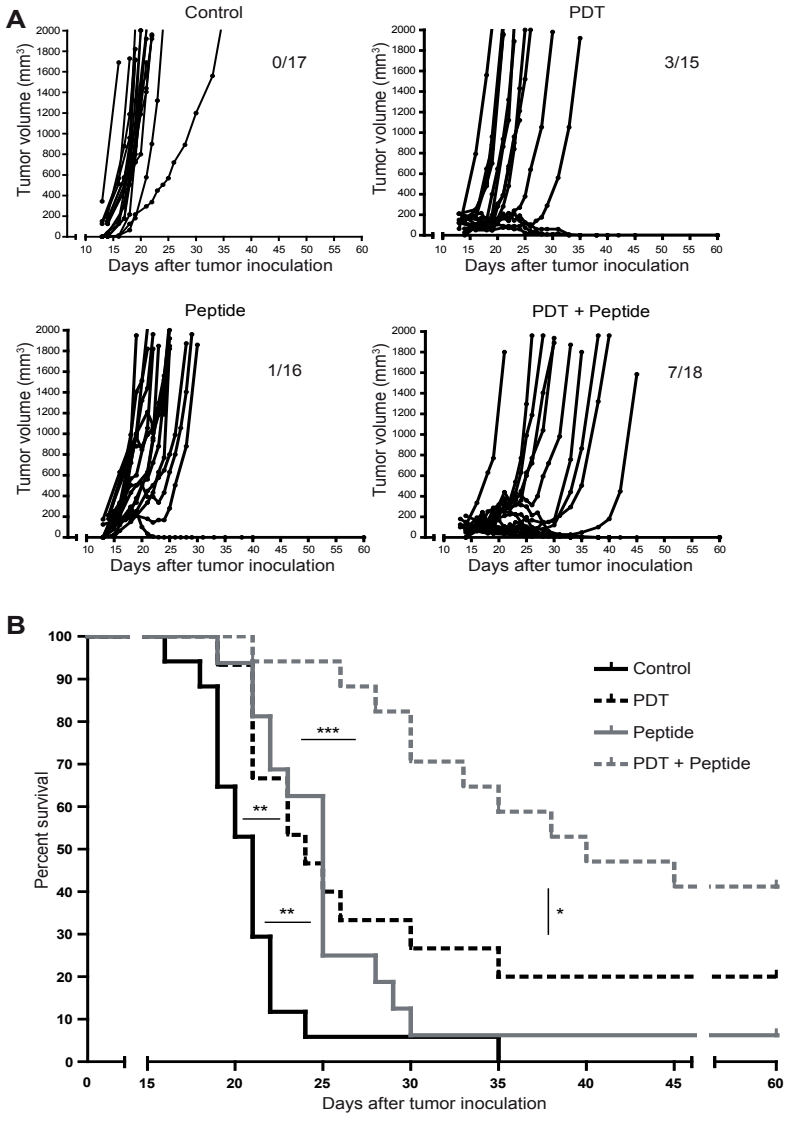

Figure 5. Therapeutic treatment of murine leukemia virus-induced lymphoma by PDT and tumor-specific peptide vaccination. (A) Tumor outgrowth curves and **(B)** survival curves of RMA tumor-bearing mice treated with PDT, peptide vaccination, or combined therapy, compared to untreated control tumors. PDT was given on day 14 after tumor inoculation, the peptide vaccine was mixed with CpG and administered subcutaneously in the tail-base in PBS on day 12. The fractions of mice that cleared the tumor are indicated. Survival curve statistics by LogRank X2 test. Statistical significance is indicated by asterisks: * $p<0.05$, ** $p<0.01$, *** $p<0.001$.

Discussion

In this study we suggest a novel therapeutic combination strategy for advanced metastatic cancer, consisting of PDT-mediated tumor ablation and tumor-specific peptide vaccination. In two independent aggressive tumor models we show that ablation of established tumors using Bremachlorin-PDT strongly reduces tumor burden and at the same time induces anti-tumor T cell responses, which was significantly enhanced when combined with therapeutic long peptide vaccination. Importantly, the systemic anti-tumor CD8 T cell response induced by combination treatment was essential for the therapeutic effect, and likely provided long-term protection since all cured mice did not develop a tumor after renewed injection of tumor cells at a different body site. The relevance of the systemic immune response was emphasized by the eradication of distant secondary tumors after combination therapy of primary tumors. Our combination protocol therefore meets the requirements of an efficient treatment strategy for advanced cancer that we discussed earlier: a strong anti-tumor effect to eradicate known tumors, and a lasting systemic immune response to identify possible metastatic tumor sites.

PDT, like other tumor ablation therapies, aims to strongly affect tumor cells while minimizing damage to healthy tissue. The non-toxic nature of the two individual components of PDT, the photosensitizer and the irradiation with visible light, allows precise restriction of the photodynamic effect to the target region. Pharmacokinetic optimization of photosensitizers has been aimed at a better accumulation in tumors and a faster clearance from other tissues. This has led to new generations of photosensitizers, which moreover are optimized for the use of higher wavelength irradiation light. This increases the effect range of PDT, as a higher wavelength of light penetrates deeper through tissue. The use of flexible interstitial optical fibers allows both precision irradiation of complexly localized tumors and the treatment of bulky tumor masses (13).

Several animal tumor models expressing known tumor antigens are available to study the immunological effects of PDT on an antigen-specific level; however, many concern artificially introduced model antigens such as chicken ovalbumin which have no clinical relevance (19). To overcome this limitation, a recent study used a murine mastocytoma tumor expressing P1A, the mouse homolog of human MAGE cancer/testis antigens, and showed antigen-specific immune responses against this clinically relevant tumor antigen and corresponding effects on tumor growth (37). In this study, we used two mouse tumor models expressing known epitopes from oncogenic viruses as a model for HPV- or Leukemia Virus-induced cancer in humans, and showed successful combination treatment of these tumors by PDT and peptide

vaccination. These tumor models expressing viral epitopes are of clinically relevance to a large group of cancer patients as around 15% to 20% of human cancer is estimated to be virally induced (38, 39). Importantly, the application of combination therapy using PDT and SLP vaccination may theoretically be extended to virtually any type of cancer, as was illustrated by recent studies identifying neo-epitopes in mouse tumors and subsequent successful vaccination with long peptides containing these tumor-specific neo-epitopes (5, 6).

Our findings in the TC-1 mouse model for HPV16-induced human tumors are of particular interest as PDT is currently already clinically studied in the treatment of HPV16-induced gynecological lesions (40-42). These studies used topical administration of the second-generation photosensitizer 5-ALA, and reported inefficient photosensitizer distribution through the target tissue leading to incomplete responses. The use of novel photosensitizers such as Bremachlorin may help to resolve this issue. Combination treatments of PDT and immunotherapy to improve the therapeutic effect are being investigated preclinically and clinically using non-specific immunostimulatory agents (43-45). However, tumor-specific immunotherapy such as therapeutic peptide vaccination with HPV antigens may be preferred to ensure a stronger and target-specific effect. Alternatively, to overcome the tumor-mediated immune suppression, T cell checkpoint blocking antibodies form an attractive therapeutic option for combination with PDT in order to boost the anti-tumor T cell response and relieve the immune system from suppression (46, 47). Taken together, this successful combination of systemic immunotherapy and local tumor ablation, which are independently already clinically applied, proposes an attractive clinical treatment strategy for advanced cancer.

Acknowledgements

The authors would like to thank A. Reshetnikov and H. Vink for expertise and supply of Bremachlorin photosensitizer; W. Benckhuijsen, N. Dolezal and J.W. Drijfhout for providing synthetic peptides and K. Franken for providing MHC-peptide tetramers.

References

1. Melief CJ, van der Burg SH. Immunotherapy of established (pre)malignant disease by synthetic long peptide vaccines. Nat Rev Cancer 2008;8:351-60.
2. Slingluff CL, Jr. The present and future of peptide vaccines for cancer: single or multiple, long or short, alone or in combination? Cancer J 2011;17:343-50.
3. Corradin G, Kajava AV, Verdini A. Long synthetic peptides for the production of vaccines and drugs: a technological platform coming of age. Sci Transl Med 2010;2:50rv3.
4. Tomita Y, Nishimura Y. Long peptide-based cancer immunotherapy targeting tumor antigen-specific CD4 and CD8 T cells. Oncoimmunology 2013;2:e25801.
5. Gubin MM, Zhang X, Schuster H, Caron E, Ward JP, Noguchi T, et al. Checkpoint blockade cancer immunotherapy targets tumour-specific mutant antigens. Nature 2014;515:577-81.
6. Castle JC, Kreiter S, Diekmann J, Lower M, van de Roemer N, de GJ, et al. Exploiting the mutanome for tumor vaccination. Cancer Res 2012;72:1081-91.
7. Zwaveling S, Ferreira Mota SC, Nouta J, Johnson M, Lipford GB, Offringa R, et al. Established human papillomavirus type 16-expressing tumors are effectively eradicated following vaccination with long peptides. J Immunol 2002;169:350-8.
8. Hu J, Budgeon LR, Balogh KK, Peng X, Cladel NM, Christensen ND. Long-peptide therapeutic vaccination against CRPV-induced papillomas in HLA-A2.1 transgenic rabbits. Trials Vaccinol 2014;3:134-42.
9. Zhang L, Chen J, Song X, Wen W, Li Y, Zhang Y, et al. Cancer/testis antigen HCA587-derived long peptide vaccine generates potent immunologic responses and antitumor effects in mouse model. Oncol Res 2014;21:193-200.
10. Kenter GG, Welters MJ, Valentijn AR, Lowik MJ, Berends-van der Meer DM, Vloon AP, et al. Vaccination against HPV-16 oncoproteins for vulvar intraepithelial neoplasia. N Engl J Med 2009;361:1838-47.
11. Kenter GG, Welters MJ, Valentijn AR, Lowik MJ, Berends-van der Meer DM, Vloon AP, et al. Phase I immunotherapeutic trial with long peptides spanning the E6 and E7 sequences of high-risk human papillomavirus 16 in end-stage cervical cancer patients shows low toxicity and robust immunogenicity. Clin Cancer Res 2008;14:169-77.
12. Poelgeest MI, Welters MJ, van Esch EM, Stynenbosch LF, Kerpershoek G, van Persijn van Meerten EL, et al. HPV16 synthetic long peptide (HPV16-SLP) vaccination therapy of patients with advanced or recurrent HPV16-induced gynecological carcinoma, a phase II trial. J Transl Med 2013;11:88.
13. Agostinis P, Berg K, Cengel KA, Foster TH, Girotti AW, Gollnick SO, et al. Photodynamic therapy of cancer: an update. CA Cancer J Clin 2011;61:250-81.
14. Dolmans DE, Fukumura D, Jain RK. Photodynamic therapy for cancer. Nat Rev Cancer 2003;3:380-7.
15. Garg AD, Nowis D, Golab J, Agostinis P. Photodynamic therapy: illuminating the road from cell death towards anti-tumour immunity. Apoptosis 2010;15:1050-71.
16. AD, Krysko DV, Verfaillie T, Kaczmarek A, Ferreira GB, Marysael T, et al. A novel pathway combining calreticulin exposure and ATP secretion in immunogenic cancer cell death. EMBO J 2012;31:1062-79.
17. Garg AD, Nowis D, Golab J, Vandenabeele P, Krysko DV, Agostinis P. Immunogenic cell death, DAMPs and anticancer therapeutics: an emerging amalgamation. Biochim Biophys Acta 2010;1805:53-71.
18. Korbelik M, Zhang W, Merchant S. Involvement of damage-associated molecular patterns in tumor response to photodynamic therapy: surface expression of calreticulin and high-mobility group box-1 release. Cancer Immunol Immunother 2011;60:1431-7.
19. P, Hashmi JT, Huang YY, Lange N, Hamblin MR. Stimulation of anti-tumor immunity by photodynamic therapy. Expert Rev Clin Immunol 2011;7:75-91.
20. Castano AP, Mroz P, Hamblin MR. Photodynamic therapy and anti-tumour immunity. Nat Rev Cancer 2006;6:535-45.
21. Castano AP, Liu Q, Hamblin MR. A green fluorescent protein-expressing murine tumour but not its wild-type counterpart is cured by photodynamic therapy. Br J Cancer 2006;94:391-7.
22. Mroz P, Szokalska A, Wu MX, Hamblin MR. Photodynamic therapy of tumors can lead to

development of systemic antigen-specific immune response. PLoS One 2010;5:e15194.
23. Gollnick SO, Brackett CM. Enhancement of anti-tumor immunity by photodynamic therapy. Immunol Res 2010;46:216-26.
24. Kabingu E, Oseroff AR, Wilding GE, Gollnick SO. Enhanced systemic immune reactivity to a Basal cell carcinoma associated antigen following photodynamic therapy. Clin Cancer Res 2009;15:4460-6.
25. Kabingu E, Vaughan L, Owczarczak B, Ramsey KD, Gollnick SO. CD8+ T cell-mediated control of distant tumours following local photodynamic therapy is independent of CD4+ T cells and dependent on natural killer cells. Br J Cancer 2007;96:1839-48.
26. Douillard S, Olivier D, Patrice T. In vitro and in vivo evaluation of Radachlorin(R) sensitizer for photodynamic therapy. Photochem Photobiol Sci 2009;8:405-13.
27. Douillard S, Lhommeau I, Olivier D, Patrice T. In vitro evaluation of Radachlorin sensitizer for photodynamic therapy. J Photochem Photobiol B 2010;98:128-37.
28. Uzdensky AB, Dergacheva OY, Zhavoronkova AA, Reshetnikov AV, Ponomarev GV. Photodynamic effect of novel chlorin e6 derivatives on a single nerve cell. Life Sci 2004;74:2185-97.
29. van Leeuwen-van ZF, van Driel PB, Gamm UA, Snoeks TJ, de Bruijn HS, van der Ploeg-van den Heuvel, et al. Microscopic analysis of the localization of two chlorin-based photosensitizers in OSC19 tumors in the mouse oral cavity. Lasers Surg Med 2014;46:224-34.
30. Kochneva EV, Filonenko EV, Vakulovskaya EG, Scherbakova EG, Seliverstov OV, Markichev NA, et al. Photosensitizer Radachlorin(R): Skin cancer PDT phase II clinical trials. Photodiagnosis Photodyn Ther 2010;7:258-67.
31. Ji W, Yoo JW, Bae EK, Lee JH, Choi CM. The effect of Radachlorin(R) PDT in advanced NSCLC: a pilot study. Photodiagnosis Photodyn Ther 2013;10:120-6.
32. Lin KY, Guarnieri FG, Staveley-O'Carroll KF, Levitsky HI, August JT, Pardoll DM, et al. Treatment of established tumors with a novel vaccine that enhances major histocompatibility class II presentation of tumor antigen. Cancer Res 1996;56:21-6.
33. Bae SM, Kim YW, Lee JM, NamKoong SE, Han SJ, Kim JK, et al. Photodynamic effects of Radachlorin on cervical cancer cells. Cancer Res Treat 2004;36:389-94.
34. Ljunggren HG, Karre K. Host resistance directed selectively against H-2-deficient lymphoma variants. Analysis of the mechanism. J Exp Med 1985;162:1745-59.
35. van Duikeren S, Fransen MF, Redeker A, Wieles B, Platenburg G, Krebber WJ, et al. Vaccine-induced effector-memory CD8+ T cell responses predict therapeutic efficacy against tumors. J Immunol 2012;189:3397-403.
36. Ossendorp F, Mengede E, Camps M, Filius R, Melief CJ. Specific T helper cell requirement for optimal induction of cytotoxic T lymphocytes against major histocompatibility complex class II negative tumors. J Exp Med 1998;187:693-702.
37. Mroz P, Vatansever F, Muchowicz A, Hamblin MR. Photodynamic therapy of murine mastocytoma induces specific immune responses against the cancer/testis antigen P1A. Cancer Res 2013;73:6462-70.
38. zur Hausen H. Viruses in human cancers. Science 1991;254:1167-73.
39. Javier RT, Butel JS. The history of tumor virology. Cancer Res 2008;68:7693-706.
40. Stern PL, van der Burg SH, Hampson IN, Broker TR, Fiander A, Lacey CJ, et al. Therapy of human papillomavirus-related disease. Vaccine 2012;30 Suppl 5:F71-F82.
41. Martin-Hirsch PL, Whitehurst C, Buckley CH, Moore JV, Kitchener HC. Photodynamic treatment for lower genital tract intraepithelial neoplasia. Lancet 1998;351:1403.
42. Soergel P, Hillemanns P. Photodynamic therapy for intraepithelial neoplasia of the lower genital tract. Photodiagnosis Photodyn Ther 2010;7:10-4.
43. Park EK, Bae SM, Kwak SY, Lee SJ, Kim YW, Han CH, et al. Photodynamic therapy with recombinant adenovirus AdmIL-12 enhances anti-tumour therapy efficacy in human papillomavirus 16 (E6/E7) infected tumour model. Immunology 2008;124:461-8.
44. Winters U, Daayana S, Lear JT, Tomlinson AE, Elkord E, Stern PL, et al. Clinical and immunologic results of a phase II trial of sequential imiquimod and photodynamic therapy for vulval intraepithelial neoplasia. Clin Cancer Res 2008;14:5292-9.
45. Bae SM, Kim YW, Kwak SY, Kim YW, Ro DY, Shin JC, et al. Photodynamic therapy-generated tumor cell lysates with CpG-oligodeoxynucleotide enhance immunotherapy efficacy in human papillomavirus 16 (E6/E7) immortalized tumor cells. Cancer Sci 2007;98:747-52.

46. Castano AP, Mroz P, Wu MX, Hamblin MR. Photodynamic therapy plus low-dose cyclophosphamide generates antitumor immunity in a mouse model. Proc Natl Acad Sci U S A 2008;105:5495-500.
47. Mroz P, Hamblin MR. The immunosuppressive side of PDT. Photochem Photobiol Sci 2011;10:751-8.

Supplementary Information

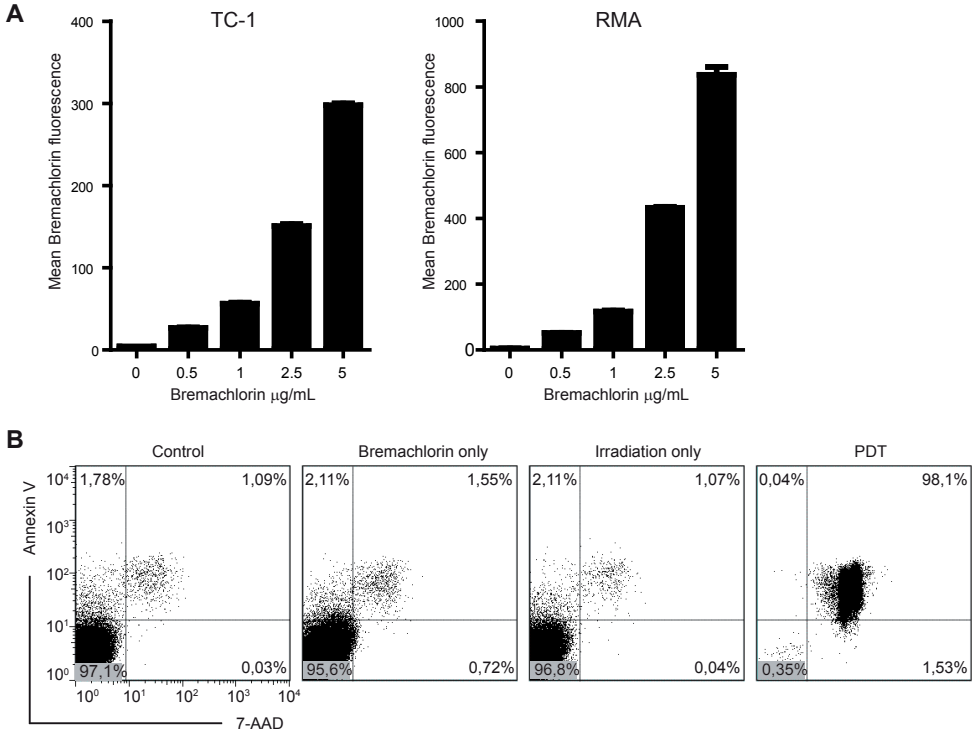

Figure S1. Efficient photosensitizer uptake enables specific killing following laser irradiation. (A) Flow cytometry of Bremachlorin fluorescence on TC-1 tumor cells incubated with different concentrations of Bremachlorin for 3 hours at 37°C. **(B)** Flow cytometry plots showing Annexin V and 7-AAD staining of TC-1 tumor cells 16 hours after in vitro PDT treatment. Cells were incubated with 1 μg/mL Bremachlorin for 3 hours, which had shown to give high cellular uptake, and irradiated for 2 minutes. Control samples were untreated cells, photosensitizer-only or irradiation-only cells. Representative plots of 3 experiments.

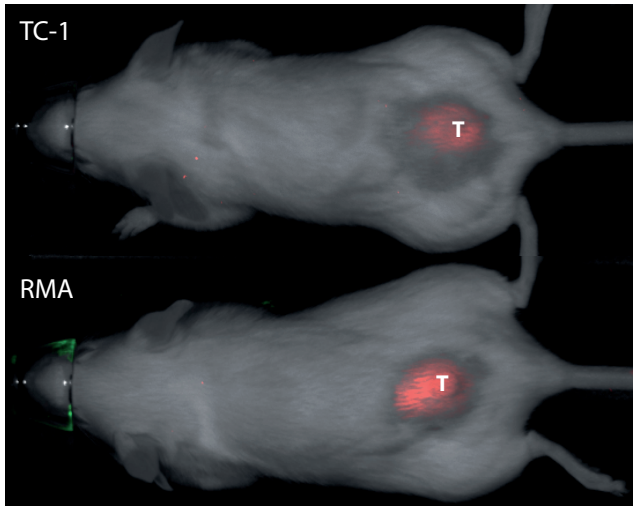

Figure S2. Bremachlorin photosensitizer accumulates in tumors. In vivo imaging of Bremachlorin fluorescence 6 hours after injection of 20 mg/kg Bremachlorin in Albino B6 mice bearing subcutaneous TC-1 or RMA tumors. Bremachlorin fluorescence in the 700 nm emission filter is represented by the red color, the tumor is indicated by a white 'T'. Representative pictures from 4 mice per tumor model.

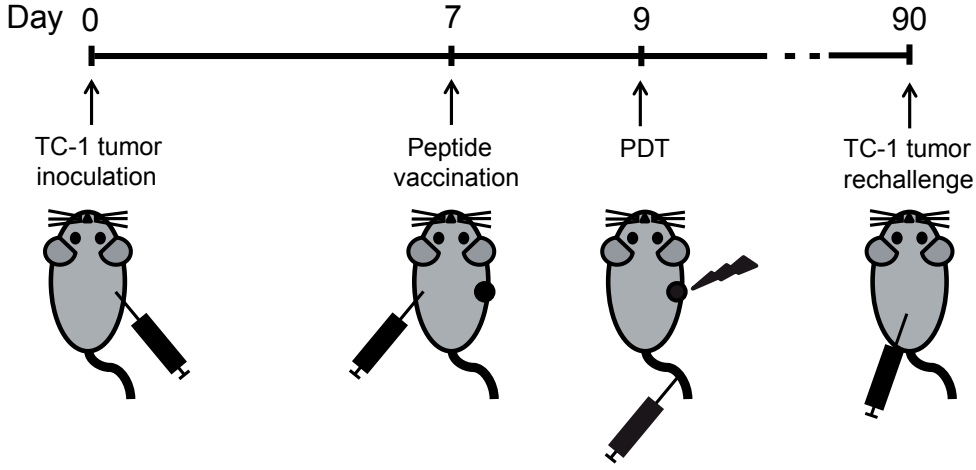

Figure S3. Graphical overview of the experimental setup in the TC-1 tumor model. The setup of the experiments using the TC-1 tumor model (single-tumor setting) is shown on a timescale starting with tumor inoculation at day 0.

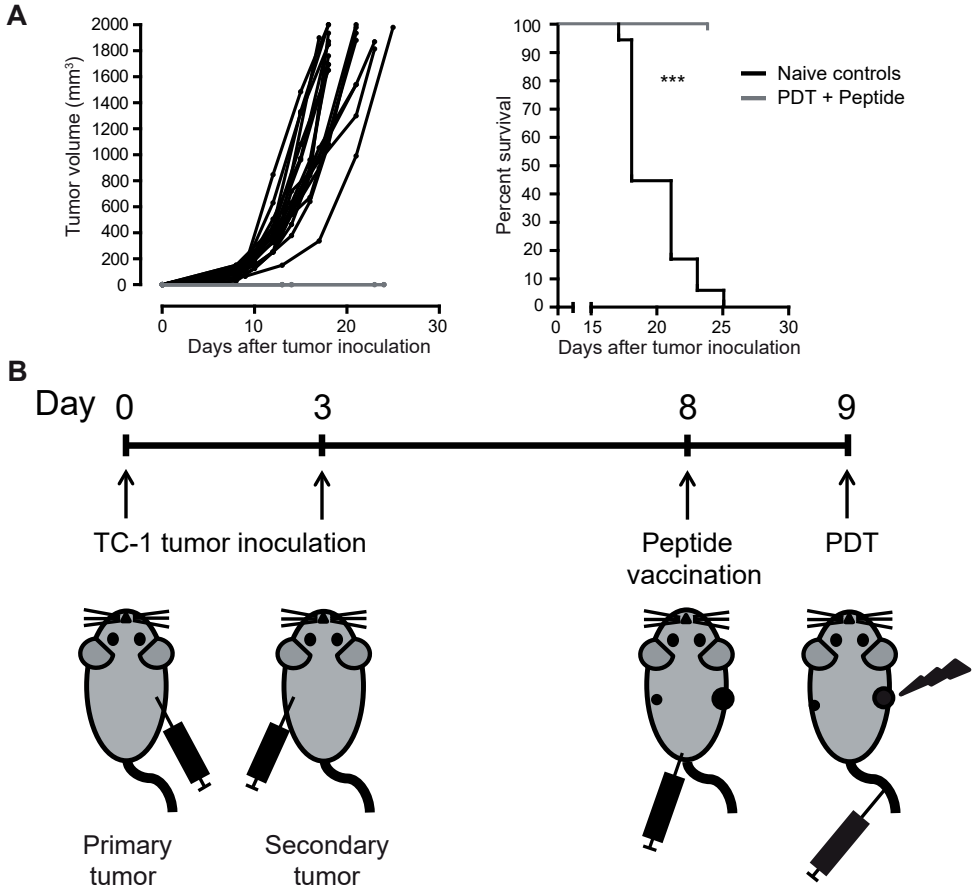

Figure S4. TC-1 tumor rechallenge and metastasis model. (A) Tumor outgrowth and survival curves after TC-1 tumor challenge in mice cured from their TC-1 tumor by combination therapy of PDT and peptide vaccination, compared to naïve control mice. Pooled data from 3 independent experiments, 13-18 mice per group. Survival curve statistics by LogRank X^2 test, statistical significance *** = $p<0.001$. **(B)** The experimental setup of the TC-1 metastasis model is shown on a timescale starting with inoculation of the primary tumor at day 0. Mice were inoculated with TC-1 tumor cells in both flanks followed by systemic peptide vaccination and PDT of only the primary tumor.

Chapter 3

Photodynamic-immune checkpoint therapy eradicates local and distant tumors by CD8 T cells

Jan Willem Kleinovink, Marieke F. Fransen, Clemens W. Löwik, Ferry Ossendorp

Cancer Immunology Research (2017) Oct;5(10):832-838

Abstract

Photodynamic Therapy (PDT) is a clinically applied tumor ablation method that reduces tumor burden and may induce T cell responses, forming an attractive therapeutic option for mutated tumors. In this study, we applied PDT in two mouse tumor models and assessed its effect on outgrowth of PDT-treated and distant untreated tumors. PDT of established tumors resulted in complete tumor eradication in the majority of mice, which were then protected against tumor re-challenge. Correspondingly, the therapeutic effect was abrogated upon systemic depletion of CD8 T cells, indicating PDT-induced tumor antigen cross-presentation and T cell activation. In a double-tumor model, PDT of primary tumors induced enhanced infiltration of untreated distant tumors by CD8 T cells, which significantly delayed their outgrowth. Combination therapy of PDT and CTLA-4 blocking antibodies significantly improved therapeutic efficacy and survival of double-tumor-bearing mice. These results show that local tumor ablation by PDT induces CD8 T cell responses crucial for systemic tumor eradication, which can be further enhanced by combination with immune checkpoint blockade. This combination of two clinically applied therapies may be a novel treatment strategy for advanced cancer without previous knowledge of tumor-specific antigens.

Introduction

Clinically apparent cancers often evade immune eradication and progress despite the presence of anti-tumor T cell responses (1). Immune evasion of tumors can be achieved through the formation of immunosuppressive tumor microenvironment including chronic exposure of T cells to cognate antigen. Based on the expression of immune checkpoint molecules such as PD-1 and CTLA-4 on functionally impaired tumor-infiltrating T cells, preclinical and clinical studies using PD-1 or CTLA-4 blocking antibodies have shown impressive results (2). However, there is considerable variation in individual responsiveness to immune checkpoint blockade, as some patients show durable tumor regression while others fail to respond to therapy (3–5). Combination strategies may improve clinical outcome, either by blocking multiple immune checkpoints or by combining immunotherapy with tumor-ablating therapies such as chemotherapy, radiotherapy or Photodynamic Therapy (PDT) (6,7). PDT is an attractive approach due to its strongly localized and non-mutagenic nature of tumor cell killing, minimizing adverse effects of therapy (8). PDT of cancer consists of localized activation of a light-sensitive photosensitizer by exposure of the tumor to visible light. Besides merely reducing tumor burden, the resulting massive tumor cell death triggers strong acute inflammation involving the influx of neutrophils and macrophages (9). Moreover, dying tumor cells can serve as source of tumor antigen and immunogenic factors able to induce or enhance tumor-specific T cell responses, which may strongly enhance the therapeutic effect (10,11). In a previous study, we showed that combination of PDT and specific peptide vaccination induced CD8 T cell responses against tumor antigens resulting in the clearance of both treated and distant untreated tumors (12). Therefore, the curative potential PDT may be superior in immunogenic tumor models in which tumor-specific T cells are present but unable to clear the tumor, mimicking a common clinical situation. In this study, we apply Bremachlorin-based PDT to MC38 and CT26 tumors, two mutated mouse tumors syngeneic to the C57BL/6 and BALB/c mouse strains, respectively. PDT treatment of established tumors resulted in complete tumor clearance dependent on CD8 T cells, which could also control outgrowth of distant untreated tumors. In a double-tumor setting, PDT of primary tumors combined with systemic CTLA-4 blockade significantly reduced the tumor burden in both MC38 and CT26 tumor models. Our findings show the immunogenic and curative potential of PDT in mutated tumors, and a potent combination treatment for advanced cancer.

Materials and Methods

Mice and tumor cell lines

C57BL/6 mice were obtained from Harlan Laboratories - ENVIGO (The Netherlands) and BALB/c mice were purchased from Charles River (France) and housed under specified pathogen-free conditions in the animal facility of the Leiden University Medical Center. All animal experimentations were approved by and according to guidelines of Dutch Animal Ethical committee. MC38 and CT26 cells (kindly provided by Mario Colombo) were cultured as described elsewhere (13). Cell lines were mycoplasma and MAP-tested before the start of experiments. For tumor inoculation, 500,000 tumor cells in 100 µL PBS were injected subcutaneously in the right flank or both flanks of the mice. In double-tumor experiments, the largest tumor on day 8 was designated primary tumor. Tumor volume was measured 3 times per week by caliper and calculated as length*width*height. Survival curves are based on the moment of sacrificing the mice upon reaching the maximally allowed tumor volume of 2000 mm3.

Photodynamic Therapy

Tumors were treated 8 days after inoculation, both at an average tumor diameter of 5 mm. Photodynamic Therapy was performed as described previously (12). In short, 20 mg/kg Bremachlorin photosensitizer (RadaPharma International) was injected intravenously, followed after 6 hours by irradiation of the tumor for 1000 seconds at 116 mW/cm² (total energy 116 J/cm²) using a 662 nm Milon Lakhta laser.

Anti-CTLA-4 antibody treatment

Antagonistic CTLA-4 blocking antibody (clone 9D9, BioXCell) was administered intraperitoneally on days 7, 10 and 14 after tumor inoculation, using 200 µg dissolved in 200 µL PBS per treatment.

T cell depletion

Depleting CD8 antibody (clone 2.43) and depleting CD4 antibody (clone GK1.5) were produced in-house using hybridomas. To deplete T cells, mice received an intraperitoneal injection of 50 µg depleting antibodies the day before treatment, followed by additional injections of 50 µg antibody when periodical screening showed return of the targeted T cell population in systemic blood. All control mice received in parallel similar amounts of isotype control rat immunoglobulin G.

Flow cytometry

Ex vivo tumor analysis was performed as described elsewhere (13). In short, single-cell suspensions of harvested tumors were stained with cell-surface markers, measured on a LSRII cytometer (BD) analyzed with FlowJo software (Tree Star).

Statistical analysis

Statistical analysis was performed using GraphPad Prism version 6.0 software. Data are shown as the mean ± SEM for each group, and comparison of groups was performed by two-tailed Student's t-test or Mann-Whitney U test depending on normality of data distribution. Survival curves were compared using the LogRank Mantel-Cox test. Statistical differences were considered significant at $p < 0.05$.

Results

Curative tumor ablation by Photodynamic Therapy (PDT) depends on CD8 T cells

We applied PDT using the photosensitizer Bremachlorin to C57BL/6 mice bearing established subcutaneous MC38 tumors and followed tumor outgrowth. Strikingly, whereas tumors in untreated mice grew out progressively, a single PDT treatment caused strong and durable tumor regression in all mice (**Figure 1a**, solid lines). As we previously observed in less immunogenic models that PDT was only curative when combined with specific induction of anti-tumor CD8 T cells, we analyzed whether the clearance of MC38 tumors by PDT monotherapy was mediated by CD8 T cells by injecting antibodies depleting CD8 T cells systemically (12). In the absence of CD8 T cells, initial tumor regression upon PDT remained intact but tumors eventually grew out. This suggests that tumor ablation by PDT works independently of CD8 T cells, whereas CD8 T cells are crucial in subsequent tumor clearance and prevention of tumor regrowth (**Figure 1a** and **Supplementary Figure S1**).

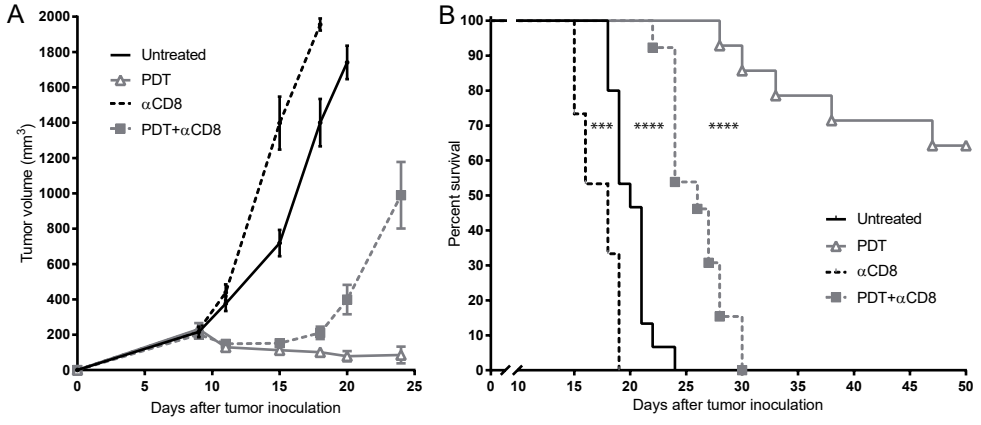

Figure 1. Curative tumor ablation by Photodynamic Therapy depends on CD8 T cells. Tumor outgrowth curves **(A)** and survival curves **(B)** of mice bearing subcutaneous MC38 tumors treated by Photodynamic Therapy (PDT) in the presence or absence of CD8 T cells, plus corresponding control groups. PDT was given on day 8 by injection of Bremachlorin photosensitizer followed after 6 hours by tumor illumination. CD8 T cells were depleted by antibodies injected periodically from day 7 until mice were sacrificed or tumor-free. Survival is defined by the time until tumor size reached the maximally allowed volume of 2000 mm³ according to local legislation. Survival differences were statistically significant by Log-Rank test: Untreated vs PDT $p<0.0001$, PDT vs PDT+αCD8 $p<0.0001$, Untreated vs αCD8 $p<0.001$, Untreated vs PDT+αCD8 $p<0.0001$. Pooled data of 2 independent experiments, 13-15 mice per group.

Consequently, PDT treatment cured the majority of mice bearing MC38 tumors resulting in significantly improved long-term survival, which was fully abrogated when CD8 T cells were depleted (**Figure 1b**). Interestingly, untreated tumors also grew out faster in the absence of CD8 T cells, suggesting that growth control of untreated tumors is mediated by CD8 T cells. Instead, depletion of CD4 T cells resulted in slower growth of untreated tumors and enhanced clearance of PDT-treated tumors, suggesting a suppressive role of CD4+ regulatory T cells (**Supplementary Figure S1**). All cured mice were protected against developing new tumors when new MC38 tumor cells were injected in the contralateral flank long after tumor clearance, suggesting the formation of immunological memory (**Supplementary Figure S2**). In summary, a single PDT treatment can fully eradicate established tumors involving CD8 T cell responses.

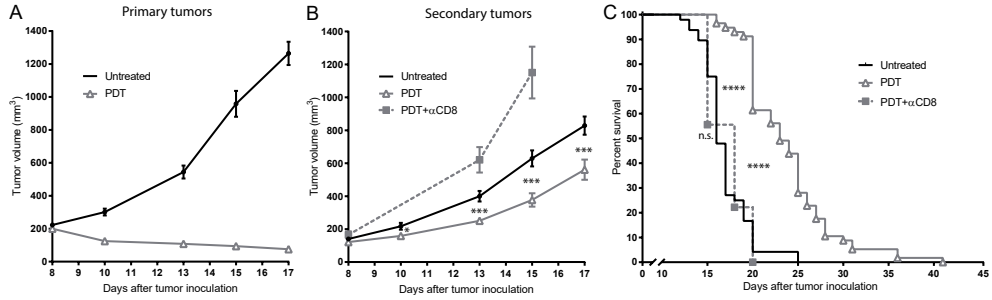

Figure 2. Local PDT induces systemic T cell responses inhibiting distant tumor growth. Primary **(A)** and secondary **(B)** tumor outgrowth curves and **(C)** survival curves of double MC38 tumor-bearing mice in which the primary tumor was left untreated or PDT-treated in the presence or absence of CD8 T cells. PDT was given on day 8 by injection of Bremachlorin photosensitizer followed after 6 hours by tumor illumination. CD8 T cells were depleted by antibodies injected periodically from day 7 until mice were sacrificed or tumor-free. Survival is defined by the time until tumor size reached the maximally allowed volume of 2,000 mm³ according to local legislation. Statistical significance of differences in secondary tumor volume (B) of untreated vs. PDT-treated mice was determined by t test (days 10 and 15) or Mann–Whitney U test (days 13 and 17). Statistical significance of survival differences (C) was determined by the log-rank test. N.s., not significant; * $p<0.05$ and *** $p<0.0001$. Pooled data of 6 independent experiments, 48–57 mice per group.

Local PDT induces systemic T cell responses inhibiting distant tumor growth

The induction of CD8 T cell responses and their involvement in tumor clearance suggests that T cells may circulate systemically and target untreated tumors growing at distant sites. We inoculated mice with MC38 tumor cells in both flanks and treated the largest tumor with PDT, following the outgrowth of both tumors in time. Also in the double tumor setting, PDT-treated tumors regressed and were cleared (**Figure 2a**). Moreover, untreated tumors grew significantly slower if the contralateral tumor received PDT treatment, an effect that was completely abrogated when CD8 T cells were systemically depleted (**Figure 2b**). Individual tumor outgrowth curves are shown in Supplementary Figure S3a-d. Altogether, local PDT caused clearance of treated tumors and delayed the growth of distant tumors, dramatically prolonging survival of double tumor-bearing mice (**Figure 2c**). Analysis of distant tumors 6 days after PDT of contralateral primary tumors showed an increased infiltration

of activated CD8 T cells compared to untreated mice, suggesting that CD8 T cells directly mediate the abscopal effect of local PDT (**Supplementary Figure S3e,f**). Together, these data indicate that local curative PDT triggers a CD8 T cell-dependent effect on untreated distant tumors.

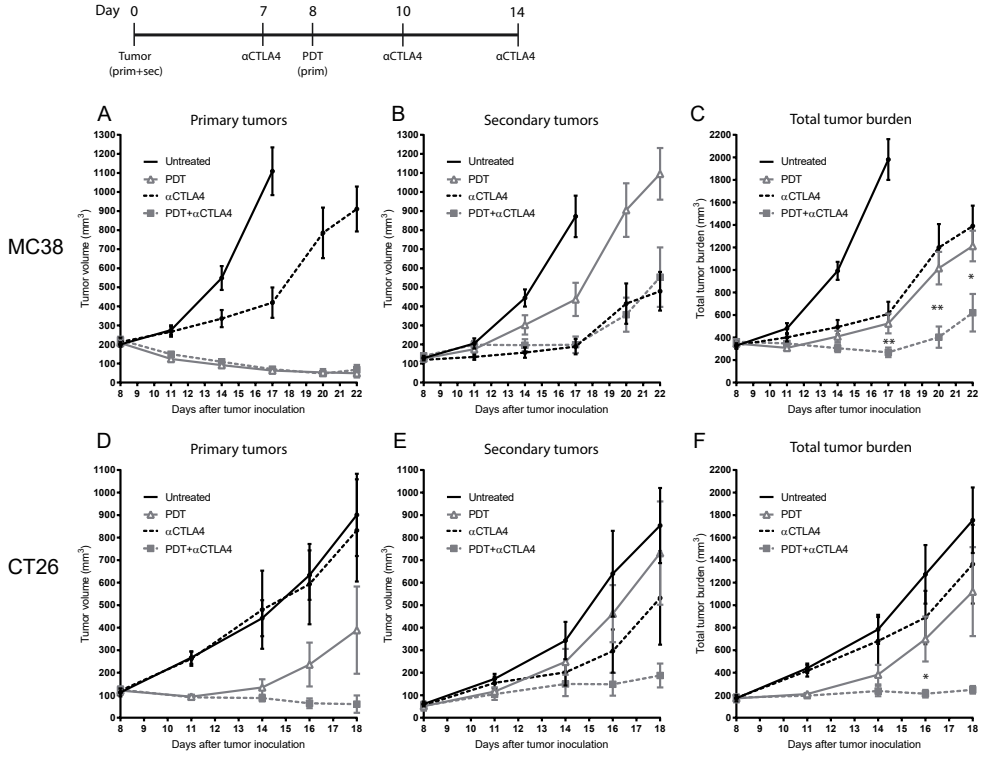

Figure 3. Efficient treatment of local and distant tumors by combined local PDT and systemic CTLA-4 blockade. Tumor growth curves. Primary tumors **(A)**, secondary tumors **(B)**, and total tumor **(C)** burden for mice bearing two MC38 tumors. Primary tumors **(D)**, secondary tumors **(E)**, and total tumor burden **(F)** for mice bearing two CT26 tumors. Mice received PDT of primary tumors on day 8, systemic CTLA-4 blocking antibody on days 7+10+14, both therapies, or were left untreated. Mann–Whitney U test (MC38 model) and t test (CT26 model) were used to determine statistical significance of differences in total tumor burden of mice receiving PDT+aCTLA-4 combination therapy compared with PDT or aCTLA-4 monotherapy. * $p<0.05$ and ** $p<0.01$. Pooled data of 2 independent experiments, 14–16 mice per group.

Efficient treatment of local and distant tumors by combined local PDT and systemic CTLA-4 blockade

As local PDT treatment slowed down the growth of distant tumors via CD8 T cells but did not fully clear them, we analyzed whether enhancing the PDT-induced CD8 T cell response by immune checkpoint blockade would enable double tumor eradication. Therefore, we treated double MC38 tumor-bearing mice with PDT of one tumor and provided systemic CTLA-4 blockade during the treatment phase. Whereas local PDT again affected the treated primary tumor much more strongly than the untreated secondary tumor, systemic CTLA-4 blockade caused a much

more pronounced growth delay of the smaller secondary tumors (**Figure 3a,b**). Combination treatment with PDT and CTLA-4 blockade combined the strong respective effects of each treatment on both tumors, and significantly reduced total tumor burden compared to either monotherapy (**Figure 3c**). Next, we also analyzed combination of PDT and CTLA-4 blockade in the more aggressively growing CT26 tumor model in BALB/c mice. Both PDT and CTLA-4 monotherapies were less efficient in delaying the growth of primary or secondary CT26 tumors compared to their effects on MC38 tumors. However, combination treatment significantly reduced CT26 tumor burden compared to either single treatment (**Figure 3d-f**). A comparison of the effects of each treatment on primary and secondary MC38 or CT26 tumors is provided in Supplementary Figure 4. This treatment strategy provides efficient combination of local tumor-destructive therapy with systemic immunomodulation in two independent tumor models.

Long-term survival after combined PDT and CTLA-4 blockade depends on CD8 T cells

Both PDT and CTLA-4 blockade as monotherapies significantly reduced MC38 tumor burden and increased survival time of double MC38 tumor-bearing mice (**Figure 4a**). The significantly lower tumor burden after combined treatment by PDT and CTLA-4 blockade resulted in a significantly further extended survival of all mice and clearance of both tumors in 20% of the mice (**Figure 4a**). A depletion experiment of CD8 T cells showed that the enhanced efficacy of combined PDT and CTLA-4 blockade is dependent on the systemic presence of CD8 T cells, as the combined treatment effect is fully lost in the absence of CD8 T cells, reducing survival to the level of untreated mice (**Figure 4b**).

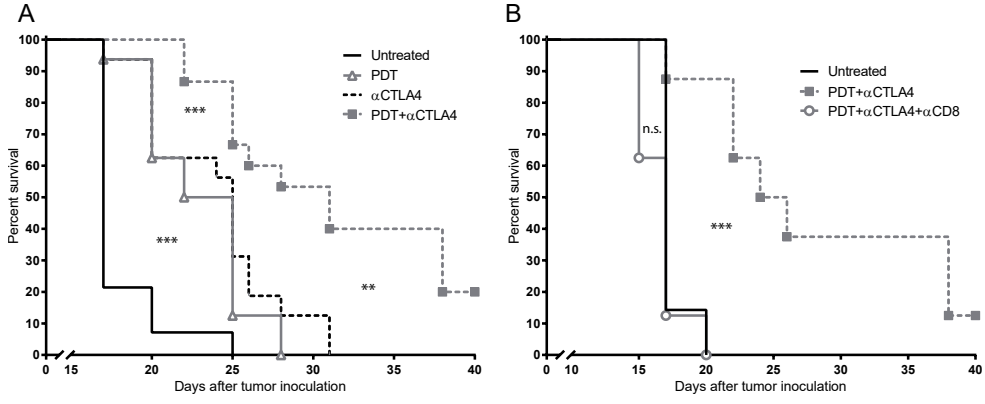

Figure 4. Long-term survival after combined PDT and CTLA-4 blockade depends on CD8 T cells. Long-term survival after combined PDT and CTLA-4 blockade depends on CD8 T cells. **(A)** Survival curves of double MC38 tumor–bearing mice receiving either PDT of primary tumors on day 8, systemic CTLA-4 blocking antibody on days 7+10+14, both therapies, or left untreated. **(B)** Survival curves of double MC38 tumor–bearing mice left untreated or receiving PDTþaCTLA-4 combination therapy with or without CD8 T-cell depletion on day 7. Survival is defined by the time until tumor size reached the maximally allowed volume of 2,000 mm³ according to local legislation. The log-rank test was used to determine significance. ** p<0.01 and *** p<0.001. Pooled data of 2 independent experiments, 14–16 mice per group.

Discussion

In this study, we show that Photodynamic Therapy (PDT) of mouse colon carcinoma tumors mediated strong tumor ablation and eradication by CD8 T cells, which also delayed distant tumor growth. This provides evidence that local tumor ablation can lead to systemically active T cell responses, likely by enhanced cross-presentation of tumor antigens by local dendritic cells and the immunostimulatory effects of PDT-induced cell death (10). Our data add to a growing body of evidence that local tumor destruction can delay the growth of identical tumors growing in other sites of the body, and stress the induction of systemic immune responses as the crucial mechanism. These tumor-specific systemic effects of local therapy, also known as the abscopal effect, have been described in several localized ablation therapies (14,15). The advent of modern immunomodulatory antibodies has triggered a range of protocols combining local tumor ablation with immune checkpoint blockade (16–18). A study combining local radiotherapy with immunomodulatory antibodies indicated that the enhanced therapeutic efficacy was mediated by tumor antigen cross-presentation by dendritic cells to CD8 T cells (19). Recent studies reported enhanced systemic efficacy of PDT combined with immune checkpoint blockade using experimental setups involving surgical resection of PDT-treated tumors or advanced nanocarrier systems (20–22). Here, we combined local PDT with systemic CTLA-4 blockade in two independent tumor models to improve the therapeutic outcome in double tumor-bearing mice. The efficacy of immunomodulatory antibodies such as CTLA-4 blockade is often largely determined by tumor size at the start of treatment. In our double-tumor models, CTLA-4 blockade indeed affected smaller secondary tumors more strongly than the bigger primary tumors, while PDT obviously affected the PDT-treated tumor more strongly. The increased efficacy of combination therapy in our double-tumor experiments may therefore be explained by the combining the strengths of each individual treatment. In addition, CTLA4 blockade has been shown to specifically deplete tumor-infiltrating regulatory T cells in several tumor models, including MC38 and CT26, favoring the subsequent expansion of intratumoral effector CD8 T cells (23,24). In a preclinical study using depletion of regulatory T cells by low-dose cyclophosphamide in the context of PDT treatment, increased anti-tumor immune responses were observed (25). These findings, suggesting a suppressive role of regulatory T cells that dampen the PDT-induced T cell response, may further explain the superior efficacy of combined PDT and CTLA4 blockade as described in this study. We have previously reported on combination therapy of PDT and specific peptide vaccination, in which PDT-induced T cell responses were further enhanced by peptide vaccination, allowing eradication of local and distant tumors (12). Combinations of PDT with specific immunotherapy

allow efficient treatment of tumors of which the antigenic profile is known, such as Human Papillomavirus (HPV)-induced gynecological and head/neck tumors expressing known HPV antigens. Here, we introduce combination therapy of PDT and CTLA-4 blockade as a more broadly applicable therapeutic option without the need to have identified the antigens expressed by the tumor. Photodynamic therapy is already clinically applied in the treatment of various tumors including HPV-induced cancer, skin tumors and gastrointestinal malignancies. CTLA-4 blockade has been approved for use in melanoma and undergoes clinical trials for several other types of human cancer, based on promising results in preclinical studies. Combinations of PDT and CTLA-4 blockade can therefore be smoothly introduced into clinical practice and may be applied to a wide variety of human cancer types.

Acknowledgements

The authors would like to thank Harrie Vink, Henk Schaminée, Toon Zeegers and Geert Haasnoot for their support.

References

1. Rosenberg SA, Sherry RM, Morton KE, Scharfman WJ, Yang JC, Topalian SL, et al. Tumor progression can occur despite the induction of very high levels of self/tumor antigen-specific CD8+ T cells in patients with melanoma. J Immunol. 2005 Nov 1;175(9):6169–76.
2. Pardoll DM. The blockade of immune checkpoints in cancer immunotherapy. Nat Rev Cancer. 2012 Mar 22;12(4):252–64.
3. Hodi FS, O'Day SJ, McDermott DF, Weber RW, Sosman JA, Haanen JB, et al. Improved survival with ipilimumab in patients with metastatic melanoma. N Engl J Med. 2010 Aug 19;363(8):711–23.
4. Topalian SL, Hodi FS, Brahmer JR, Gettinger SN, Smith DC, McDermott DF, et al. Safety, Activity, and Immune Correlates of Anti–PD-1 Antibody in Cancer. N Engl J Med. 2012 Jun 28;366(26):2443–54.
5. Postow MA, Callahan MK, Wolchok JD. Immune Checkpoint Blockade in Cancer Therapy. J Clin Oncol. 2015 Jun 10;33(17):1974–82.
6. Callahan MK, Postow MA, Wolchok JD. CTLA-4 and PD-1 Pathway Blockade: Combinations in the Clinic. Front Oncol. 2014;4:385.
7. Drake CG. Combination immunotherapy approaches. Ann Oncol. 2012 Sep 1;23(suppl 8):viii41-viii46.
8. Ibbotson SH. Adverse effects of topical photodynamic therapy. Photodermatol Photoimmunol Photomed. 2011 Jun;27(3):116–30.
9. Agostinis P, Berg K, Cengel KA, Foster TH, Girotti AW, Gollnick SO, et al. Photodynamic therapy of cancer: An update. CA Cancer J Clin. 2011 Jul;61(4):250–81.
10. Mroz P, Hashmi JT, Huang Y-Y, Lange N, Hamblin MR. Stimulation of anti-tumor immunity by photodynamic therapy. Expert Rev Clin Immunol. 2011 Jan 10;7(1):75–91.
11. Mroz P, Szokalska A, Wu MX, Hamblin MR, Theoret M. Photodynamic Therapy of Tumors Can Lead to Development of Systemic Antigen-Specific Immune Response. Mosley RL, editor. PLoS One. 2010 Dec 10;5(12):e15194.

12. Kleinovink JW, Van Driel PB, Snoeks TJ, Prokopi N, Fransen MF, Cruz LJ, et al. Combination of photodynamic therapy and specific immunotherapy efficiently eradicates established tumors. Clin Cancer Res. 2016 Mar 15;22(6):1459–68.
13. Kleinovink JW, Marijt KA, Schoonderwoerd MJA, van Hall T, Ossendorp F, Fransen MF. PD-L1 expression on malignant cells is no prerequisite for checkpoint therapy. Oncoimmunology. 2017 Apr 3;6(4):e1294299.
14. Bastianpillai C, Petrides N, Shah T, Guillaumier S, Ahmed HU, Arya M. Harnessing the immunomodulatory effect of thermal and non-thermal ablative therapies for cancer treatment. Tumor Biol. 2015 Dec 30;36(12):9137–46.
15. Formenti SC, Demaria S. Systemic effects of local radiotherapy. Lancet Oncol. 2009 Jul;10(7):718–26.
16. Sharabi AB, Nirschl CJ, Kochel CM, Nirschl TR, Francica BJ, Velarde E, et al. Stereotactic Radiation Therapy Augments Antigen-Specific PD-1-Mediated Antitumor Immune Responses via Cross-Presentation of Tumor Antigen. Cancer Immunol Res. 2015 Apr 1;3(4):345–55.
17. Waitz R, Solomon SB, Petre EN, Trumble AE, Fasso M, Norton L, et al. Potent Induction of Tumor Immunity by Combining Tumor Cryoablation with Anti-CTLA-4 Therapy. Cancer Res. 2012 Jan 15;72(2):430–9.
18. Belcaid Z, Phallen JA, Zeng J, See AP, Mathios D, Gottschalk C, et al. Focal radiation therapy combined with 4-1BB activation and CTLA-4 blockade yields long-term survival and a protective antigen-specific memory response in a murine glioma model. PLoS One. 2014;9(7):1–9.
19. Rodriguez-Ruiz ME, Rodriguez I, Garasa S, Barbes B, Solorzano JL, Perez-Gracia JL, et al. Abscopal effects of radiotherapy are enhanced by combined immunostimulatory mAbs and are dependent on CD8 T cells and crosspriming. Cancer Res. 2016;137(8):canres.0549.2016.
20. Gao L, Zhang C, Gao D, Liu H, Yu X, Lai J, et al. Enhanced anti-tumor efficacy through a combination of integrin ??v??6-targeted photodynamic therapy and immune checkpoint inhibition. Theranostics. 2016;6(5):627–37.
21. He C, Duan X, Guo N, Chan C, Poon C, Weichselbaum RR, et al. Core-shell nanoscale coordination polymers combine chemotherapy and photodynamic therapy to potentiate checkpoint blockade cancer immunotherapy. Nat Commun. 2016 Aug 17;7:12499.
22. Duan X, Chan C, Guo N, Han W, Weichselbaum RR, Lin W. Photodynamic Therapy Mediated by Nontoxic Core–Shell Nanoparticles Synergizes with Immune Checkpoint Blockade To Elicit Antitumor Immunity and Antimetastatic Effect on Breast Cancer. J Am Chem Soc. 2016 Dec 28;138(51):16686–95.
23. Simpson TR, Li F, Montalvo-Ortiz W, Sepulveda MA, Bergerhoff K, Arce F, et al. Fc-dependent depletion of tumor-infiltrating regulatory T cells co-defines the efficacy of anti?CTLA-4 therapy against melanoma. J Exp Med. 2013 Aug 26;210(9):1695–710.
24. Selby MJ, Engelhardt JJ, Quigley M, Henning KA, Chen T, Srinivasan M, et al. Anti-CTLA-4 antibodies of IgG2a isotype enhance antitumor activity through reduction of intratumoral regulatory T cells. Cancer Immunol Res. 2013;1(1):32–42.
25. Reginato E, Mroz P, Chung H, Kawakubo M, Wolf P, Hamblin MR. Photodynamic therapy plus regulatory T-cell depletion produces immunity against a mouse tumour that expresses a self-antigen. Br J Cancer. 2013;109(8):2167–74.

Supplementary Information

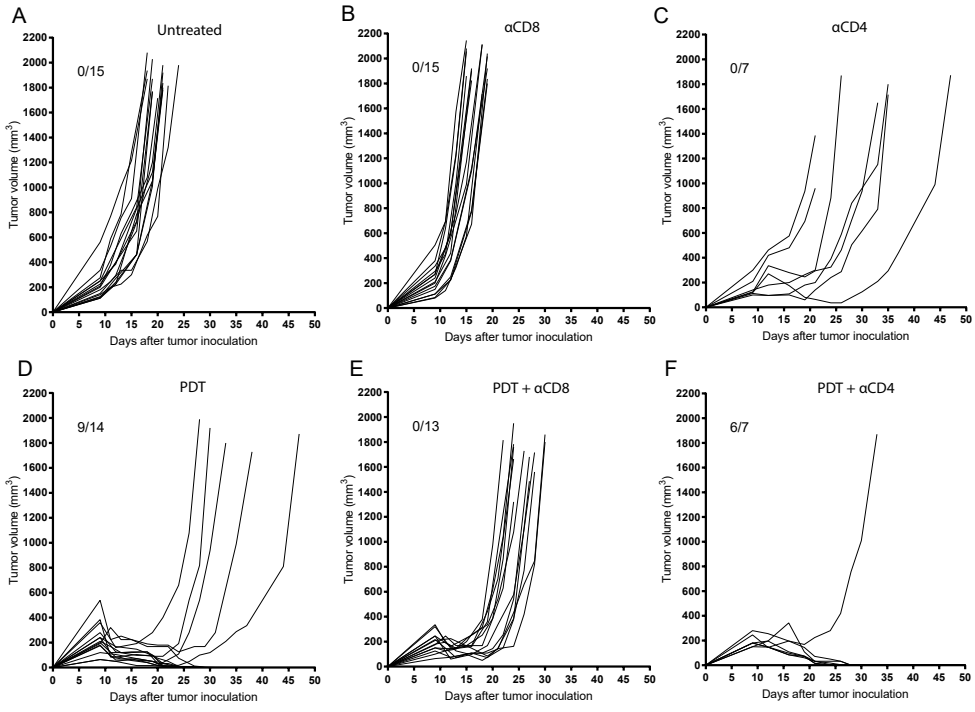

Supplementary Figure S1. Curative tumor ablation by Photodynamic Therapy depends on CD8 T cells. Tumor outgrowth curves of individual mice bearing subcutaneous MC38 tumors treated by Photodynamic Therapy (PDT) in the presence of T cells or with CD8 or CD4 T cell depletion (αCD8, αCD4). PDT was given on day 8 by injection of Bremachlorin photosensitizer followed after 6 hours by tumor illumination. T cells were depleted by antibodies injection on day 7 to assure complete absence of T cells until mice were sacrificed or tumor-free. The number of cured mice is indicated by fractions.

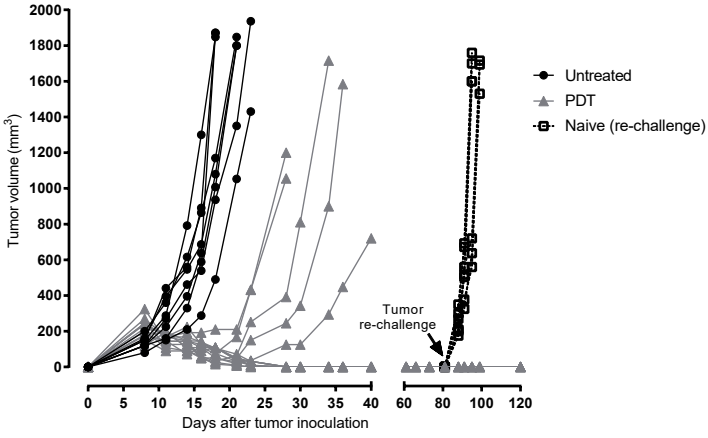

Supplementary Figure S2. Mice cured by PDT are protected against tumor rechallenge. Tumor outgrowth curves of untreated and PDT-treated MC38 tumor-bearing mice. PDT-cured mice (8 out of 13) and naïve control mice were injected with new MC38 tumor cells on day 80 and tumor outgrowth was monitored. All 8 mice remained tumor-free.

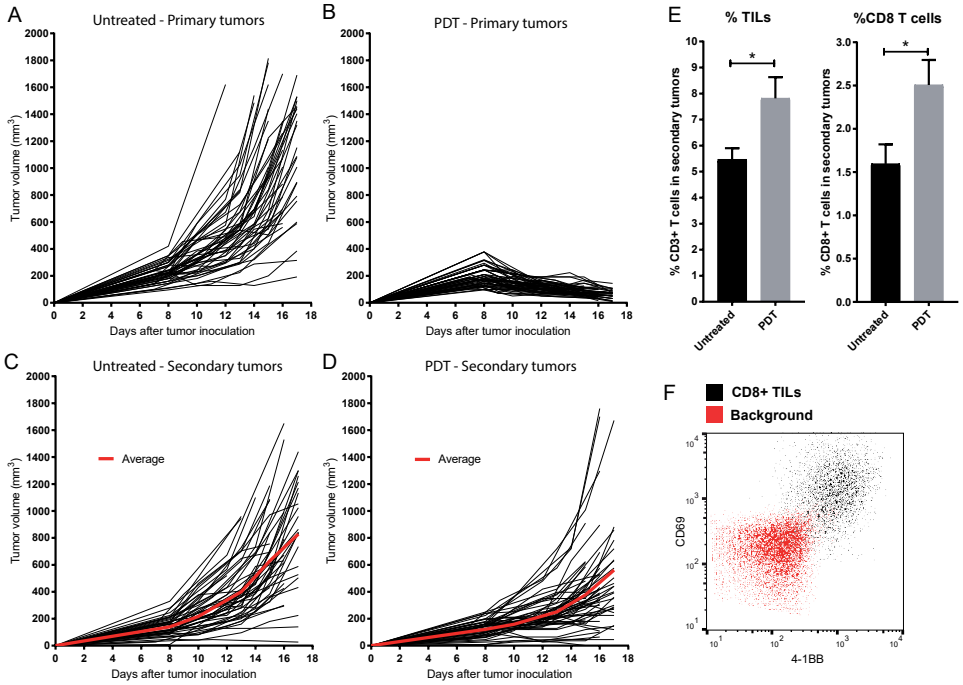

Supplementary Figure S3. Local PDT inhibits distant tumor growth. (A-D) Outgrowth curves of primary and secondary tumors of individual double MC38 tumor-bearing mice receiving PDT or left untreated. PDT was given on day 8 by injection of Bremachlorin photosensitizer followed after 6 hours by primary tumor illumination. Group average tumor volume of secondary tumors is indicated by the red line. Pooled data of 6 independent experiments, 48-57 mice per group. **(E)** Ex vivo analysis of secondary tumors by flow cytometry, showing percentage of total CD3+ tumor-infiltrating lymphocytes (TILs) or CD8 T cells from total CD45+ cells in the tumor. Asterisks indicate statistically significant differences ($p<0.05$) between untreated and PDT-treated mice. **(F)** Tumor-infiltrating CD8 T cells have an activated phenotype. Representative flow cytometry plot showing 4-1BB and CD69 activation marker expression.

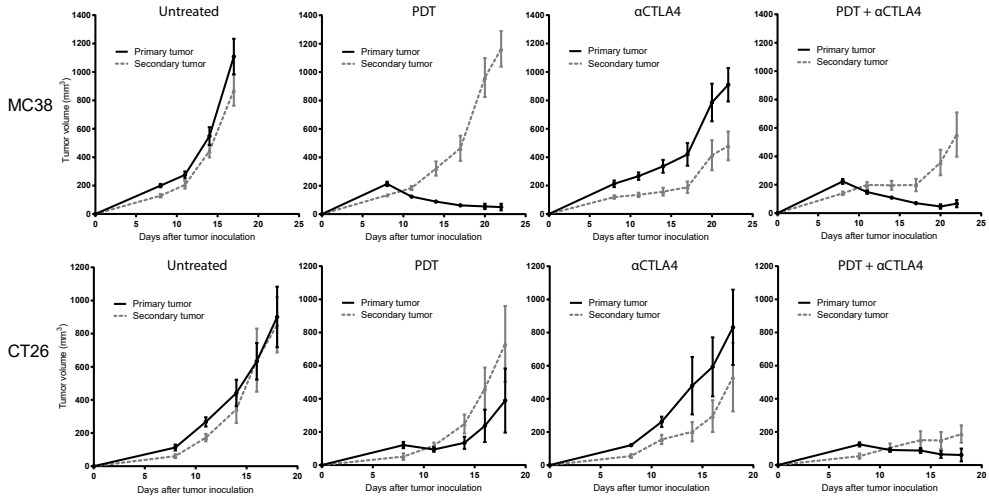

Supplementary Figure S4. Responses of primary and secondary tumors to therapy. Group average tumor outgrowth curves of primary and secondary MC38 tumors (upper graphs) or CT26 tumors (lower graphs). Mice received PDT of primary tumors on day 8, systemic CTLA4-blocking antibody on days 7, 10 and 14, both therapies, or were left untreated. Pooled data of 2 independent experiments, 14-16 mice per group.

Chapter 4

Vaccine tracking by in vivo near-infrared fluorescence imaging of emulsified peptide antigen

Jan Willem Kleinovink, Laura Mezzanotte, Henrik Gold, Nico Meeuwenoord, Luis J. Cruz, Alan B. Chan, Cornelis J.M. Melief, Hermen S. Overkleeft, Marieke F. Fransen, Clemens Löwik, Ferry Ossendorp

Manuscript in preparation

Abstract

Information on the fate of vaccines after *in vivo* administration may help optimize vaccination strategies. Optical imaging is a non-invasive visualization method capable of locating and quantifying light-producing molecules in vivo, which can be applied for vaccine visualization. We conjugated synthetic peptide vaccines to the near-infrared (NIR) fluorescent dye NIRD1. Using a NIRD1-labeled peptide of the OVA model antigen, we showed the feasibility of visualizing vaccines at the injection site and local lymph nodes. Distinct kinetics of different vaccine formulations were well-identified by live NIR fluorescence imaging. Small-droplet Montanide water-in-oil emulsions prepared by a syringe extrusion (SE) method showed remarkably slower vaccine kinetics than Vortex-prepared emulsions with larger droplets, which was visualized at the injection site and in draining lymph nodes. Differential vaccine drainage to lymph nodes was reflected in the ability to prime vaccine-specific CD8 T cells in local vaccine-draining lymph nodes, whereas systemic T cell levels were not significantly different. In conclusion, we have developed a NIR fluorescence imaging protocol for visualization of the fate of vaccines, which can be used to optimize vaccination strategies for several applications such as infectious disease and cancer.

Introduction

Immunotherapy of cancer aims to induce or enhance immune responses against tumors. Immune recognition can involve a variety of immune cells, but CD8 T cells are crucial immune cells capable of inducing tumor cell death through the delivery of cytotoxic T cell effector molecules. T cells recognize peptide epitopes presented in MHC molecules on the surface of target cells, and recent literature has shown T cell recognition of tumor cells driven by neo-epitopes in mutated cellular proteins (1–3). Indeed, highly mutated types of human cancer such as melanoma and lung cancer show higher numbers of neo-epitopes, correlating with a stronger immune recognition and in particular with the presence of T cells inside the tumor (4–6). Immunotherapy with immunomodulatory antibodies enhancing existing T cell responses has shown promising clinical results in patients with highly mutated and T cell-infiltrated tumors (7–9). Therapeutic vaccination is a form of cancer immunotherapy aiming to induce T cell responses by providing an exogenous source of tumor-specific antigen. The delivery of minimal peptide epitopes of tumor antigens results in direct binding to MHC molecules on any nucleated cell, resulting in T cell anergy due to antigen presentation in the absence of co-stimulatory signals. To restrict vaccine antigen presentation to professional APCs capable of priming functional T cells, the concept of synthetic long peptide (SLP) vaccines was established, which require antigen processing by professional APCs to create the MHC-binding epitope (10,11). Preclinical studies indicated that SLP vaccination may not only be applied in virally induced cancer by vaccinating with viral epitopes widely shared among individuals, both also by using individual unique neo-epitopes as a therapeutic peptide vaccine (12–14). Clinical application of SLP vaccination using a series of overlapping peptides covering the E6 and E7 oncoproteins of human papillomavirus 16 (HPV16) has shown promising results in patients with pre-malignant HPV16-induced gynecological lesions, but failed to induce strong responses in patients with established HPV16+ tumors despite the presence of vaccine-induced T cell responses (15–17). Mouse studies combining SLP vaccination with chemotherapy or photodynamic therapy have suggested combination therapy to improve the limited efficacy of SLP vaccination against advanced cancer (18,19). In addition, the efficacy of SLP vaccination as such may be improved, for example in terms of peptide formulation and routing. For instance, the fate of the vaccine peptides after injection is currently largely unknown, which could be addressed by live vaccine visualization techniques. Near-infrared (NIR) fluorescent dyes are very suitable for in vivo optical imaging studies due to their high excitation and emission wavelength, enhancing tissue penetration of the fluorescence signal (20–23). The widely used and clinically approved NIR dye Indocyanine Green (ICG) has

good optical properties as a standalone dye but is less suitable for conjugation to biomolecules (24,25). In this preclinical study, we labeled a model SLP vaccine with the novel NIR fluorescent dye NIRD1 to establish a fluorescence-based imaging platform for live SLP visualization and quantification. We visualized the vaccine at the injection site and draining lymph nodes and correlated vaccine kinetics to functionality. In conclusion, this study shows that NIR fluorescence imaging of vaccines is feasible and provides detailed information on vaccine kinetics, which can be used to optimize therapeutic vaccination strategies.

Materials and Methods

Mice and cell lines

Wildtype C57BL/6 mice and BALB/c nude mice were obtained from Charles River Laboratories (France). Albino B6 mice (tyrosinase-deficient immunocompetent C57BL/6 mice) and OT-I mice ($OVA_{257-264}$ (SIINFEKL)-specific T cell receptor-transgenic mice of C57BL/6 background) were bred in the animal breeding facility of the Leiden University Medical Center, the Netherlands. All experiments were approved by the animal ethical committee of Leiden University. D1 is a dendritic cell line and B3Z is a T cell hybridoma expressing beta-galactosidase upon presentation of its cognate antigen SIINFEKL, both are of C57BL/6 background and were used as described elsewhere (26). Cells were assured to be free of rodent viruses and *Mycoplasma* by PCR analysis.

Synthetic long peptide vaccines

For vaccine tracking experiments, the near-infrared (NIR) fluorescent dye NIRD1 was conjugated to synthetic long peptides using an aminohexanoid acid (Ahx) linker. This NIRD1-Ahx construct, amounting to approximately 1 kDa, was used to label the OVA SLP (DEVSGLEQLESIINFEKLAAAAAK). The purity of NIR-SLP conjugate preparations was visualized by Odyssey Imager (LI-COR) after tricine gel electrophoresis as described elsewhere (27). For *in vivo* vaccine tracking experiments, the NIR-SLP was injected subcutaneously in the tail-base of the mice in a volume of 100 µL, formulated in PBS or in Montanide emulsions consisting of a 1:1 ratio of a vaccine-containing PBS fraction and the mineral oil Montanide ISA 51 (Seppic). Vortex emulsions were prepared by vortexing the mixture for 30 minutes at room temperature. Syringe Extrusion emulsions were prepared by syringe extrusion of the PBS-Montanide mixture using two 1 mL syringes (Codan) connected to a three-way stopcock (Braun Discofix C3), using a protocol of 40 slow passages through the stopcock in 20 seconds followed by 160 passages at full speed. Dosing and formulation are indicated in the Figures legends.

NIR Fluorescence imaging

For live *in vivo* imaging, vaccinated mice were anaesthetized by isoflurane inhalation on the indicated time points. NIR fluorescent signals were measured by IVIS Spectrum (PerkinElmer) using excitation for 2 seconds at 745 nm and measuring the emission in the 840 nm filter, with Field Of View C and medium binning. Accompanying LivingImage software (Caliper Life Sciences) was used for data analysis. Signal quantification in specific regions of interest (ROI) was performed by using fixed-size ROIs throughout the experiments. Figures show the fluorescent signal as the Total Radiant Efficiency (TRE), expressed in (photons/second)/(μW/cm²) or as a percentage of the TRE at the start of the experiment.

Adoptive T cell transfer and T cell flow cytometry

For adoptive transfer of OVA SLP-specific OT-I CD8 T cells, the spleen of OT-I mice was harvested and mashed on 70 μm cell strainers (BD Biosciences) to create single-cell suspensions, followed by erythrocyte lysis and CD8 T cell isolation using a negative magnetic selection kit (BD). Adoptive transfer consisted of $1*10^6$ purified CD8 OT-I cells injected intravenously in 200 μL PBS in the tail vein. On indicated time points after transfer, the spleen and/or lymph nodes of recipient mice were harvested, mashed and deprived of erythrocytes, stained for CD3ε, CD8β and the OT-I congenic marker CD90.1, and analyzed by flow cytometry (BD LSR-II). To visualize OT-I proliferation, OT-I cells were labeled with the fluorescent dye carboxyfluorescein succinimidyl ester (CFSE) that is distributed among daughter cells upon cellular proliferation, reducing the fluorescence intensity per cell, which can be visualized by flow cytometry. To measure the HPV SLP-induced endogenous CD8 T cell response, venous blood samples were taken from the tail vein 8 days after vaccination. After erythrocyte lysis of the blood samples, the tumor-specific CD8 T cell response was determined by flow cytometry analysis after staining of the cells with fluorescently labeled antibodies against CD3ε, CD8β, and with 7-AAD and APC-conjugated tetramers (own production) binding the H-2Db RAHYNIVTF complex on the CD8 T cell.

Statistical analysis

Statistical analysis was performed using GraphPad Prism version 7.0 software. Data are shown as the mean ± SEM for each group, and comparison of groups was performed by two-tailed Student's t-test. Statistical differences were considered significant at $p < 0.05$.

Results and Discussion

Subcutaneously injected peptide vaccines drain to lymph nodes

In order to track the fate of antigen vaccines after vaccination, we used the near-infrared (NIR) fluorescent dye NIRD1 to label a model SLP of the chicken ovalbumin (OVA) CD8 T cell epitope SIINFEKL, creating conjugated NIR-OVASLP. To validate NIR fluorescence as a measure of vaccine presence, we tested whether no unbound NIRD1 dye was present in the conjugate preparation. Using tricine gel electrophoresis to distinguish small size differences between proteins, we show that the NIR-OVASLP conjugate (approximately 3.5 kDa) does not contain any free NIRD1 dye (approximately 1 kDa including the Ahx linker) (**Figure 1a**). Subcutaneous injection in the flank is a common vaccination route in mice, which drains primarily to the inguinal lymph node in that flank. The proximity of injection site and draining lymph node likely hampers their distinction by optical imaging. As an alternative injection site, we injected NIR-OVASLP subcutaneously in the tail-base of a BALB/c nude mouse. This mouse strain is immunodeficient, but ideal for optical imaging due to the complete absence of hair and pigment. Within minutes after injection in the tail-base, lymph drainage towards the inguinal lymph node was clearly visible by live NIR fluorescence imaging (**Figure 1b**). The signal beyond the inguinal lymph node suggests further lymph transport by efferent vessels towards the axillary lymph node, as has been described before (28). We therefore injected B6 mice with NIR-OVASLP in the central tail-base and harvested inguinal and axillary lymph nodes from both flanks 90 minutes after injection, and quantified the NIR fluorescence signal.

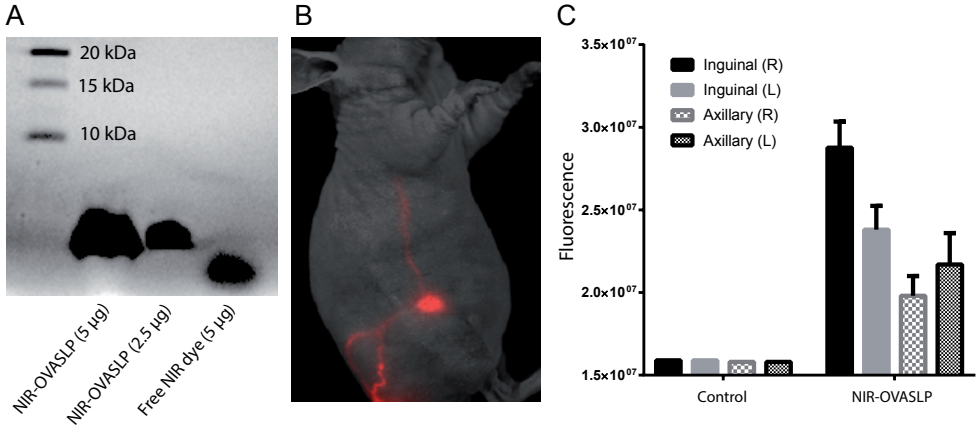

Figure 1. Inguinal and axillary lymph nodes drain the tail-base vaccination site. (A) Tricine gel electrophoresis of indicated amounts of NIRD1-labeled OVA24 SLP or free unbound NIRD1 dye, showing that the NIRD1-OVASLP conjugate does not contain unbound NIRD1 dye. The smallest three bands of a standard protein ladder are shown in the top. **(B)** NIR Fluorescence image of a BALB/c nude mouse 5 minutes after subcutaneous injection of NIR-OVASLP in the tail-base (not visible), and the drainage by the inguinal lymph node. **(C)** Measurement of NIR fluorescence in the left (L) and right (R) inguinal and axillary lymph nodes harvested from C57BL/6 mice 90 minutes after injection of NIR-OVASLP s.c. in the tail-base. Y-axis show the mean and SEM of the total radiant efficiency expressed in (photons/second) / ($\mu W/cm^2$). Lymph nodes from non-injected control mice are included as controls.

Injection in the tail-base results in vaccine accumulation primarily in the inguinal lymph nodes, whereas axillary lymph nodes showed lower fluorescence (**Figure 1c**). In summary, using a protocol of subcutaneous injection in the tail-base, we visualize drainage of SLP vaccines via lymphatic vessels to lymph nodes.

Fluorescence imaging of peptide vaccine kinetics

Our results show that the NIR-OVASLP construct can be visualized in draining lymph nodes by live imaging. Next, we analyzed whether NIRD1-labeling is sufficiently sensitive to visualize differential vaccine kinetics. We formulated the labeled vaccine in PBS, which is drained from the injection site rapidly, or in water-in-oil formulations using the mineral oil Montanide, which is used as a sustained-release formulation. Whereas clinical use of Montanide applies syringe extrusion as an emulsification method, preclinical studies most commonly mix the water and oil phase by vortex, which in general produces less stable emulsions with larger droplets (29,30). After subcutaneous injection of NIR-OVASLP in the tail-base of immunocompetent Albino B6 mice, NIR fluorescence imaging clearly identified the presence of the vaccine at the injection site (**Figure 2a**). To assess whether this NIR fluorescence-based vaccine tracking can be used to identify the kinetics of an administered vaccine, we formulated the NIR-OVASLP in three different ways: soluble peptide in saline (PBS), or 50/50 water-in-oil emulsions of the mineral oil Montanide emulsified either by Vortex or by Syringe Extrusion (SE). In order to follow the presence of the vaccine at the injection site and lymph nodes in time, we performed repeated measurements and quantified the NIR fluorescence signal in these areas of interest. The three formulations showed a clearly distinguishable pattern of clearance of the vaccine at the injection site, as shown by the drop in the fluorescent signal (**Figure 2b**). Corresponding with the expected pharmacokinetics of the different formulations, soluble SLP in PBS showed the fastest drop in fluorescent signal at the injection site. Interestingly, the SE formulation of Montanide-SLP showed a longer presence of peptide at the injection site than the exact same Montanide-SLP mixture prepared by Vortex. The NIR signal of Vortex-prepared emulsions at the injection site showed a two-phased pattern of a fast immediate drop followed by gradual decrease, consistent with heterogeneity in emulsion droplet size. Moreover, measurement of the flanks of the mice showed a clear NIR fluorescence signal in the vaccine-draining inguinal lymph nodes in the earliest days after injection (**Figure 2c,d**). The highest signal was found for the PBS free-peptide formulation, while the SE-formulated peptide was nearly undetectable in lymph nodes, and Vortex-formulated peptide showing an intermediate profile. Hence, a faster drop in fluorescence signal in the vaccination site corresponded with a higher signal in the lymph nodes, suggesting that our NIR fluorescence imaging protocol successfully quantified SLP drainage from the vaccination site to lymph nodes. In summary, these data show

the feasibility of SLP tracking by using NIR-labeled peptides. This imaging protocol allowed vaccine quantification at the injection site and visualization of lymph drainage, with sufficient sensitivity to distinguish vaccine formulations with distinct kinetics. Brewer et al. used MRI of iron-labeled Montanide to show that the oil remains at the injection site while the peptide epitope content encapsulated in liposomes gradually disappeared (31). Although the peptide length and formulation are different, this confirms the gradual release of peptide from Montanide depots as we visualized by NIR fluorescence imaging, a considerably less laborious and more subject-friendly technique compared to MRI (32).

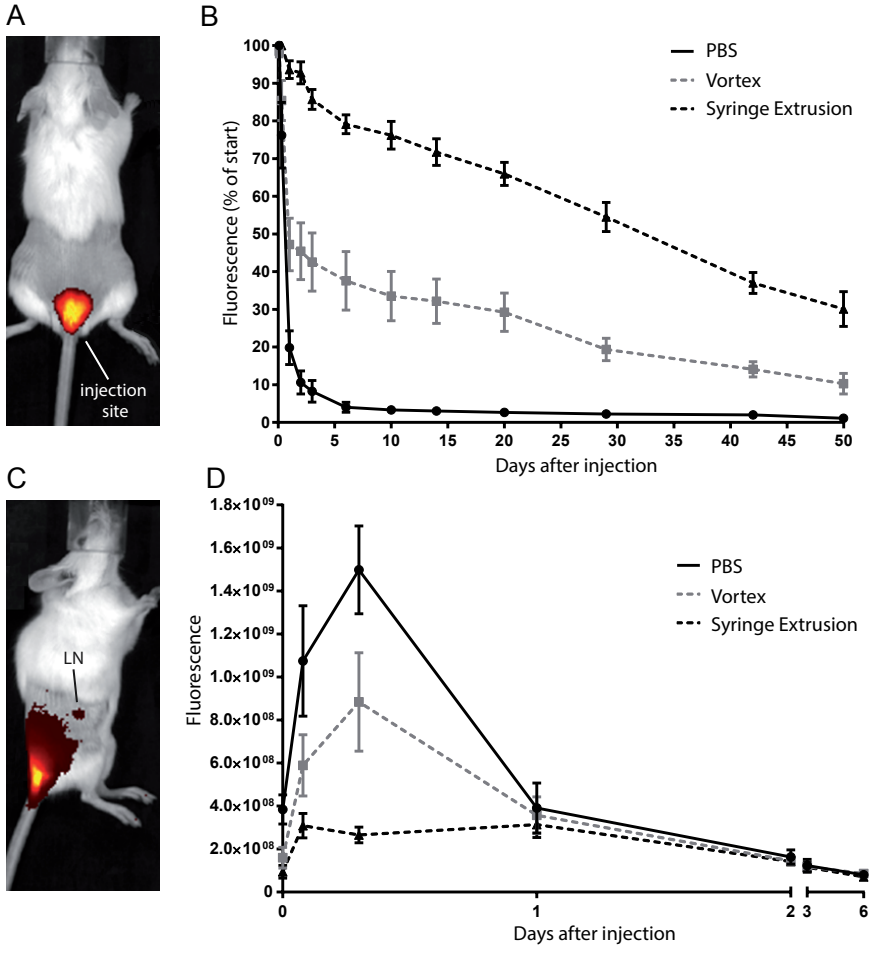

Figure 2. Visualization of peptide vaccine kinetics by fluorescence imaging. Examples of NIR-OVASLP fluorescence at the tail-base injection site (A) and the vaccine-draining inguinal lymph node (C) after injection in PBS. Quantification of vaccine fluorescence at the injection site (B) and vaccine-draining inguinal lymph nodes (D) of NIR-OVASLP formulated in PBS or in Montanide emulsions prepared by Vortex or Syringe Extrusion, as indicated. Fixed-size region of interest were used to quantify fluorescence, expressed as Total Radiant Efficiency in (photons/second) / (μW/cm²). The Y-axis shows the fluorescence signal either as a percentage of the starting signal after injection (B) or in absolute numbers (D).

SLP labeling does not hamper vaccine functionality

The validity of vaccine tracking using conjugated NIR dyes depends on the degree to which the presence of the dye affects the functional properties of the SLP vaccine. For instance, fluorescent and radioactive labeling of proteins and antibodies can significantly hamper the functional activity of the molecule of interest (33–35). To analyze whether NIRD1 conjugation hampered the immunogenicity of the SLP, we incubated D1 dendritic cells with labeled or unlabeled OVASLP and added the OVA-specific CD8 T cell hybridoma B3Z. T cell receptor (TCR) signaling in B3Z cells results in expression of the beta-galactosidase reporter as a measure of antigen presentation by dendritic cells and of vaccine functionality as such. The presence of NIRD1 on the OVASLP results in equal antigen processing and presentation as the unlabeled OVASLP (**Figure 3a**).

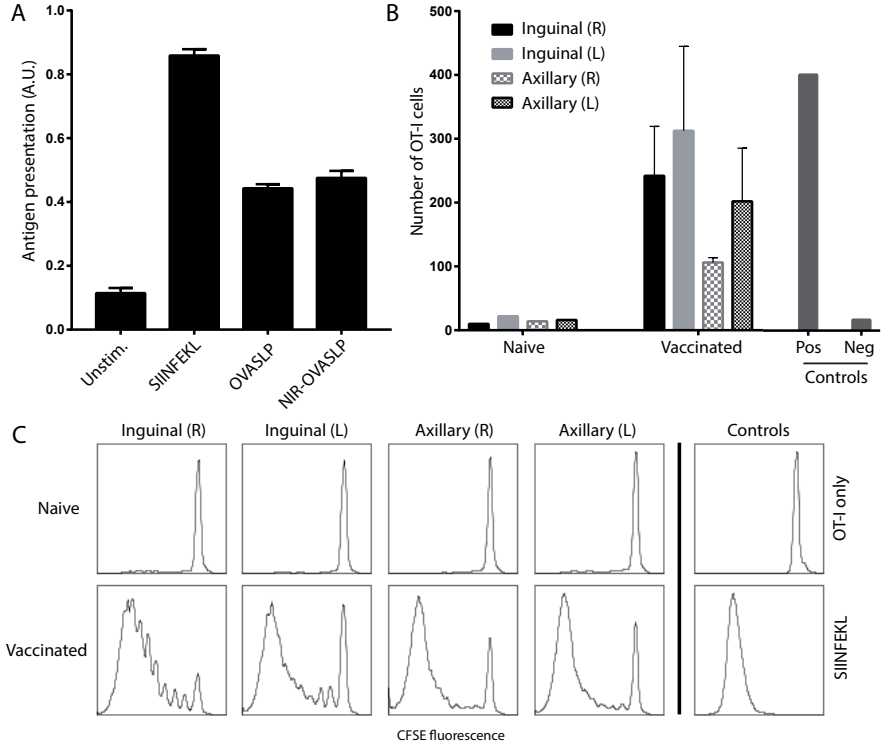

Figure 3. SLP labeling does not hamper vaccine functionality. (A) In vitro antigen presentation assay using OVA-specific B3Z CD8 T cell reporter cells. NIRD1-labeled or unlabeled OVA SLP was added to D1 dendritic cells and incubated overnight, followed by addition of B3Z cells. Presentation of the SIINFEKL epitope of OVA by dendritic cells to B3Z cells induces T cell receptor downstream signaling resulting in beta-galactosidase production, which enables a colorimetric assay as a measure of antigen presentation. Addition of SIINFEKL minimal epitope was used as positive control, non-incubated dendritic cells as negative control. **(B)** Proliferation of OT-I CD8 T cells incubated 4 days with single-cell suspensions of inguinal or axillary lymph nodes isolated from mice 90 minutes after vaccination with NIR-OVASLP in PBS the tail-base. The Y-axis shows the OT-I cell count normalized per 100 beads. Addition of SIINFEKL minimal epitope to a mixture of lymph node cells was used as positive control, OT-I cells not incubated with any lymph node cells or peptide served as negative control. **(C)** Visualization of OT-I cell proliferation from Figure 3B by showing CFSE fluorescence. Prior to incubation, OT-I cells were labeled with CFSE, which is distributed between daughter cells during proliferation, reducing CFSE fluorescence intensity per cell.

The superior result of the minimal peptide epitope SIINFEKL shows that B3Z activation functions in the absence of co-stimulatory signals. To assure NIR-OVASLP vaccine functionality in vivo, we mashed the tail-base vaccine-draining lymph nodes from Figure 1c and incubated them 4 days with OT-I cells, which are SIINFEKL-specific CD8 T cells isolated from a TCR-transgenic mouse. OT-I cells were pre-labeled with CFSE, a dye that is divided among daughter cells during proliferation and thereby allows visualization of T cell proliferation by the intensity of CFSE fluorescence in flow cytometry. OT-I cells incubated with vaccine-draining lymph nodes accumulated to much higher numbers than OT-I cells incubated with lymph nodes of naïve mice, or without lymph nodes (**Figure 3b**). FACS measurement of CFSE fluorescence confirmed that OT-I cells had massively proliferated after vaccination, as shown by the presence of cells with reduced CFSE fluorescence (horizontal axis) as a result of dilution by proliferation (**Figure 3c**). These results indicate that the conjugated NIRD1 dye leaves SLP functionality fully intact in vitro and in vivo, which validates correlation studies between SLP imaging and vaccine functionality.

Differential vaccine kinetics reflect local but not systemic T cell responses

To assess whether the varying vaccine kinetics were reflected in the ability to induce systemic T cell responses, we vaccinated mice with NIR-OVASLP formulated in PBS or in Montanide emulsions prepared by either Vortex or SE. On day 0, 3 or 14 after vaccination, mice received an adoptive transfer of vaccine-specific T cell receptor-transgenic OT-I CD8 T cells. Three days after T cell transfer, vaccine-draining lymph nodes and spleens were harvested to analyze the expansion of OT-I T cells as a measure of vaccine-induced T cell priming. Both formulations of Montanide emulsions induced strong vaccine-specific T cell proliferation in vaccine-draining lymph nodes and in the spleen (**Figure 4**). The higher SLP accumulation in lymph nodes draining Vortex emulsions, as compared to SE emulsions, was reflected in slightly stronger local T cell proliferation in lymph nodes, whereas differences in the spleen were not statistically significant. As expected, the non-adjuvanted peptide vaccine in PBS induced poor T cell proliferation due to the absence of T cell co-stimulation, despite the high levels of SLP in the lymph nodes after vaccination. This finding underscores the well-established important role of Montanide emulsions as vaccine adjuvants (11, 36). In conclusion, local differences in the presence of vaccine at the vaccination site and vaccine-draining lymph nodes are not necessarily reflected in the magnitude of systemic T cell responses. A previous study comparing different emulsions of a minimal peptide epitope vaccine in IFA, showed slightly lower T cell responses induced by Vortex-prepared vaccines when compared to Syringe Extrusion (37). We share their advice that vaccine emulsion protocols should be standardized to avoid large variability and undesired artefacts such as the inclusion of air bubbles in the emulsion, which favors the use of the Syringe Extrusion protocol.

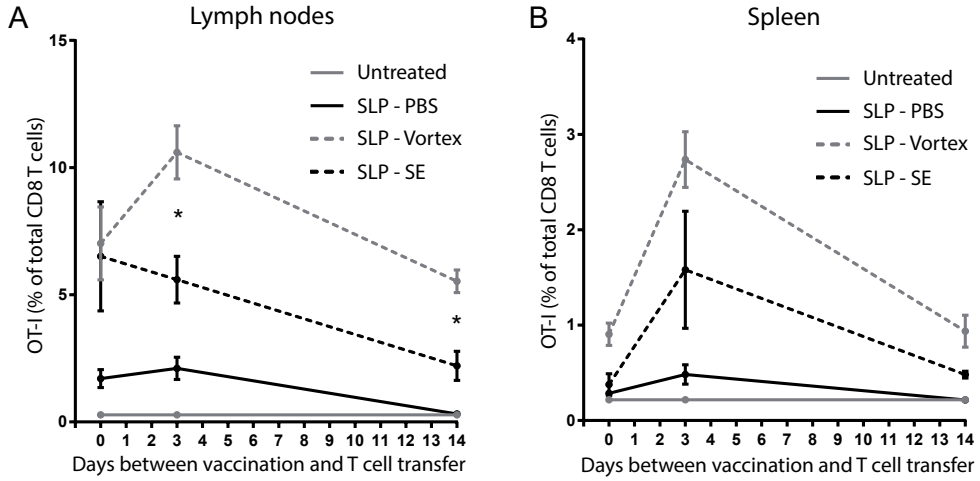

Figure 4. Differential vaccine kinetics reflect local but not systemic T cell responses. Expansion of vaccine-specific OT-I cells in vaccine-draining inguinal lymph nodes **(A)** and spleens **(B)** of mice 3 days after adoptive intravenous transfer of 1 million OT-I CD8 T cells. On day 0, 3 or 14 before OT-I transfer, mice were vaccinated in the tail-base with OVASLP formulated in PBS or in Montanide emulsions prepared by either Vortex or Syringe Extrusion (SE). Untreated naïve mice served as negative controls. The expansion of OT-I cells was quantified by flow cytometry and is presented as OT-I T cells as a percentage of total CD8 T cells. Statistically significant differences ($p<0.05$) by Student's t-test are indicated by asterisks (SLP-Vortex vs SLP-SE).

In summary, we show the feasibility of live NIR fluorescence SLP visualization and quantification at the injection site and in draining lymph nodes, and correlate vaccine kinetics to functionality in terms of T cell. We show that vaccine tracking can identify differences between vaccine formulations with varying kinetics. This does not exclude that besides the formulation, the characteristics of the peptide itself also influence vaccine kinetics (38). This issue can be addressed by comparing peptides with different lengths and physicochemical properties. Our NIRD1-based live fluorescence imaging platform serves as a useful tool to investigate fundamental and applied scientific questions in the field of vaccinology.

References

1. Castle JC, Loewer M, Boegel S, de Graaf J, Bender C, Tadmor AD, et al. Immunomic, genomic and transcriptomic characterization of CT26 colorectal carcinoma. BMC Genomics. 2014;15:190.
2. Yadav M, Jhunjhunwala S, Phung QT, Lupardus P, Tanguay J, Bumbaca S, et al. Predicting immunogenic tumour mutations by combining mass spectrometry and exome sequencing. Nature. 2014;515:572–6.
3. Kreiter S, Vormehr M, van de Roemer N, Diken M, Löwer M, Diekmann J, et al. Mutant MHC class II epitopes drive therapeutic immune responses to cancer. Nature. 2015;520:692–6.
4. Alexandrov LB, Nik-Zainal S, Wedge DC, Aparicio SAJR, Behjati S, Biankin A V, et al. Signatures of mutational processes in human cancer. Nature. 2013;500:415–21.

5. Van Allen EM, Miao D, Schilling B, Shukla SA, Blank C, Zimmer L, et al. Genomic correlates of response to CTLA-4 blockade in metastatic melanoma. Science. 2015;350:207–11.
6. Rizvi NA, Hellmann MD, Snyder A, Kvistborg P, Makarov V, Havel JJ, et al. Mutational landscape determines sensitivity to PD-1 blockade in non-small cell lung cancer. Science. 2015;348:124–8.
7. Topalian SL, Hodi FS, Brahmer JR, Gettinger SN, Smith DC, McDermott DF, et al. Safety, Activity, and Immune Correlates of Anti–PD-1 Antibody in Cancer. N Engl J Med. 2012;366:2443–54.
8. Hodi FS, O'Day SJ, McDermott DF, Weber RW, Sosman JA, Haanen JB, et al. Improved survival with ipilimumab in patients with metastatic melanoma. N Engl J Med. 2010;363:711–23.
9. Topalian SL, Drake CG, Pardoll DM. Immune Checkpoint Blockade: A Common Denominator Approach to Cancer Therapy. Cancer Cell. 2015;27:450–61.
10. Melief CJM, van der Burg SH. Immunotherapy of established (pre)malignant disease by synthetic long peptide vaccines. Nat Rev Cancer. 2008;8:351–60.
11. Slingluff CL. The present and future of peptide vaccines for cancer: single or multiple, long or short, alone or in combination? Cancer J. 2011;17:343–50.
12. Gubin MM, Zhang X, Schuster H, Caron E, Ward JP, Noguchi T, et al. Checkpoint blockade cancer immunotherapy targets tumour-specific mutant antigens. Nature. 2014;515:577–81.
13. Castle JC, Kreiter S, Diekmann J, Lower M, van de Roemer N, de Graaf J, et al. Exploiting the Mutanome for Tumor Vaccination. Cancer Res. 2012;72:1081–91.
14. Zwaveling S, Ferreira Mota SC, Nouta J, Johnson M, Lipford GB, Offringa R, et al. Established human papillomavirus type 16-expressing tumors are effectively eradicated following vaccination with long peptides. J Immunol. 2002;169:350–8.
15. Kenter GG, Welters MJP, Valentijn ARPM, Lowik MJG, Berends-van der Meer DMA, Vloon APG, et al. Vaccination against HPV-16 oncoproteins for vulvar intraepithelial neoplasia. N Engl J Med. 2009;361:1838–47.
16. Kenter GG, Welters MJP, Valentijn ARPM, Lowik MJG, Berends-van der Meer DMA, Vloon APG, et al. Phase I immunotherapeutic trial with long peptides spanning the E6 and E7 sequences of high-risk human papillomavirus 16 in end-stage cervical cancer patients shows low toxicity and robust immunogenicity. Clin Cancer Res. 2008;14:169–77.
17. van Poelgeest MIE, Welters MJP, van Esch EMG, Stynenbosch LFM, Kerpershoek G, van Persijn van Meerten EL, et al. HPV16 synthetic long peptide (HPV16-SLP) vaccination therapy of patients with advanced or recurrent HPV16-induced gynecological carcinoma, a phase II trial. J Transl Med. 2013;11:88.
18. van der Sluis TC, van Duikeren S, Huppelschoten S, Jordanova ES, Beyranvand Nejad E, Sloots A, et al. Vaccine-Induced Tumor Necrosis Factor-Producing T Cells Synergize with Cisplatin to Promote Tumor Cell Death. Clin Cancer Res. 2015;21:781–94.
19. Kleinovink JW, Van Driel PB, Snoeks TJ, Prokopi N, Fransen MF, Cruz LJ, et al. Combination of photodynamic therapy and specific immunotherapy efficiently eradicates established tumors. Clin Cancer Res. 2016;22:1459–68.
20. Etrych T, Lucas H, Janoušková O, Chytil P, Mueller T, Mäder K. Fluorescence optical imaging in anticancer drug delivery. J Control Release. 2016;226:168–81.
21. Leblond F, Davis SC, Valdés PA, Pogue BW. Pre-clinical whole-body fluorescence imaging: Review of instruments, methods and applications. J Photochem Photobiol B. 2010;98:77–94.
22. Vahrmeijer AL, Hutteman M, van der Vorst JR, van de Velde CJH, Frangioni J V. Image-guided cancer surgery using near-infrared fluorescence. Nat Rev Clin Oncol. 2013;10:507–18.
23. van Driel PBAA, van de Giessen M, Boonstra MC, Snoeks TJA, Keereweer S, Oliveira S, et al. Characterization and evaluation of the artemis camera for fluorescence-guided cancer surgery. Mol Imaging Biol. 2015;17:413–23.
24. Schaafsma BE, Mieog JSD, Hutteman M, van der Vorst JR, Kuppen PJK, Löwik CWGM, et al. The clinical use of indocyanine green as a near-infrared fluorescent contrast agent for image-guided oncologic surgery. J Surg Oncol. 2011;104:323–32.

25. Reinhart MB, Huntington CR, Blair LJ, Heniford BT, Augenstein VA. Indocyanine Green. Surg Innov. 2016;23:166–75.
26. Rahimian S, Kleinovink JW, Fransen MF, Mezzanotte L, Gold H, Wisse P, et al. Near-infrared labeled, ovalbumin loaded polymeric nanoparticles based on a hydrophilic polyester as model vaccine: Invivo tracking and evaluation of antigen-specific $CD8^+$ T cell immune response. Biomaterials. 2015;37.
27. Schägger H. Tricine–SDS-PAGE. Nat Protoc. 2006;1:16–22.
28. Harrell MI, Iritani BM, Ruddell A. Lymph node mapping in the mouse. J Immunol Methods. 2008;332:170–4.
29. Aucouturier J, Dupuis L, Deville S, Ascarateil S, Ganne V. Montanide ISA 720 and 51: a new generation of water in oil emulsions as adjuvants for human vaccines. Expert Rev Vaccines. 2002;1:111–8.
30. Fillmore PD, Brace M, Troutman SA, Blankenhorn EP, Diehl S, Rincon M, et al. Genetic analysis of the influence of neuroantigen-complete Freund's adjuvant emulsion structures on the sexual dimorphism and susceptibility to experimental allergic encephalomyelitis. Am J Pathol. 2003;163:1623–32.
31. Brewer KD, Lake K, Pelot N, Stanford MM, DeBay DR, Penwell A, et al. Clearance of depot vaccine SPIO-labeled antigen and substrate visualized using MRI. Vaccine. 2014;32:6956–62.
32. Kosaka N, Ogawa M, Choyke PL, Kobayashi H. Clinical implications of near-infrared fluorescence imaging in cancer. Future Oncol. 2009;5:1501–11.
33. Vira S, Mekhedov E, Humphrey G, Blank PS. Fluorescent-labeled antibodies: Balancing functionality and degree of labeling. Anal Biochem. 2010;402:146–50.
34. Gahlmann A, Moerner WE. Exploring bacterial cell biology with single-molecule tracking and super-resolution imaging. Nat Rev Microbiol. 2013;12:9–22.
35. Vergara I, Castillo E, Romero-Piña M, Torres-Viquez I, Paniagua D, Boyer L, et al. Biodistribution and Lymphatic Tracking of the Main Neurotoxin of Micrurus fulvius Venom by Molecular Imaging. Toxins. 2016;8:85.
36. Khong H, Overwijk WW. Adjuvants for peptide-based cancer vaccines. J Immunother Cancer. 2016;4:56.
37. Koh YT, Higgins SA, Weber JS, Kast WM. Immunological consequences of using three different clinical/laboratory techniques of emulsifying peptide-based vaccines in incomplete Freund's adjuvant. J Transl Med. 2006;4.
38. Weijzen S, Meredith SC, Velders MP, Elmishad AG, Schreiber H, Kast WM. Pharmacokinetic Differences Between a T Cell-Tolerizing and a T Cell-Activating Peptide. J Immunol. 2001;166.

Chapter 5

Near-infrared labeled, ovalbumin loaded polymeric nanoparticles based on a hydrophilic polyester as model vaccine: In vivo tracking and evaluation of antigen-specific CD8+ T cell immune response

Sima Rahimian*, Jan Willem Kleinovink*, Marieke F. Fransen, Laura Mezzanotte, Henrik Gold, Patrick Wisse, Hermen Overkleeft, Maryam Amidi, Wim Jiskoot, Clemens W. Löwik, Ferry Ossendorp and Wim E. Hennink

* Shared first authorship

Biomaterials (2015) Jan;37:469-77

Abstract

Particulate antigen delivery systems aimed at the induction of antigen-specific T cells form a promising approach in immunotherapy to replace pharmacokinetically unfavorable soluble antigen formulations. In this study, we developed a delivery system using the model protein antigen ovalbumin (OVA) encapsulated in nanoparticles based on the hydrophilic polyester poly(lactide-co-hydroxymethylglycolic acid) (pLHMGA). Spherical nanoparticles with size 300-400 nm were prepared and characterized and showed a strong ability to deliver antigen to dendritic cells for cross-presentation to antigen-specific T cells in vitro. Using near-infrared (NIR) fluorescent dyes covalently linked to both the nanoparticle and the encapsulated OVA antigen, we tracked the fate of this formulation in mice. We observed that the antigen and the nanoparticles are efficiently co-transported from the injection site to the draining lymph nodes, in a more gradual and durable manner than soluble OVA protein. OVA-loaded pLHMGA nanoparticles efficiently induced antigen cross-presentation to OVA-specific CD8 T cells in the lymph nodes, superior to soluble OVA vaccination. Together, these data show the potential of pLHMGA nanoparticles as attractive antigen delivery vehicles.

Introduction

Immunotherapy aims at the induction or enhancement of cellular immune responses against the target of interest, and has the advantage of a high efficacy and less side effects based on antigen-specificity (1). One of the challenging aspects in the development of effective strategies for immunotherapy is to secure efficient antigen presentation by dendritic cells (DCs) in a targeted and sustained manner to subsequently result in activation of antigen-specific T cells (2). Dendritic cells are professional antigen-presenting cells (APCs) and have a pivotal role in the initiation and orchestration of T cell immune responses (3-6). Immature DCs constantly engulf and process soluble and particulate antigens, as well as necrotic and apoptotic cells via various mechanisms (7). Upon maturation, DCs migrate to draining lymph nodes and present the processed protein antigens in the form of linear peptide epitopes to CD4 and CD8 T cells through major histocompatibility complex (MHC) class I and class II molecules to initiate a proper immune response against the antigens (6,8,9). The crucial role of DCs in adaptive immunity makes them an important target for the development of antigen vaccines. The weak immunogenicity of soluble protein antigens has led to the development of carrier systems that aim for DC targeting and intracellular antigen delivery (2,10-17). Particulate delivery systems have several advantages such as protection of antigen against enzymatic degradation and enhanced uptake by DCs, the possibility of co-delivery of antigen and adjuvants to DCs, and the possibility of introducing targeting ligands on the surface of the particle as well as prolonged antigen delivery for sustained antigen-presentation by DCs (2,3,7,15,18-22). Especially biodegradable polymeric nanoparticles (NPs) have been used extensively as antigen delivery vehicles (3,15,19,23). In particular, particles based on poly(lactic-coglycolic acid) (pLGA), a biodegradable polyester, have been widely investigated for diverse pharmaceutical applications including protein and antigen delivery (24-29). Several studies have shown the efficacy of antigen-loaded pLGA particulate systems in the induction of immune responses both in vitro and in animal models (18,30,31). pLGA particles are far more efficient in generating long-lasting CD8 T cell immunity than soluble antigen and antigen in incomplete Freund's adjuvant (IFA) (32). Nevertheless, pLGA systems have several drawbacks as peptide/protein-releasing formulations. Upon degradation, acidification inside the particles results in aggregation and denaturation of the loaded peptide/protein (33). Moreover, peptide/protein encapsulated in pLGA are prone to chemical modifications such as acylation (34,35). Altogether these drawbacks lead to incomplete release (36) of the content from the particles and possible undesired immunogenicity and other adverse reactions (37). To overcome pLGA pitfalls, functionalized polyesters such as poly(lactic-co-glycolic-hydroxymethyl glycolic

acid) (pLGHMGA) and poly(lactic-co-hydroxymethyl glycolic acid) (pLHMGA) have been developed. These polymers are more hydrophilic than pLGA and therefore degrade faster, do not show a pH drop inside the degrading particles (38) and cause much lower acylation. Moreover, they show complete and faster release in comparison to pLGA particles (39-41). The fate of vaccines after administration has been investigated in several in vivo imaging studies (42-46). Fluorescence imaging has received considerable attention during the past few years because of its advantages such as the ease of translation from in vitro imaging studies and being non-invasive, fast and cost-effective (47-51). Several in vivo near-infrared (NIR) fluorescent dyes have been developed with excitation/emission maxima between 700 and 900 nm to minimize tissue absorbance and light scattering, resulting in increased depth of penetration, low fluorescence background, and high intensity signals (45). These dyes can be modified or conjugated to antigens or NPs/polymers (50). A considerable number of vaccine tracking studies with NIR fluorescent dyes focuses on tracking of DCs rather than the vaccine. Moreover, the fluorescent dye is often encapsulated in the particles which brings the risk of dye leakage from the particles (46,52), or is attached to other contrast agents such as superparamagnetic iron oxide particles (53,54). The use of NIR fluorescent dyes coupled both to the antigen of interest and to the delivery system may therefore be preferred. In this study, we evaluate the feasibility of polymeric pLHMGA nanoparticles as a protein antigen delivery system. The particulate antigen showed a superior ability to induce antigen cross-presentation to antigen-specific T cells compared to soluble antigen, both in vitro and in vivo. Using NIR dyes covalently linked to both the nanoparticle and the model protein antigen, we visualized the delivery system and its content in real-time, showing gradual relocation from the injection site to the draining lymph nodes. This shows the potential of pLHMGA nanoparticles as an efficient antigen delivery system for the induction of antigen-specific cellular immune responses and suggests its experimental application in cancer research.

Materials and Methods

Materials

Ovalbumin Low Endo™ (OVA, batch X2N13844) was purchased from Worthington, USA. IRDye800CW and IRDye680RD N-hydroxysuccinimide ester (NHS ester) were purchased from LI-COR Biosciences, USA. Alexa647-labeled ovalbumin was obtained from Molecular probes, The Netherlands. 5-Hexyn-1-ol, polyvinyl alcohol (PVA; Mw 30000-70000; 88% hydrolyzed), palladium on carbon (Pd/C; 10 % wt. loading dry support), tin(II) 2-ethylhexanoate ($SnOct_2$), copper(I) acetate, dimethyl sulfoxide (DMSO) and tris((1-benzyl-1H-1,2,3-triazol-4-yl)methyl)

amine (TBTA) were obtained from Sigma-Aldrich, USA. Benzyl alcohol, sodium dihydrogen phosphate (NaH_2PO_4) and disodium hydrogen phosphate (Na_2HPO_4) were obtained from Merck, Germany. D,l-Lactide was from Purac, the Netherlands. N,N-dimethylformamide (DMF), chloroform, dichloromethane (DCM), n-propanol, methanol, tetrahydrofuran (THF) and toluene were from Biosolve, the Netherlands. Sodium azide (NaN_3, 99%), sodium hydroxide (NaOH) and sodium dodecyl sulfate 20% (SDS) were purchased from Fluka, the Netherlands. Bicinchoninic acid assay (Micro BCA) reagents were obtained from Thermo Scientific (USA). Pyrogen-free water was purchased from Carl Roth (Germany). Phosphate buffered saline (1.8 mM NaH_2PO_4, 8.7 mM Na_2HPO_4, 163.9 mM Na^+, 140.3 mM Cl^-) (PBS) was obtained from B Braun, Germany. Toluene and DMF were dried on 3Å molecular sieves prior to use. Chemicals were used as received without further purification, unless otherwise stated. Azide-functionalized water-soluble near-infrared fluorescent dye 10 (azide-NIR10) was prepared as described elsewhere (55). (Experimental details are provided in supporting information).

Synthesis of copolymers of 3S-(benzyloxymethyl)-6S-methyl-1,4-dioxane-2,5-dione with d,l-lactide (pLHMGA).

3S-(benzyloxymethyl)-6S-methyl-1,4-dioxane-2,5-dione (benzyloxymethylmethyl-glycolide) (BMMG) was synthesized as described before (56). A copolymer of d,l-lactide and BMMG (50:50 molar ratio) was synthesized via ring opening polymeriztion at 130 °C using benzyl alcohol as initiator with a 100/1 monomer-to-initiator molar ratio and stannous octoate ($SnOct_2$) as catalyst (**Figure 1**) (39,56). In a typical procedure, vacuum dried monomers (BMMG (2840 mg, 11.35 mmol) and d,l-lactide (1630 mg, 11.35 mmol)) were introduced into a dry schlenk tube under a nitrogen atmosphere. Next, benzyl alcohol (24.5 mg, 0.226 mmol; 223.1 µL from a 109.8 mg/mL stock solution in toluene) and $Sn(Oct)_2$ (45.9 mg, 0.113 mmol; 409.8 µL from a 112 mg/mL stock solution in toluene) were added. Toluene was evaporated under vacuum for 2 hours, the tube was closed and immersed into a preheated 130°C oil bath for 16 hours while stirring. Next, the obtained polymer was dissolved in 10 mL chloroform and subsequently precipitated in 500 ml cold methanol to remove the unreacted monomers and to precipitate the polymer, which was collected by filtration and vacuum dried to yield 4.5 g (90%) poly (d,l-lactic-co-benzyloxymethylglycolic acid) (pLBMGA). Subsequently, pLBMGA was dissolved in 500 mL THF, and 5 g of 10 % w/w Pd/C catalyst was added. The flask was filled with hydrogen in three consecutive steps of subsequent evacuation and refilling with H_2 and the reaction mixture was stirred for 16 hours under a H_2 pressure. Next, Pd/C was removed using a glass filter and THF was removed by evaporation. The obtained polymer was then dissolved in 5 mL chloroform and precipitated in 200 mL n-propanol and vacuum dried after filtration to yield 3 g of pLHMGA (84%).

Synthesis of hexyn-poly(d,l lactide)(hexyn-pDLLA) to couple to azide-NIR10 via click chemistry

Hexyn-pDLLA was synthesized via ring opening polymerization similar to the method described in section 2.2.1. Briefly, vacuum dried d,l lactide (396 mg, 2.75 mmol) was transferred into a dry schlenk tube under a nitrogen atmosphere. Next, the initiator, 5-hexyn-1-ol (monomer-to-initiator ratio was 70 to 1, 3.85, 0.039 mmol; 75.5 µL from a 51 mg/mL stock solution in toluene and $Sn(Oct)_2$ (7.9 mg, 0.020 mmol; 71.2 µL from a 112 mg/mL stock solution in toluene) were introduced into the schlenk tube. The tube was evacuated for 2 h, sealed, and immersed in an oil bath thermostated at 130 °C. The polymerization was performed for 16 hours and the formed polymer was purified by dissolution in chloroform and precipitation in n-propanol followed by filtration and vacuum drying to yield 370 mg of hexyn-pDLLA (Yield: 92 %).

Conjugation of azide-NIR10 to hexyn-pDLLA by click chemistry

Conjugation of the azide-NIR10 to hexyn-pDLLA was performed using copper catalyzed azide-alkyne cycloaddition (57-60). In a typical procedure, 30.4 mg hexyn-pDLLA (1.84 µmole) and 2 mg azide-NIR10 (1.84 µmole) were transferred into a vial. Then copper (I) acetate (0.2 mole per mole of polymer) and TBTA (0.05 mole per mole of polymer) were added to the vial from their stock solution in dried DMF and the volume was adjusted with DMF to 250 µL. The system was flushed with nitrogen for 20 minutes and the reaction was performed at 40 °C overnight. The obtained conjugate (NIR10-pDLLA) was purified by precipitation in water. The obtained precipitate was washed with water and freeze dried at -50 °C and 0.7 mbar overnight (Chris Alpha 1-2 freeze-drier, Germany). The conjugation efficiency was calculated using GPC analysis by dividing the area under the chromatogram of the conjugated polymer using UV detection by the area under the curve of reaction mixture (Yield: 76%).

Polymer characterization

NMR Spectroscopy: A Gemini 300 MHz spectrometer (Varian Associates Inc., USA) was used to conduct ^{1}H-NMR measurements at 298 K. Chemical shifts are reported in ppm with reference to the solvent peak (δ) 7.26 ppm for $CDCl_3$. *Gel Permeation Chromatography (GPC):* Molecular weight and molecular weight distribution (polydispersity index (PDI); weight average molecular weight/ number average molecular weight) of the synthesized pLHMGA was measured by using a Waters Alliance system (Waters, USA) with a Waters 2695 separating module equipped with Waters 2414 refractive index detector. Fifty µL of 5 mg/ mL sample was injected onto two PL-gel 5 µm mixed-D columns fitted with a guard column (Polymer Laboratories, M_w range 0.2-400 kDa). Polystyrene

standards were used to calibrate the columns and AR grade THF was used as eluent at a flow rate of 1 mL/min and a run time of 30 minutes. For hexyn-pDLLA and NIR10-pDLLA, DMF containing LiCl 10 mM was used as eluent and a Waters 2478 UV detector was connected to the system and the UV absorbance of the dye was measured at 700 nm. Polyethylene glycol (PEG) standards were used to calibrate the column. The flow rate was set at 0.7 mL/min with a run time of 40 minutes. The results were analyzed using Empower software v. 2 (Waters, USA).
Differential Scanning Calorimetry (DSC): The thermal properties of the polymers were established by using differential scanning calorimetry (Discovery DSC, TA instrument, USA). Two to five mg of polymer sample was loaded into an aluminum pan which was subsequently heated from room temperature to 120 °C, with a heating rate of 5 °C/min, followed by cooling down to −50 °C. Thereafter, the sample was heated to 120 °C with a temperature modulation of ±1 °C and a ramping rate of 2 °C/min. The glass transition temperature (T_g) was recorded as the midpoint of the heat capacity change in the second heating run.

Labeling OVA with NIR fluorescent dyes
OVA was labeled with either IRDye800CW (IR800) or IRDye680RD (IR680) by coupling the NHS ester of the dyes to the protein. In a typical procedure, 20 mg of OVA was dissolved in 1 mL PBS (B Braun, Germany) pH 7.4 and the pH was adjusted to 8.5 by adding 0.1 mL of K_2HPO_4 1 M pH 9. The IRDye680RD NHS ester was dissolved in DMSO (4 mg/mL) and 0.25 mL of the stock solution containing 1 mg of the dye was added to the OVA solution at a 2:1 molar ratio. The reaction was carried out at room temperature for two hours. The unreacted dye was subsequently removed with pyrogen-free water by using Zeba™ spin desalting columns equilibrated with pyrogen-free water in two consecutive steps and IR680-OVA was collected after freeze drying (yield: 85%). IR800CW was conjugated and purified by using the same procedure with a dye/OVA feed molar ratio of 1.7 to 1 (yield: 79%).

Characterization of labeled-OVA
IR680-OVA was characterized by GPC using a Waters UPLC Acquity system equipped with a fluorescence detector. Two channels were used: channel 1 for detection of the protein (excitation at 280 nm and emission at 340 nm) and channel 2 for detection of the IR680 signal (excitation at 672 nm and emission at 694 nm). Seven and a half µL of IR680-OVA (10 µg/mL in PBS) was injected onto a BEH450 SEC 2.5 µm column (Waters, USA). PBS was used as elution buffer and the flow rate was set at 0.25 mL/min. To calculate the dye/OVA molar ratio, the UV spectrum of the freeze-dried labeled OVA was recorded (Shimadzu 2450, Japan) and the absorbance values at 280 nm (A_{280}) and 672 nm (A_{672}) were used to calculate the degree of conjugation according to the following formula: (Dye/OVA) = (A_{672}/ε*Dye*) / ((A_{280} – 0.07*A_{672})/

ε*OVA*)). Dye/OVA is the molar ratio of IR680 to OVA and the molar extinction coefficient of IR680 (ε_{Dye}) is 165,000 M^{-1} cm^{-1} (according to the manufacturer) and the molar extinction coefficient of OVA (ε_{OVA}) is 30590 M^{-1} cm^{-1} (61). IR800-OVA was characterized similarly by using the corresponding wavelengths suitable for IR800.

Preparation of nanoparticles

OVA loaded nanoparticles (NPs) were prepared by using a double emulsion solvent evaporation method essentially as described before (62). In brief, 50 µL of 30 mg/mL OVA solution in pyrogen-free water was emulsified by sonication (30 s, 20 W-ultrasonic homogenizer (Labsonic P, B. Braun Biotech, Germany) in a solution of 50 mg of pLHMGA in 1 mL of DCM to obtain a water -in-oil emulsion (W_1/O). Next, 2 mL of PVA 1% w/v solution in pyrogen-free water (filtered through a 0.2 µm filter) was added to this first emulsion and a water-in-oil-in-water emulsion was formed by a second round of sonication for 30 seconds. The double emulsion (W_1/O/W_2) was then added dropwise to 25 mL of PVA 0.3% w/v in pyrogen-free water at 40 °C while stirring for rapid removal of DCM. After 1 hour, the particles were collected by centrifugation for 30 min at 20,000 g, washed with PBS and consecutively with water, resuspended in pyrogen-free water, and freeze-dried overnight. Dual labeled NPs containing NIR10-labeled pLHMGA and IR680-OVA were prepared using the same method by addition of 4 mg of NIR10-pDLLA to 50 mg of pLHMGA and using IR680-OVA (20 mg/ml) as internal water phase. For preparation of empty NPs, NPs loaded with IR800-OVA or Alexa647-OVA, 50 µl pyrogen-free, 50 µl of 20 mg/mL IR800-OVA or Alexa647-OVA was used as internal water phase.

Nanoparticle characterization: Size and morphology analysis

Dynamic light scattering: The size of NPs was measured with dynamic light scattering (DLS) on an ALV CGS-3 system (Malvern Instruments, Malvern, UK) equipped with a JDS Uniphase 22 mW He–Ne laser operating at 632.8 nm, an optical fiber-based detector, and a digital LV/LSE-5003 correlator. Freeze dried NPs were suspended in deionized water (RI = 1.332 and viscosity 0.8898 cP) and measurements were done at 25 °C at an angle of 90°.

Transmission electron microscopy (TEM): The size and morphology of NPs were analyzed by using transmission electron microscopy (TEM, FEI Tecnai T10). A droplet of nanoparticle suspension in water was placed on a carbon coated copper grid and the sample was stained with 2% uranyl acetate. NPs were visualized with 7-73 k fold magnification and analyzed by MeasureIT software.

Nanoparticle characterization: OVA content and loading efficiency of NPs

OVA loading efficiency of the NPs was determined by measuring the protein content of digested NPs essentially as described before (63). In short, about 5 mg of particles (accurately weighed) was dissolved in 0.5 mL of DMSO followed by addition of

2.5 mL of 50 mM NaOH containing 0.5% (w/v) SDS. After complete degradation of the particles, the resulting solution was analyzed by using the Micro BCA™ Protein Assay Kit (Thermo Scientific), a calorimetric method that quantifies protein concentration based on peptide bond and specific amino acid residues. Calibration was done by using 2-40 µg/mL of OVA solution in DMSO:NaOH 50 mM/SDS 0.5% (1:5). Loading efficiency (LE%) is defined as the amount of OVA encapsulated in the nanoparticles divided by the amount of protein added × 100%. Loading percentage (L%) is reported as the amount of OVA entrapped in the particles per total dry mass of the nanoparticles × 100%. In case of dual labeled NPs (containing IR680-OVA) or IR800-OVA NPs, the degraded particle solution was analyzed for its OVA content based on the NIR label by using an Odyssey™ scanner (LI-COR Biosciences, USA) at the 700 nm channel for IR680-OVA and the 800 nm channel for IR800-OVA and the calibration was done by using IR680-OVA or IR800-OVA.

Nanoparticle characterization: *In vitro* release of OVA from NPs

About 5 mg of freeze-dried dual labeled NPs (containing IR680-OVA) was accurately weighed and suspended in 5 mL phosphate buffered saline (pH 7.4, 49 mM NaH_2PO_4, 99 mM Na_2HPO_4, 6 mM NaCl and 0.05% (w/v) NaN_3). The particle suspension was incubated at 37 °C under mild agitation. At different time points, 300 µl was removed and centrifuged at 24000 g for 15 minutes. The amount of protein released and present in the supernatant was quantified by using an Odyssey™ scanner using the 700 nm channel for visualization of IR680-OVA. Calibration was done by using IR680-OVA in PBS.

Mice and cells

WT C57BL/6 (CD45.2/Thy1.2; H-2K^b) mice were obtained from Charles River Laboratories (France). Albino BL/6 mice (B6(Cg)-Tyr^{c-2J}/J tyrosinase-deficient immunocompetent BL/6 mice) were bred in the animal breeding facility of the Leiden University Medical Center, the Netherlands. All experiments were approved by the animal experimental committee of Leiden University, the Netherlands. D1 cells are a dendritic cell line of BL/6 background (64), and B3Z is a CD8$^+$ T cell hybridoma specific for the SIINFEKL epitope from OVA and carrying the *lacZ* (E.coli β-galactosidase) reporter gene induced by NFAT (nuclear factor of activated T-cells) (65). Antigen-specific activation of B3Z cells leads to T cell receptor-mediated triggering of NFAT, and the subsequent production of β-galactosidase can be quantified by addition of CPRG, a substrate for the β-galactosidase, as a measure of antigen cross-presentation (66). Cells were cultured in Iscove's Modified Dulbecco's Medium (IMDM, Lonza) containing 8% fetal calf serum (FCS, Greiner), supplemented with 2 mM GlutaMax (Gibco) and 80 IU/mL sodium-penicillin G (Astellas, the Netherlands) for D1 cells, or supplemented with 100 IU/mL penicillin/streptomycin (Gibco), 2 mM glutamin

(Gibco), 25 µM 2-mercaptoethanol and 500 µg/mL Hygromycin B (AG Scientific) for B3Z cells. OT-I*Thy1.1 mice are TCR-transgenic mice on B6 background whose $CD8^+$ T cells recognize the OVA-epitope SIINFEKL presented in H2-K^b, crossed to Thy1.1 mice to obtain a congenic marker for distinction from endogenous $CD8^+$ T cells in transfer experiments. Naïve OT-I $CD8^+$ T cells were obtained by creating single-cell suspensions from spleens and lymph nodes of OT-I*Thy1.1 mice and subsequent purification of $CD8^+$ cells.

Dendritic Cell viability assay

D1 dendritic cells (50,000 cells/well in 96-well plates) were incubated with dispersions of unlabeled and labeled NPs (7.8-1000 µg/ml) overnight at 37 °C, and cell viability was measured by flow cytometry using the DNA-binding fluorescent dye 7-amino-actinomycin-D (7-AAD) to stain dead cells.

Analysis of cellular uptake

D1 cells (100,000 cells/well in 96-well plates) were incubated with Alexa 647-OVA nanoparticles (final concentration of OVA in medium: 6 µg/ml) overnight. D1 cells were subsequently transferred onto a confocal slide without washing or fixation. The intracellular localization of NPs was studied by confocal laser scanning microscopy imaging using inverted Leica SP2 confocal microscope and the samples were analyzed using the corresponding Leica confocal software in DIC mode.

***In vitro* antigen cross-presentation assay**

In vitro cross-presentation of OVA by DCs was studied by incubating titrated amounts of OVA encapsulated in NPs or in soluble form with 50,000 D1 cells (100 µl of 0.2-25 µg OVA/mL in PBS corresponding to 0.12 to 1.5 mg/ml of NPs) for two hours at 37°C followed by addition of 50,000 B3Z cells and incubation overnight at 37°C in 96-well plates. The cells were then incubated with a lysis buffer containing the CPRG substrate for *lacZ* (PBS +1% 9 mg/mL CPRG + 0.9% 1M $MgCl_2$ + 0.125% NP40 + 0.71% 14.3M β-mercaptoethanol) at 37 °C until the color reaction had progressed sufficiently for readout in a plate reader measuring the optical density at 590 nm. The direct MHC-binding minimal epitope SIINFEKL (100 ng/mL in PBS) was used as a positive control, and unstimulated D1 cells were negative controls.

***In vivo* tracking of labeled NPs**

Albino BL/6 mice were vaccinated subcutaneously with 50 µg OVA encapsulated in dual labeled NPs dispersed in 100 µl PBS or 50 µg/100 µl PBS IR800-OVA. Vaccine kinetics were then studied at several time points after administration by using the IVIS spectrum preclinical *in vivo* imaging system (PerkinElmer). Kinetics were measured by quantifying the fluorescent intensity in pre-set regions of interest (ROI) at the injection site and the two vaccine-draining inguinal lymph nodes, expressed

as the total radiant efficiency in (p/s)/(μW/cm^2). The fluorescent signal in the injection site at each time point is presented as the as percentage of the maximum recorded value, to show percentual decrease in time. In the lymph nodes the data is presented as the signal to background ratio and it is calculated by dividing the fluorescence signal of the lymph nodes by the background signal at each time point (67).

***In vivo* antigen cross-presentation**

To establish antigen-presentation *in vivo*, BL/6 mice were vaccinated with OVA encapsulated in NPs or in its soluble form. Mice were injected subcutaneously with 200 μL of a 2 mg/mL suspension of NPs in PBS containing 50 μg of encapsulated OVA or 50 μg of soluble OVA. One day after vaccination, 500,000 OVA-specific OT-I CD8$^+$ T cells were injected intravenously in the tail vein in 200 μL PBS. Mice were sacrificed 4 days after T cell transfer to analyze the expansion of the transferred OVA-specific T cells caused by presentation of the OVA antigen. Vaccine-draining inguinal lymph nodes and the spleen were taken out, mashed on 70 μm cell strainers (Becton Dickinson) and the cells were stained with fluorescently labeled antibodies for CD8β and the OT-I congenic marker CD90.1 (Thy1.1), and analyzed by flow cytometry. T cell expansion expressed as the number of transferred (OT-I) T cells as a percentage from total CD8$^+$ T cells (68).

Statistical analysis

GraphPad Prism software was used for statistical analysis. Two groups were comparing by unpaired two-tailed Student's t-test with alpha=0.05. Statistical significance was considered when $p < 0.05$.

Results and Discussion

Synthesis and characterization of pLHMGA

A random copolymer of BMMG and d,l-lactide was synthesized by using BnOH and $SnOct_2$ as initiator and catalyst, respectively, via ring opening polymerization in the melt (**Figure 1**) and the polymer was obtained in high yield (~100%). The protective benzyl groups were subsequently removed overnight by hydrogenation to yield pLHMGA (83%). The structures of the synthesized polymers were confirmed by ^{1}H NMR spectroscopy and this analysis showed that the molar ratio of BMMG and d,l-lactide in pLBMGA (protected polymer) was 48/52, which is close to feed ratio (50/50). Both pLBMGA and pLHMGA were amorphous with T_g values of 39 °C and 57 °C, respectively, which were similar to values reported earlier (39) and confirmed the random structure of the polymers. GPC analysis showed that the number average molecular weight of pLHMGA (16.2 kDa) was close to the aimed

molecular weight based on monomer-to-initiator molar ratio (15.8 kDa) and the PDI was 1.6. Based on previous studies using the same polymers, in our study we chose a relatively low molecular weight polymer in order to achieve small nanoparticles with high loading and fast release.

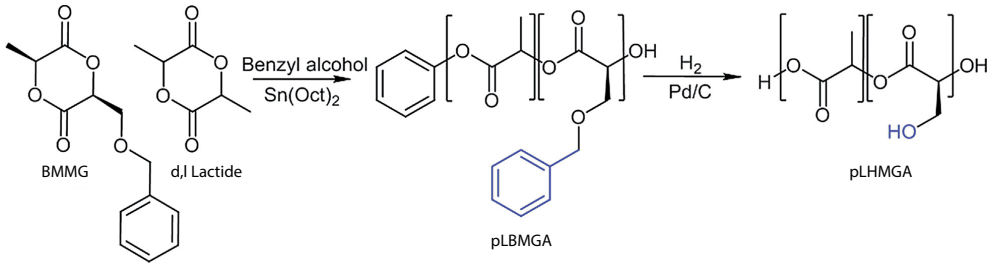

Figure 1. Synthesis of poly(lactic-co-hydroxymethylglycolic acid) (pLHMGA) in two steps. Synthesis of poly(lactic-co-benzyloxymethylglycolic acid) (pLBMGA) via ring opening polymerization of BMMG and D,L-lactide, followed by removing the benzyl group by hydrogenation to yield pLHMGA.

Synthesis and characterization of hexyn-pDLLA and NIR10-pDLLA

An alkyne-bearing homopolymer of d,l lactide (hexyn-pDLLA) was synthesized by using 1-hexyn-6-ol as initiator and stannous octoate as catalyst. The alkyne functionality in this polymer provides the possibility to conjugate azide-bearing molecules via click chemistry. The obtained polymer was amorphous with a T_g of 50 °C, similar to values reported in the literature (69). GPC analysis showed that the number average molecular weight of hexyn-pDLLA (11.0 kDa) was close to that of the aimed molecular weight based on monomer-to-initiator ratio (10.1 kDa). To obtain a NIR fluorescent-labeled polymer, the azide-NIR10 was coupled to hexyn-pDLLA by click reaction. Analysis of the reaction mixture after 16 hours by GPC with UV detection confirmed the presence of labeled polymer at a retention time of 20 minutes corresponding to that of the polymer, while a peak was also observed at 23.5 min, which corresponds to the retention time of the free dye. From the chromatogram a coupling efficiency of 85% was calculated. After purification, GPC analysis showed that the polymer contained 8% of free dye. GPC analysis of the freeze dried particles containing NIR10-pDLLA showed that only a negligible amount of free dye was present in the particles indicating that most of the free dye was removed during particle preparation process.

Characterization of IR680-OVA and IR800-OVA

In order to prepare a traceable OVA for *in vivo* imaging, the NHS ester of IRdye680RD was conjugated to OVA and the obtained IR680-OVA was analyzed by GPC. Overlapping peaks corresponding to OVA (excitation 280 and emission 340 nm) and IR680 (excitation 672 and emission 694 nm) in the GPC chromatogram of the purified IR680-OVA confirmed that the IR680 was indeed conjugated to OVA. No additional peaks (fluorescence detection) were observed, indicating that the

free dye was completely removed by purification. Conjugation efficiency calculated by UV measurements showed an average molar dye/protein ratio of 1.7. IR800-OVA was successfully prepared and purified as described for IR680-OVA. The average molar dye/protein ratio was 1.0.

Table 1. Characteristics of NPs. Average ± SD (n=3) of representative data.

	Size (nm) (DLS)	PDI (DLS)	Loading (%)	Loading efficiency (%)
Empty NPs	364 ± 40	0.22 ± 0.08	-	-
OVA NPs	340 ± 4	0.19 ± 0.04	1.71 ± 0.01	57.4 ± 0.4
Dual labeled NPs	293 ± 3	0.15 ± 0.02	1.37 ± 0.01	69.0 ± 0.4
Alexa-OVa NPs	384 ± 20	0.33 ± 0.05	1.15 ± 0.02	57.6 ± 0.4

Preparation and characterization of empty and OVA loaded NPs

Empty and OVA-loaded NPs particles were prepared by a double emulsion-solvent evaporation method, which is a well-known procedure and has been used frequently for encapsulation of hydrophilic drugs as well as biotherapeutics (70-73). Empty and OVA loaded NPs with NIR fluorescent dyes on the polymer and/or the protein antigen had comparable characteristics in terms of morphology and size. DLS analysis showed that the mean hydrodynamic diameter of the NPs ranged from 290-370 nm with a PDI of 0.16 - 0.27 (**Table 1**). The particle preparation procedure was optimized in order to obtain nanoparticles with a size of around 300 nm because nanoparticles of 300 nm were most efficient in activation of dendritic cells and inducing a systemic immune response as compared to bigger particles (74). Analysis of freeze-dried samples with TEM showed spherical NPs with a size ranging from 150-250 nm (**Figure 2**), which is smaller than the sizes obtained with DLS. This is due to the fact that DLS reports the hydrodynamic diameter of the particles based on scattering intensity which is proportional to the 6^{th} power of the particle diameter, and therefore in polydisperse samples, relatively low scattering intensities of small particles are overshadowed by high scattering intensities of big particles, resulting in a skewed average size (75,76). The loading efficiency of unlabeled as well as labeled OVA in NPs was about 60%. The *in vitro* release of OVA from pLHMGA particles was studied by using dual labeled NPs (containing IR680-OVA).

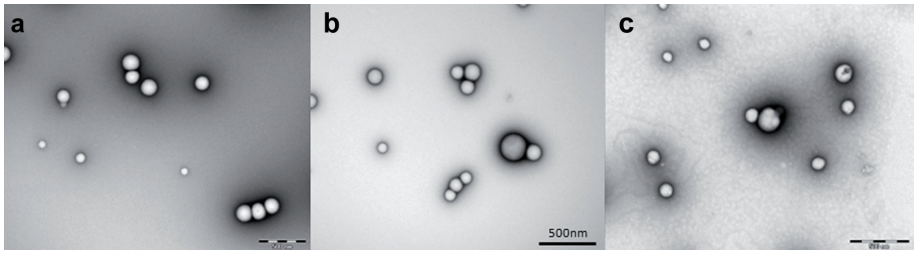

Figure 2. TEM images of **(a)** empty NPs, **(b)** unlabeled OVA NPs and **(c)** dual-labeled NPs. Bar scale = 500 nm.

Figure 3 shows that the particles had a low burst release of about 5%, followed by sustained release up to 70% for 30 days. These data are in line with previous studies of pLHMGA particles with the same copolymer composition and loaded with bovine serum albumin (77). Considering slight variations in the loading efficiency of the nanoparticles and in order to allow a fair comparison in functional experiments, a fixed amount of OVA was used in various in vitro and in vivo studies.

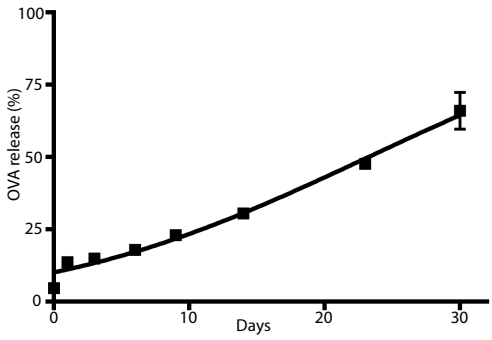

Figure 3. In vitro release of IR680-OVA from pLHMGA NPs. Dual labeled NPs were dispersed in PBS (1 mg/mL) and kept at 37 °C under mild agitation. Following a low burst release of about 5%, IR680-OVA was release in a sustained manner in 30 days up to 70%.

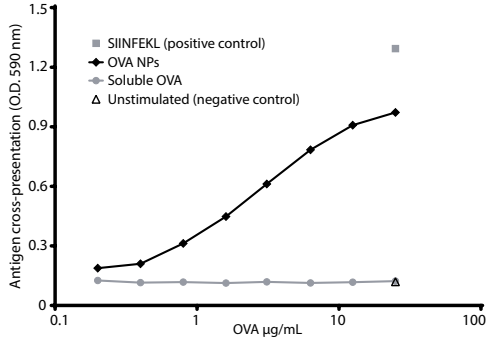

Figure 4. In vitro protein cross-presentation of OVA-encapsulated NPs. DCs were incubated with 0.2-25 µg OVA/mL encapsulated in NPs or in soluble form, and co-cultured with OVA-specific B3Z hybridoma T cells overnight. Optical density (O.D.) at 590 nm is a measure of OVA cross-presentation by DCs to B3Z cells. The SIINFEKL peptide positive control was used at 100 ng/mL. n=3, representative graph of 5 independent experiments.

Cytocompatibility of empty and OVA loaded NPs

To assess the cytocompatibility of NPs, dendritic cells were incubated with empty and OVA NPs as well as dual labeled NPs for 16 hours at 37 °C. Dead cells were quantified by using 7-AAD, a DNA binding fluorescent dye which stains cells that have lost membrane integrity (78). Dendritic cells incubated with LPS and soluble OVA corresponding to the amounts of OVA in the loaded nanoparticles were used as controls. Cell viability was about 90% for dendritic cells incubated with empty and OVA-loaded nanoparticles (concentration of NPs ranging from 7.8-1000 µg/mL, data not shown), showing the cytocompatibility of these particles.

Antigen cross-presentation *in vitro*

D1 dendritic cells were incubated with (Alexa 647-OVA)-loaded NPs overnight and visualized by confocal microscopy to verify that OVA NPs are efficiently taken up by dendritic cells (data not shown). Subsequently, we wanted to test whether the uptake of OVA NPs by DCs leads to processing and cross-presentation of the OVA antigen to OVA-specific T cells. To this end, DCs were incubated with OVA NPs and co-cultured with OVA-specific B3Z hybridoma T cells. **Figure 4** shows that OVA NPs induced antigen-specific T cell activation in a dose-dependent manner, while soluble OVA failed to activate T cells even at high doses. Since this assay is based on

the immunological principle of antigen-specificity of T cells, the T cell activation is the result of uptake, processing and cross-presentation of the antigen by DCs to T cells. Furthermore, the dual labeled NPs were equally efficient in T cell activation as the unlabeled NPs (data not shown), showing that labeling did not affect the ability of NPs to induce *in vitro* cross-presentation.

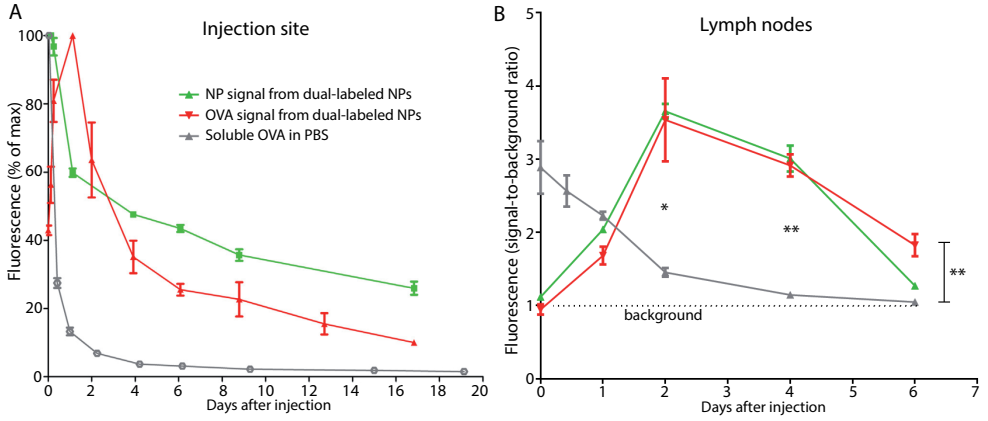

Figure 5. In vivo tracking of NPs and OVA antigen. Quantification of the fluorescent signal of IR680 and NIR10 in dual labeled NPs (containing NIR10 dye on the polymer and IR680 on the OVA), and IR800 signal of soluble antigen (IR800-OVA in PBS) after s.c. injection of 50 µg OVA in NPs or in soluble form. **(A)** Fluorescent signal at the injection site expressed as a percentage of maximum signal. **(B)** Fluorescent signal in the draining lymph nodes expressed as signal to background ratio. Statistical significance is indicated by asterisks comparing IR680 signal in NPs vs soluble IR800-OVA. Statistical analysis was performed by unpaired Student's t-test, * = $p < 0.05$, ** = $p < 0.01$. n=mice per group.

In vivo tracking of labeled NPs

As our aim was to develop an antigen-delivery system that ensures a prolonged supply of antigen to the immune system, we visualized the presence of OVA NPs in the injection site and in the draining lymph nodes, where immune responses are initiated. The tail-base injection site was chosen as it drains specifically to the inguinal lymph nodes which are located at sufficient distance in the mouse to be able to distinguish the injection site from the lymph nodes, and to visualize and quantify their respective signals accurately. Using a dual-color *in vivo* imaging setup based on two distinct NIR fluorescent dyes, we were able to visualize the antigen and the delivery vehicle simultaneously. The NIR fluorescent dye IR680 (excitation 675 nm, emission 720 nm) was coupled to the OVA antigen and the dye NIR10 (excitation 745 nm and emission 840 nm) was coupled to the polymer to track the delivery vehicle. **Figure 5a** shows the presence of the double-labeled OVA NPs at the injection site in time, compared to a soluble formulation of NIR-labeled OVA protein in PBS. As expected, the vast majority of soluble OVA antigen leaves the injection site within the first day, leading to a short peak presence in the lymph nodes immediately after injection that rapidly decreases (**Figure 5b**). In contrast, OVA encapsulated in NPs was cleared from the injection site more gradually,

corresponding with gradual accumulation in the draining lymph nodes and remaining there for several days. **Figure 6** shows examples of the presence of NP OVA at the injection site and in the draining lymph nodes. Interestingly, the signals from the NP vehicle and its OVA content show similar patterns in the injection site and lymph nodes, suggesting that the OVA antigen arrives in the lymph nodes in encapsulated form. The increasing fluorescent signal of encapsulated IR680-OVA in the first day after injection may be caused by initial quenching of the signal, for example by the hydrophobic environment in the NPs or by self-aggregation and stacking of the dye at high concentrations (79). Hydration of the NPs and a decreased stacking of NPs at the injection site during the first day would relieve the IR680 dye from both these quenching effects.

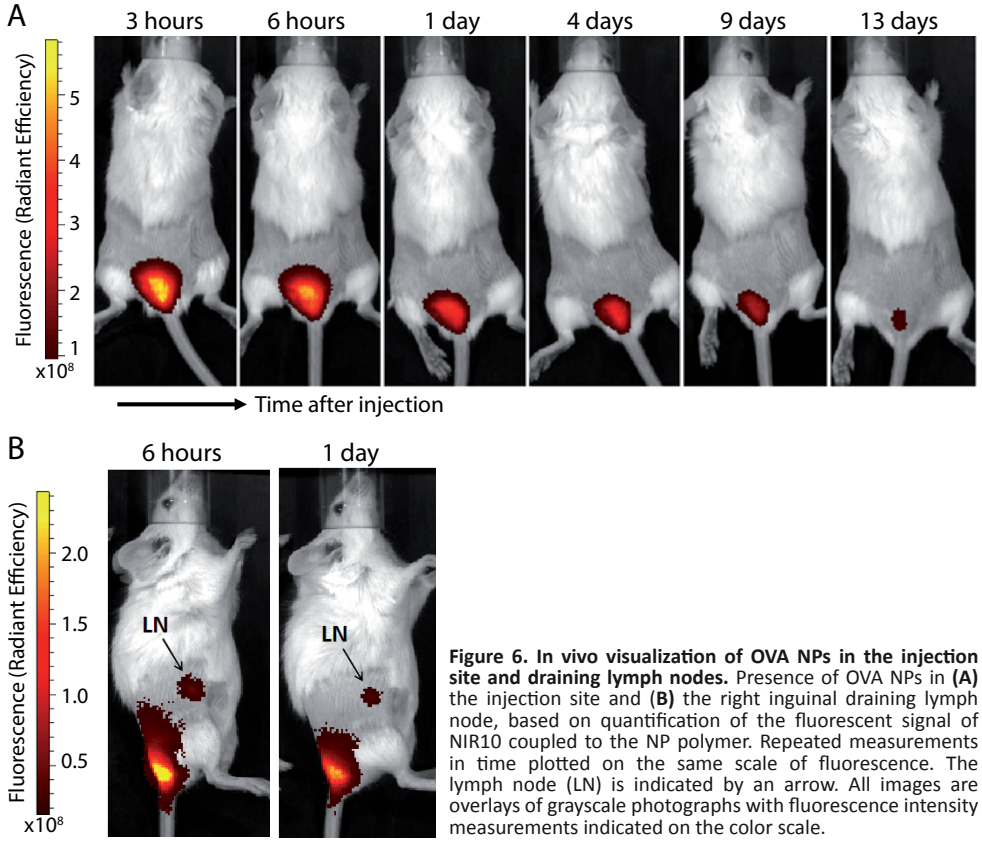

Figure 6. In vivo visualization of OVA NPs in the injection site and draining lymph nodes. Presence of OVA NPs in **(A)** the injection site and (**B)** the right inguinal draining lymph node, based on quantification of the fluorescent signal of NIR10 coupled to the NP polymer. Repeated measurements in time plotted on the same scale of fluorescence. The lymph node (LN) is indicated by an arrow. All images are overlays of grayscale photographs with fluorescence intensity measurements indicated on the color scale.

In vivo antigen cross-presentation

The efficient and prolonged delivery of antigen to the draining lymph nodes by OVA NPs led us to test their ability to induce antigen cross-presentation *in vivo*. To test this hypothesis, we administered OVA NPs to mice, followed after one day by

an adoptive transfer of OVA-specific CD8+ T cells (OT-I cells). By transferring these high numbers of OT-I T cells, we increase the precursor frequency of OVA-specific T cells to artificially high levels, which allows us to detect subtle effects in terms of cross-presentation of OVA antigen. Four days after T cell transfer, the proliferation of these transferred OT-I T cells as a result of *in vivo* cross-presentation of the OVA antigen was assessed in the vaccine-draining lymph nodes and the spleen (**Figure 7**). A strong expansion of OT-I cells was found in the lymph nodes and spleen of mice treated with OVA NPs, which proved far superior to the administration of soluble OVA. The absence of T cell proliferation after injection of equal amounts of empty NPs shows that the delivery system itself plays no role and emphasizes the antigen-specific nature of T cell activation. These results correspond with the superior ability of OVA NPs over soluble OVA to induce *in vitro* antigen cross-presentation to OVA-specific CD8+ T cells (**Figure 4**).

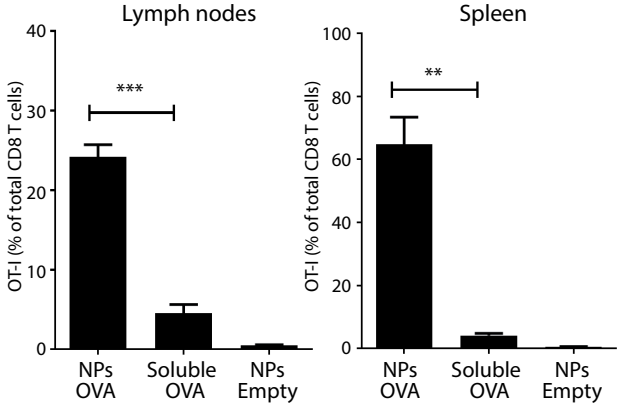

Figure 7. In vivo cross-presentation of OVA antigen to OVA-specific CD8 T cells. Expansion of TCR-transgenic OVA-specific CD8 T cells (OT-I) in the draining lymph nodes and spleen, 4 days after transfer into recipient mice. One day before the OT-I transfer, mice were treated subcutaneously with 50 µg OVA either in soluble form or in 400 µg of NPs or with 400 µg of empty NPs. In vivo expansion of the transferred OT-I T cells was quantified by ex vivo flow cytometry and expressed as the percentage of total CD8 T cells. n = 3-4 mice per group, representative of 2 independent experiments. Student's t-test showed significant difference in OT-I T cell expansion between mice treated with OVA NPs versus soluble OVA, ** = $p < 0.01$, *** = $p < 0.001$.

Conclusion

We developed an antigen delivery system based on pLHMGA nanoparticles encapsulating the model protein antigen OVA. The nanoparticles showed sustained release of antigen *in vitro* and were able to induce *in vitro* antigen cross-presentation by DCs to antigen-specific T cells. Near-infrared fluorescence imaging showed that the antigen is efficiently transported from the injection site to the draining lymph nodes, both in encapsulated and in free form. In these lymph nodes, the OVA NPs exhibited a strong capacity to induce antigen-specific $CD8^+$ T cell proliferation through cross-presentation of the antigen. In conclusion, pLHMGA nanoparticles are attractive vehicles for protein antigen delivery for effective stimulation of the cellular immune system.

Acknowledgements

We thank Ana Luisa Silva, Paul Werkhoven, Nataschja Ho and Joep van den Dikkenberg for technical assistance and useful suggestions. This research was performed within the framework of the Cancer Vaccine Tracking project (#03O-302), Center for Translational Molecular Medicine (CTMM).

References

1. Silva JM, Videira M, Gaspar R, Preat V, Florindo HF. Immune system targeting by biodegradable nanoparticles for cancer vaccines. J Control Release 2013;168:179e99.
2. Reddy ST, Swartz MA, Hubbell JA. Targeting dendritic cells with biomaterials: developing the next generation of vaccines. Trends Immunol 2006;27:573e9.
3. Akagi T, Baba M, Akashi M. Biodegradable nanoparticles as vaccine adjuvants and delivery systems: regulation of immune responses by nanoparticle-based vaccine. Polym Nanomedicine 2012;247:31e64.
4. Banchereau J, Briere F, Caux C, Davoust J, Lebecque S, Liu YJ, et al. Immunobiology of dendritic cells. Annu Rev Immunol 2000;18:767e811.
5. Banchereau J, Palucka A. Dendritic cells as therapeutic vaccines against cancer. Nat Rev Immunol 2005;5:296e306.
6. Banchereau J, Steinman RM. Dendritic cells and the control of immunity. Nature 1998;392:245e52.
7. Lanzavecchia A. Mechanisms of antigen uptake for presentation. Curr Opin Immunol 1996;8:348e54.
8. Vyas JM, Van der Veen AG, Ploegh HL. The known unknowns of antigen processing and presentation. Nat Rev Immunol 2008;8:607e18.
9. Schuurhuis D, Laban S, Toes R, Ricciardi-Castagnoli P, Kleijmeer M, van der Voort E, et al. Immature dendritic cells acquire CD8(+) cytotoxic T lymphocyte priming capacity upon activation by T helper cell-independent or –dependent stimuli. J Exp Med 2000;192:145e50.
10. Elamanchili P, Diwan M, Cao M, Samuel J. Characterization of poly(D,L-lacticco- glycolic acid) based nanoparticulate system for enhanced delivery of antigens to dendritic cells. Vaccine 2004;22:2406e12.
11. Elamanchili P, Lutsiak CME, Hamdy S, Diwan M, Samuel J. “Pathogenmimicking” nanoparticles for vaccine delivery to dendritic cells. J Immunother 2007;30:378e95.
12. Gregory AE, Titball R, Williamson D. Vaccine delivery using nanoparticles. Front Cell Infect Microbiol 2013;3.
13. Bolhassani A, Safaiyan S, Rafati S. Improvement of different vaccine delivery systems for cancer therapy. Mol Cancer 2011;10(3).
14. Joshi MD, Unger WJ, Storm G, van Kooyk Y, Mastrobattista E. Targeting tumor antigens to dendritic cells using particulate carriers. J Control Release 2012;161:25e37.
15. Krishnamachari Y, Geary SM, Lemke CD, Salem AK. Nanoparticle delivery systems in cancer vaccines. Pharm Res 2011;28:215e36.
16. Mahapatro A, Singh DK. Biodegradable nanoparticles are excellent vehicle for site directed in-vivo delivery of drugs and vaccines. J Nanobiotechnol 2011;9:55.
17. Park YM, Lee SJ, Kim YS, Lee MH, Cha GS, Jung ID, et al. Nanoparticle-based vaccine delivery for cancer immunotherapy. Immune Netw 2013;13:177e83.
18. Zhang Z, Tongchusak S, Mizukami Y, Kang YJ, Ioji T, Touma M, et al. Induction of anti-tumor cytotoxic T cell responses through PLGA-nanoparticle mediated antigen delivery. Biomaterials 2011;32:3666e78.

19. Hamdy S, Haddadi A, Hung RW, Lavasanifar A. Targeting dendritic cells with nano-particulate PLGA cancer vaccine formulations. Adv Drug Deliv Rev 2011;63:943e55.
20. Demento SL, Cui W, Criscione JM, Stern E, Tulipan J, Kaech SM, et al. Role of sustained antigen release from nanoparticle vaccines in shaping the T cell memory phenotype. Biomaterials 2012;33:4957e64.
21. Melief CJM. Cancer immunotherapy by dendritic cells. Immunity 2008;29:372e83.
22. van Montfoort N, Camps MG, Khan S, Filippov DV, Weterings JJ, Griffith JM, et al. Antigen storage compartments in mature dendritic cells facilitate prolonged cytotoxic T lymphocyte cross-priming capacity. Proc Natl Acad Sci USA 2009;106:6730e5.
23. Ma W, Chen M, Kaushal S, McElroy M, Zhang Y, Ozkan C, et al. PLGA nanoparticle-mediated delivery of tumor antigenic peptides elicits effective immune responses. Int J Nanomedicine 2012;7:1475e87.
24. Ye M, Kim S, Park K. Issues in long-term protein delivery using biodegradable microparticles. J Control Release 2010;146:241e60.
25. Giteau A, Venier-Julienne MC, Aubert-Pouessel A, Benoit JP. How to achieve sustained and complete protein release from PLGA-based microparticles? Int J Pharm 2008;350:14e26.
26. Sinha V, Trehan A. Biodegradable microspheres for protein delivery. J Control Release 2003;90:261e80.
27. van de Weert M, Hennink WE, Jiskoot W. Protein instability in poly(lactic-coglycolic acid) microparticles. Pharm Res 2000;17:1159e67.
28. Brannon-Peppas L, Blanchette J. Nanoparticle and targeted systems for cancer therapy. Adv Drug Deliv Rev 2004;56:1649e59.
29. Jain R. The manufacturing techniques of various drug loaded biodegradable poly(lactide-co-glycolide) (PLGA) devices. Biomaterials 2000;21:2475e90.
30. O'Hagan D, Singh M, Gupta R. Poly(lactide-co-glycolide) microparticles for the development of single-dose controlled-release vaccines. Adv Drug Deliv Rev 1998;32:225e46.
31. Rosalia RA, Silva AL, Camps M, Allam A, Jiskoot W, van der Burg SH, et al. Efficient ex vivo induction of T cells with potent anti-tumor activity by protein antigen encapsulated in nanoparticles. Cancer Immunol Immunother 2013;62:1161e73.
32. Mueller M, Schlosser E, Gander B, Groettrup M. Tumor eradication by immunotherapy with biodegradable PLGA microspheres-an alternative to incomplete Freund's adjuvant. Int J Cancer 2011;129:407e16.
33. Ding AG, Schwendeman SP. Acidic microclimate pH distribution in PLGA microspheres monitored by confocal laser scanning microscopy. Pharm Res 2008;25:2041e52.
34. Sophocleous AM, Zhang Y, Schwendeman SP. A new class of inhibitors of peptide sorption and acylation in PLGA. J Control Release 2009;137:179e84.
35. Houchin ML, Topp EM. Chemical degradation of peptides and proteins in PLGA: a review of reactions and mechanisms. J Pharm Sci 2008;97:2395e404.
36. Kim HK, Park TG. Microencapsulation of human growth hormone within biodegradable polyester microspheres: protein aggregation stability and incomplete release mechanism. Biotechnol Bioeng 1999;65:659e67.
37. Hermeling S, Crommelin DJA, Schellekens H, Jiskoot W. Structure-immunogenicity relationships of therapeutic proteins. Pharm Res 2004;21:897e903.
38. Liu Y, Ghassemi AH, Hennink WE, Schwendeman SP. The microclimate pH in poly(D,L-lactide-co-hydroxymethyl glycolide) microspheres during biodegradation. Biomaterials 2012;33:7584e93.
39. Ghassemi AH, van Steenbergen MJ, Talsma H, van Nostrum CF, Jiskoot W, Crommelin DJA, et al. Preparation and characterization of protein loaded microspheres based on a hydroxylated aliphatic polyester, poly(lactic-cohydroxymethyl glycolic acid). J Control Release 2009;138:57e63.
40. Ghassemi AH, van Steenbergen MJ, Barendregt A, Talsma H, Kok RJ, van Nostrum CF, et al. afs controlled release of octreotide and assessment of peptide acylation from poly(D,L-lactide-co-

hydroxymethyl glycolide) compared to PLGA microspheres. Pharm Res 2012;29:110e20.
41. Samadi N, van Nostrum CF, Vermonden T, Amidi M, Hennink WE. Mechanistic studies on the degradation and protein release characteristics of poly(lactic co-glycolic-co-hydroxymethylglycolic acid) nanospheres. Biomacromolecules 2013;14:1044e53.
42. Srinivas M, Cruz LJ, Bonetto F, Heerschap A, Figdor CG, de Vries IJM. Customizable, multi-functional fluorocarbon nanoparticles for quantitative in vivo imaging using F-19 MRI and optical imaging. Biomaterials 2010;31: 7070e7.
43. Verdijk P, Scheenen TWJ, Lesterhuis WJ, Gambarota G, Veltien AA, Walczak P, et al. Sensitivity of magnetic resonance imaging of dendritic cells for in vivo tracking of cellular cancer vaccines. Int J Cancer 2007;120:978e84.
44. Long CM, van Laarhoven HWM, Bulte JWM, Levitsky HI. Magnetovaccination as a novel method to assess and quantify dendritic cell tumor antigen capture and delivery to lymph nodes. Cancer Res 2009;69:3180e7.
45. Yang Z, Zheng S, Harrison WJ, Harder J, Wen X, Gelovani JG, et al. Longcirculating near-infrared fluorescence core-cross-linked polymeric micelles: synthesis, characterization, and dual nuclear/optical imaging. Biomacromolecules 2007;8:3422e8.
46. Heo MB, Lim YT. Programmed nanoparticles for combined immunomodulation, antigen presentation and tracking of immunotherapeutic cells. Biomaterials 2014;35:590e600.
47. Christian NA, Benencia F, Milone MC, Li G, Frail PR, Therien MJ, et al. In Vivo dendritic cell tracking using fluorescence lifetime imaging and near-infraredemissive polymersomes. Mol Imaging Biol 2009;11:167e77.
48. Frangioni J. In vivo near-infrared fluorescence imaging. Curr Opin Chem Biol 2003;7:626e34.
49. Escobedo JO, Rusin O, Lim S, Strongin RM. NIR dyes for bioimaging applications. Curr Opin Chem Biol 2010;14:64e70.
50. Key J, Leary JF. Nanoparticles for multimodal in vivo imaging in nanomedicine. Int J Nanomedicine 2014;9:711e26.
51. Rao J, Dragulescu-Andrasi A, Yao H, Yao H. Fluorescence imaging in vivo: recent advances. Curr Opin Biotechnol 2007;18:17e25.
52. Mou Y, Hou Y, Chen B, Hua Z, Zhang Y, Xie H, et al. In vivo migration of dendritic cells labeled with synthetic superparamagnetic iron oxide. Int J Nanomedicine 2011;6:2633e40.
53. Su H, Mou Y, An Y, Han W, Huang X, Xia G, et al. The migration of synthetic magnetic nanoparticle labeled dendritic cells into lymph nodes with optical imaging. Int J Nanomedicine 2013;8:3737e44.
54. Chen YC, Wen S, Shang SA, Cui Y, Luo B, Teng GJ. Magnetic resonance and near-infrared imaging using a novel dual-modality nano-probe for dendritic cell tracking in vivo. Cythotherapy 2014;16:699e710.
55. Lee H, Mason JC, Achilefu S. Heptamethine cyanine dyes with a robust CeC bond at the central position of the chromophore. J Org Chem 2006;71:7862e5.
56. Leemhuis M, van Nostrum C, Kruijtzer J, Zhong Z, ten Breteler M, Dijkstra P, et al. Functionalized poly(alpha-hydroxy acid)s via ring-opening polymerization: toward hydrophilic polyesters with pendant hydroxyl groups. Macromolecules 2006;39:3500e8.
57. Kolb H, Finn M, Sharpless K. Click chemistry: diverse chemical function from a few good reactions. Angew Chemie Int Ed 2001;40:2004.
58. van Dijk M, Rijkers DTS, Liskamp RMJ, van Nostrum CF, Hennink WE. Synthesis and applications of biomedical and pharmaceutical polymers via click chemistry methodologies. Bioconjug Chem 2009;20:2001e16.
59. Moses JE, Moorhouse AD. The growing applications of click chemistry. Chem Soc Rev 2007;36:1249e62.
60. Binder WH, Sachsenhofer R. 'Click' chemistry in polymer and material science: an update. Macromol Rapid Commun 2008;29:952e81.
61. Gill SC, von Hippel PH. Calculation of protein extinction coefficients from amino acid sequence

data. Anal Biochem 1989;182:319e26.
62. Silva AL, Rosalia RA, Sazak A, Carstens MG, Ossendorp F, Oostendorp J, et al. Optimization of encapsulation of a synthetic long peptide in PLGA nanoparticles: low-burst release is crucial for efficient CD8(þ) T cell activation. Eur J Pharm Biopharm 2013;83:338e45.
63. Sah H. A new strategy to determine the actual protein content of poly(lactideco-glycolide) microspheres. J Pharm Sci 1997;86:1315e8.
64. Winzler C, Rovere P, Rescigno M, Granucci F, Penna G, Adorini L, et al. Maturation stages of mouse dendritic cells in growth factor-dependent longterm cultures. J Exp Med 1997;185:317e28.
65. Karttunen J, Sanderson S, Shastri N. Detection of rare antigen-presenting cells by the lacZ T-cell activation assay suggests an expression cloning strategy for T-cell antigens. PNAS 1992;89:6020e4.
66. Shastri N, Gonzalez F. Endogenous generation and presentation of the ovalbumin peptide/k(b) complex to T-cells. J Immunol 1993;150:2724e36.
67. Filonov GS, Piatkevich KD, Ting L, Zhang J, Kim K, Verkhusha VV. Bright and stable near-infrared fluorescent protein for in vivo imaging. Nat Biotechnol 2011;29:757e61.
68. Hogquist KA, Jameson SC, Heath WR, Howard JL, Bevan MJ, Carbone FR. T cell receptor antagonist peptides induce positive selection. Cell 1994;76:17e27.
69. Perego G, Cella GD, Bastioli C. Effect of molecular weight and crystallinity on poly(lactic acid) mechanical properties. J Appl Polym Sci 1996;59:37e43.
70. Cohen S, Yoshioka T, Lucarelli M, Hwang L, Langer R. Controlled delivery systems for proteins based on poly(lactic glycolic acid) microspheres. Pharm Res 1991;8:713e20.
71. Mundargi RC, Babu VR, Rangaswamy V, Patel P, Aminabhavi TM. Nano/micro technologies for delivering macromolecular therapeutics using poly(D,L-lactide-co-glycolide) and its derivatives. J Control Release 2008;125:193e209.
72. Zambaux M, Bonneaux F, Gref R, Maincent P, Dellacherie E, Alonso M, et al. Influence of experimental parameters on the characteristics of poly(lactic acid) nanoparticles prepared by a double emulsion method. J Control Release 1998;50:31e40.
73. Couvreur P, Puisieux F. Nanoparticles and microparticles for the delivery of polypeptides and proteins. Adv Drug Deliv Rev 1993;10:141e62.
74. Joshi VB, Geary SM, Salem AK. Biodegradable particles as vaccine delivery systems: size matters. Aaps J 2013;15:85e94.
75. Dhawan A, Sharma V. Toxicity assessment of nanomaterials: methods and challenges. Anal Bioanal Chem 2010;398:589e605.
76. Patterson JP, Robin MP, Chassenieux C, Colombani O, O'Reilly RK. The analysis of solution self-assembled polymeric nanomaterials. Chem Soc Rev 2014;43:2412e25.
77. Ghassemi AH, van Steenbergen MJ, Talsma H, van Nostrum CF, Crommelin DJA, Hennink WE. Hydrophilic polyester microspheres: effect of molecular weight and copolymer composition on release of BSA. Pharm Res 2010;27:2008e17.
78. Zembruski NCL, Stache V, Haefeli WE, Weiss J. 7-Aminoactinomycin D for apoptosis staining in flow cytometry. Anal Biochem 2012;429:79e81.
79. Zhegalova NG, He S, Zhou H, Kim DM, Berezin MY. Minimization of selfquenching fluorescence on dyes conjugated to biomolecules with multiple labeling sites via asymmetrically charged NIR fluorophores. Contrast Media Mol Imaging 2014;9:355e62.

Chapter 6

A dual-color bioluminescence reporter mouse for simultaneous in vivo imaging of T cell localization and activation

Jan Willem Kleinovink, Laura Mezzanotte, Giorgia Zambito, Marieke Fransen, Luis J. Cruz, Sjef Verbeek, Alan Chan, Ferry Ossendorp, Clemens Löwik

In revision

Abstract

Non-invasive imaging technologies to visualize the location and functionality of T cells are of great value in immunology. Here, we describe the design and generation of a transgenic mouse whose T cells contain both a constitutively expressed green-emitting click-beetle luciferase (CBG99) and a T cell activation-dependent red-emitting firefly luciferase (PpyRE9), allowing multicolor bioluminescence imaging of T cell location and activation. This dual-luciferase mouse, which we named TbiLuc, showed a high constitutive luciferase expression in lymphoid organs such as lymph nodes and the spleen. Ex vivo purified lymphocytes showed functional expression in both CD8 and CD4 T cells, whereas B cells showed no detectable signal. We cross-bred TbiLuc mice to T cell receptor-transgenic OT-I mice to obtain luciferase-expressing naïve CD8 T cells with defined antigen-specificity. TbiLuc*OT-I T cells showed a fully antigen-specific induction of the T cell activation-dependent luciferase. In vaccinated mice, we visualized T cell localization and activation in vaccine-draining lymph nodes with high sensitivity using two distinct luciferase substrates, D-luciferin and CycLuc1, of which the latter specifically reacts with the PpyRE9 enzyme. This dual-luciferase T cell reporter mouse can be applied in many experimental models studying the location, expansion and functional state of T cells.

Introduction

Bioluminescence imaging (BLI) is an optical molecular imaging technique based on the emission of light produced by luciferase enzymes expressed in cells or whole animals. It has been extensively used to study gene expression, using genetic constructs in which expression of the luciferase is driven by the promoter of the gene of interest (1). A common application of BLI is the monitoring of tumor cell growth using luciferase-expressing tumor cells (2). Besides functioning as a quantitative measure for cell number, BLI also provides information on cell viability as the light-producing reaction mediated by firefly or click beetle luciferases requires ATP, oxygen, and $Mg2^{+}$, thus the context of a living cell (3,4). Commonly, retroviral or lentiviral constructs harboring the luciferase gene coupled to a specific promoter are designed to integrate the luciferase gene into cells by viral transduction. Alternatively, luciferase-transgenic reporter mouse strains can be developed using similar constructs, requiring more time and effort but becoming a source of luciferase-expressing cells without the need for further modification. Such transgenic models are especially valuable if the cells of interest are to be studied in their natural, unmodified state.

BLI technology is highly suited to analyze the immune system in vivo, because it allows real-time visualization of the typically strong dynamics of many immune cells, which often change location and expand or contract in number over short periods of time. These characteristics are particularly true for T lymphocytes, also known as T cells, which are crucial effector cells in the cellular arm of the immune system. In particular, T cells are responsible for the clearance of viral infections and the eradication of tumors. T cells are found in high numbers in lymphoid organs such as the spleen and lymph nodes, but also circulate in the bloodstream to patrol the body and enter peripheral tissues in case these harbor their target. These properties make T cells an attractive target for BLI. Thus far, many attempts to create luciferase-expressing T cells have used viral transduction of T cells. However, T cells in their untouched natural state, immunologically referred to as ‘naïve T cells’, are practically impossible to transduce. Therefore, in order to allow their transduction, T cells are first artificially activated in vitro which facilitates their transduction, and often rested for several days before use in an experiment (5–9). However, the transition of a T cell from the naïve to the activated state is not fully reversible, as T cell activation starts transcriptional programs that cannot be reversed. Hence, although commonly ignored, the results obtained with BLI of such transduced T cells cannot be directly compared to the natural situation in which new T cell responses start with naïve T cells. These drawbacks have led to the production of a number of T cell luciferase-transgenic mouse models to allow the tracking of T cells

(10–12). While definitely a step forward from using transduced T cells, these single-luciferase transgenic models have the limitation that they only provide information on the location of T cells, but not their functional state.

We have previously shown that the click-beetle green luciferase mutant CBG99 and the red-emitting firefly mutant PpyRE9 can be efficiently combined for multicolor in vivo bioluminescence imaging of transplanted cells previously transduced with a single luciferase, using the substrate D-luciferin (13). In this study, we show the design and generation of a transgenic mouse model called TbiLuc, which contains the genes of the two abovementioned luciferases, expressed in T cells, allowing dual color visualization of T cell location and activation. In TbiLuc, naïve T cells constitutively express CBG99 luciferase driven by the CD2 promoter, while activated T cells will also express PpyRE9 luciferase driven by the NFAT promoter. We show that luciferase expression is restricted to T cells, and that antigen-specific or non-specific activation of T cells successfully induces the expression of the activation-dependent luciferase. However, the expression level of the two luciferases influences the ability to efficiently separate the two light signals in vivo using a single substrate. Therefore, we combined the recently developed luciferase substrate CycLuc1(14) as a specific substrate for firefly luciferases (such as PPyRE9) with D-luciferin as a substrate for the CBG99 enzyme. Our finding that CycLuc1 is not an efficient substrate for CBG99 allowed us to efficiently separate light signals in vivo using TbiLuc T cells. We cross-bred TbiLuc mice to T cell receptor-transgenic OT-I mice and subsequently localized vaccine-specific CD8 T cells in lymphoid organs and visualize their activation upon vaccination and addition of the two distinct luciferase substrates.

In summary, we have developed a dual-luciferase T cell reporter mouse which allows live bioluminescence imaging of T cell location and activation, which has numerous possible applications in many experimental models where T cells play a central role.

Materials and Methods

Mice and cell lines

The following construct was designed for the generation of the TbiLuc transgenic mouse. The PpyRE9 gene (Photinus pyralis red-emitting luciferase 9, a kind gift of Prof. Branchini (29)) was cloned downstream of 3 NFAT repetitive elements and minimal promoter derived from the pGL4.30 plasmid (Promega). The sequence of the human CD2 promoter was cloned upstream of the CBG99 green click beetle luciferase gene (15,25). These two cassettes were cloned to form a bidirectional construct, separated by an insulator. TbiLuc mice were generated by injection of the

bicistronic construct into pronuclei of fertilized oocytes of CBA*C57BL/6 mice. In the pups born the presence of the transgene was determined by a specific PCR using genomic DNA from tail biopsy and its activity/ function was measured by evaluation of light emission from tail-vein blood after addition of the luciferase substrate D-luciferin. Mice were back-crossed to the C57BL/6 strain for several generations before use in experiments. Albino B6 mice (tyrosinase-deficient immunocompetent C57BL/6 mice), TbiLuc mice (dual T cell luciferase transgenic mice), OT-I mice (T cell receptor-transgenic mice carrying the CD45.1 congenic marker) and crossed TbiLuc*OT-I mice were bred in the animal breeding facility of the Leiden University Medical Center, the Netherlands. All experiments were approved by the animal ethical committee of Leiden University. D1 is a GM-CSF-dependent immature dendritic cell line derived from C57BL/6 mice, and B3Z is an OVA-specific CD8 T cell hybridoma carrying the lacZ reporter gene induced by NFAT (30,31). Cell lines were assured to be free of rodent viruses and Mycoplasma by regular PCR analysis. Cells were cultured as previously described (32).

Bioluminescence imaging (BLI)

Cell samples were prepared for in vitro BLI analysis in sterile black-walled flat-bottom 96-wells plates (Greiner). Cells were suspended in 100 µL PBS containing 1 mM D-luciferin potassium salt (SynChem) or 1 mM CycLuc1 (Aobious), incubated for 5 minutes at 37°C. For in vivo BLI, mice were injected with 150 mg/kg D-luciferin or 7,6 mg/kg CycLuc1 intraperitoneally, left for 5 minutes and anaesthetized by isoflurane inhalation. In experiments using both substrates, the substrates were injected with a 3-hour interval. BLI imaging was performed using an IVIS Spectrum small animal imager (PerkinElmer) that measured the light signal using open filter and a series of 20 nm wavelength band filters from 500 nm to 700 nm, with an acquisition time of 30 seconds. Accompanying LivingImage 4.2 software (Perkin Elmer) was used for spectral unmixing of the full-spectrum measurement to identify individual signals in vitro. Signal quantification in specific regions of interest (ROI) was performed by using fixed-size ROIs throughout the experiments.

Isolation of organs and immune cells

Organs from TbiLuc mice were taken out, weighed and homogenized before BLI analysis. Immune cells were obtained from the spleen by mashing on 70 µm cell strainers (BD Biosciences) to create single-cell suspensions, followed by erythrocyte lysis. Then, CD4 and CD8 T cells were isolated separately by negative magnetic selection (BD IMag enrichment kits), B cells by positive magnetic selection of B220+ cells (BD), while NK cells were obtained by FACS-sorting for NK1.1+ cells.

T cell activation in vitro

T cells isolated from spleens of TbiLuc or TbiLuc*OT-I mice were stimulated overnight with 100 ng/mL Phorbol 12-myristate 13-acetate (PMA) + 1500 ng/mL ionomycin (both Sigma-Aldrich), with agonistic anti-CD3 and anti-CD28 antibodies (BD Biosciences) pre-coated at 1 µg/mL at 37°C for 30 minutes, or with 50,000 D1 dendritic cells pre-loaded with OVA immune complexes. OVA immune complexes were formed by incubating a 1:300 mass ratio of OVA protein (Worthington) and anti-OVA antibody (LSBio) for 30 minutes at 37°C, after which the immune complexes were added to D1 dendritic cells and incubated overnight. Unloaded D1 cells were incubated overnight in parallel to serve as control cells.

Adoptive transfer and vaccination

Adoptive transfer consisted of 1 million purified OT-I CD8 T-cells (unless stated otherwise) isolated as described above, injected intravenously in 200 µL PBS in the tail vein. Vaccination consisted of subcutaneous injection of 1 million D1 cells pre-loaded with OVA immune complexes, or unloaded control D1 cells, in 50 µL PBS in the tail-base region.

Western Blot

Expression of PpyRE9 luciferase by activated T cells was confirmed by Western Blot. T cells were isolated and stimulated overnight as described above. Then, 3*106 cells were lysed and the total protein content of each sample was determined by a Pierce BCA protein assay kit (Thermo Scientific). Next, 20 µg of total cell extract was applied to a 10% SDS-PAGE and transferred onto a nitrocellulose membrane. After washing, the membrane was incubated overnight with rabbit anti-luciferase polyclonal antibody in TPBS at 1/500 dilution (Fitzgerald). The GAPDH antibody (Cell Signaling Technology) was used to correct for the amount of total protein. The blots were washed, exposed to an HRP-conjugated secondary antibody for 1 hour, and detected using enhanced chemiluminescence (ECL) reagents (Thermo Scientific). Detection of ECL signals was performed with the IVIS Spectrum and quantification of bands using Living Image Software 4.2.

Flow cytometry

Before adoptive transfer of CD8 T cells, their CD8-purity and naïve phenotype was assessed by flow cytometry. In short, spleen cells were suspended in FACS buffer (PBS with 0.5% FCS and 0.02% sodium azide), surface-stained with antibodies against CD8β, CD44, CD45.1 and CD62L (BioLegend) and analyzed on a BD Accuri C6 flow cytometer. Analysis was performed on FlowJo software (FlowJo).

Statistical analysis

Statistical analysis was performed using GraphPad Prism 6.0 software. Data are shown as the mean ± SEM for each group, and comparison of groups was performed by two-tailed Student's t-test. Statistical differences were considered significant at $p < 0.05$.

Results

Design and development of the dual-luciferase transgenic TbiLuc mouse

We designed a bicistronic vector containing the click beetle green luciferase (CBG99) sequence under the control of the human CD2 (hCD2) promoter and the red-emitting firefly luciferase (PpyRE9) sequence under the control of the nuclear factor of activated T cells (NFAT) minimal promoter (**Figure 1A**). NFAT expression is absent in naïve T cells and increases strongly after T cell activation, making it an ideal promoter to visualize activated T cells. The hCD2 promoter is expressed in both T cells and B cells in humans, but is T cell-specific when used in mice (15). This bicistronic vector was used to generate the TbiLuc transgenic mouse on a C57BL/6*CBA mixed background (F1). Founders were selected based on high light emission in blood and further back-crossed towards C57BL/6 background. As expected, the CD2-driven CBG99 luciferase was constitutively expressed in lymphoid organs, which was evident both in live in vivo BLI and in isolated spleen, lymph nodes and thymus (**Figure 1B, C**).

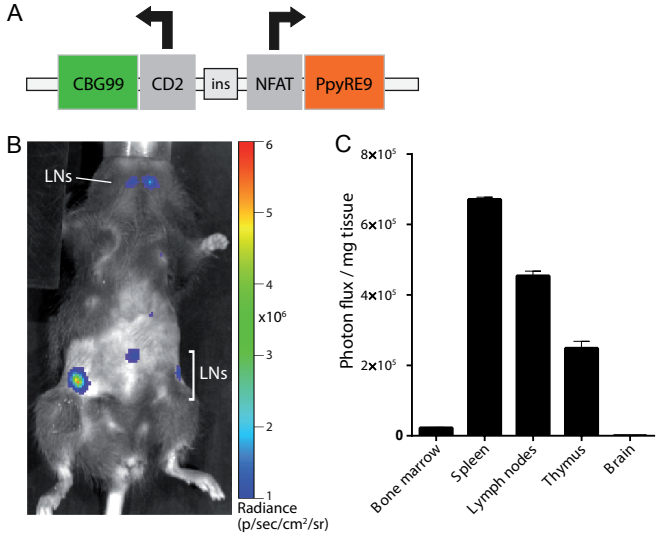

Figure 1. Design and development of the dual-luciferase transgenic TbiLuc mouse. (A) Simplified schematic overview of the dual-luciferase reporter bicistronic vector. NFAT = nuclear factor of activated T cells, CBG99 = click beetle green luciferase 99, PpyRE9 = Photinus pyralis red-emitting luciferase 9. **(B)** Bioluminescence measurement of a TbiLuc mouse, showing luciferase expression in secondary lymphoid organs. The abdomen is shaved to reduce signal absorption. Cervical, mesenteric and inguinal lymph nodes (LNs) are indicated. **(C)** Quantification of luciferase signals in several organs of TbiLuc mice (n=3), shown as photon flux per mg of tissue (mean + SEM).

Luciferase expression is restricted to T cells

Next, we analyzed in more detail which cells in the lymphoid organs express luciferase by isolating B cells, CD4 T cells, CD8 T cells and NK cells from the spleens of TbiLuc mice. Constitutive expression of CBG99 luciferase in unstimulated cells was completely restricted to T cells, as B cells and NK cells showed no detectable bioluminescence signal (**Figure 2A**, top half). CD8 T cells produced a two-fold higher luciferase activity than CD4 T cells. The amount of the luciferase activity was proportional to the number of T cells. In parallel, we tested the validity of the dual-luciferase construct by stimulating these isolated immune cells with PMA and ionomycin, which are chemical compounds often used in combination to trigger NFAT by activating the protein kinase C (PKC) pathway and increasing intracellular levels of calcium, respectively. Also after PMA/ionomycin treatment, strong luciferase activity was observed only in T cells, except for a weakly detectable signal in NK cells (**Figure 2A**, bottom half).

T cell activation results in NFAT-induced luciferase expression

We next analyzed if the increased light signal after PMA/ionomycin treatment was mediated by the NFAT-driven PpyRE9 luciferase. A spectral unmixing algorithm was applied to separate the independent emission spectra within the sample and quantify these spectra separately. Two distinct emission patterns were identified corresponding to the emission spectra of the green CBG99 and the red PpyRE9 luciferases (**Figure 2B**). By representing the unmixed signals in artificial green and red colors, the emission spectra of the two luciferases can be assessed per single sample. Unstimulated naïve T cells expressed only the constitutive hCD2-driven CBG99 luciferase, while PMA/ionomycin treatment induced the expression of NFAT-driven red PpyRE9 luciferase, resulting in a yellow color based on overlaying green and red colors (**Figure 2C**). The low signal observed in NK cells after PMA/ionomycin treatment was confirmed to be NFAT-induced, as shown by the red color. The induction of PpyRE9 luciferase expression by PMA/ionomycin treatment was further analyzed by Western Blotting, showing a clear presence of PpyRE9 luciferase protein band after stimulation of TbiLuc CD8 T cells with PMA/ionomycin (**Supplemental Figure 1A**).

Dual-luciferase imaging of antigen-specific T cells

In order to study dual-bioluminescent T cells with known antigen specificity, the TbiLuc mouse was crossed to T cell receptor-transgenic OT-I mice whose CD8 T cells recognize the SIINFEKL epitope of chicken ovalbumin (OVA) as presented in H-2Kb MHC class I molecules. The resulting TbiLuc*OT-I mice showed constitutive luciferase expression in lymphoid organs, identical to their parental TbiLuc mice (**Figure 3A**). To study NFAT-luciferase induction in an antigen-specific manner, we purified CD8 T cells from the spleens of TbiLuc*OT-I mice by magnetic selection. This procedure yielded >90% pure CD8 T cells with a naïve phenotype (**Supplemental Figure 1b**).

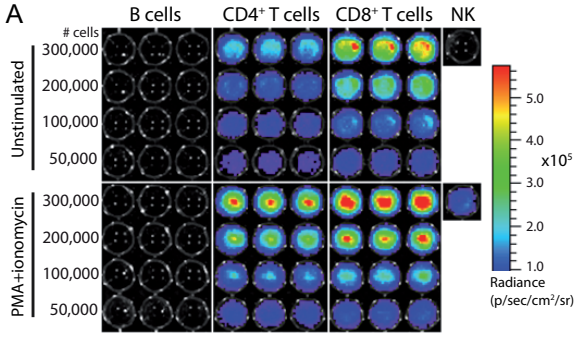

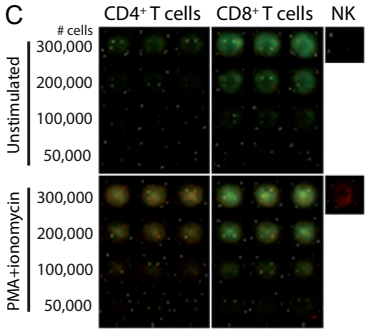

Figure 2. T cell-specific expression of constitutive and inducible luciferases in the TbiLuc mouse. B cells, T cells and NK cells were isolated from splenocytes of TbiLuc mice, plated in different amounts, and stimulated overnight with PMA and ionomycin to activate the inducible red luciferase. **(A)** Luciferase expression is restricted to CD4 and CD8 T cells and signal strength correlates to the number of T cells, both in unstimulated (top half) and PMA+ionomycin stimulated cells (bottom half). **(B)** Spectral unmixing of the total BLI signal identifies two emission spectra matching the constitutive CBG99 luciferase (green) and the inducible PpyRE9 luciferase (red). **(C)** Spectral unmixing applied to the signals from Figure A indicates that naïve T cells express only constitutive CBG99 luciferase (top half, green color), while activated T cells express both luciferases (bottom half, overlay of green and red signals).

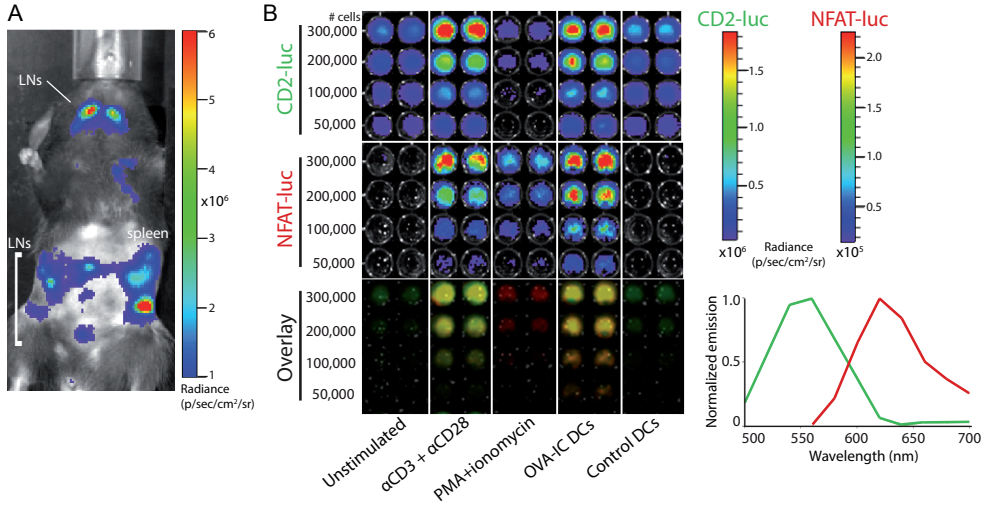

Figure 3. Dual-luciferase imaging of antigen-specific T cells. (A) Bioluminescence measurement of a TbiLuc*OT-I mouse, showing luciferase expression in secondary lymphoid organs. The abdomen is shaved to reduce signal absorption. The spleen and various lymph nodes (LNs) are indicated. **(B)** Titrations of CD8 T cells, isolated from the spleen of TbiLuc*OT-I mice, were stimulated overnight with agonistic CD3/CD28 antibodies, PMA + ionomycin, dendritic cells loaded with OVA protein immune complexes (OVA-IC DCs) or with unloaded control DCs, as indicated. Subsequent bioluminescence imaging shows constitutive CBG99 expression (CD2-luc, top), activation-induced PpyRE9 expression (NFAT-luc, middle) and an overlay of artificial green and red colors (bottom) corresponding to the spectral unmixing as shown in the bottom-right graph.

The isolated CD8 T cells were then co-incubated in vitro with dendritic cells presenting the SIINFEKL epitope processed from the OVA protein after uptake of immune-complexes (OVA-IC), which we have previously reported as an efficient CD8 T cell vaccine (16). This led to a strong induction of NFAT-luciferase, which was completely antigen-specific as control dendritic cells did not induce any expression, identical to unstimulated naïve T cells (**Figure 3B**). Again, Western Blot analysis showed the presence of PpyRE9 protein (**Supplemental Figure 1C**). Although the use of a single D-luciferin substrate was sufficient for dual color imaging in vitro, the weak NFAT-induced red light signal did not allow efficient in vivo detection of T cell activation (data not shown). Therefore, we tested a new luciferin substrate, CycLuc1, that was specifically designed to improve light emission from firefly luciferases such as our NFAT-induced PpyRE9 red luciferase (14). By using T cell hybridomas expressing either one of the two luciferases also used in TbiLuc, we show that CycLuc1 is an inefficient substrate for CBG99 green luciferase, as indicated by the 30-fold lower signal at the emission peak as compared to D-luciferin (**Supplemental Figure 2**). This allows specific detection of PpyRE9 luciferase in TbiLuc T cells using the CycLuc1 substrate. Moreover, these data indicate that substrates given in combination compete for the active site of the enzymes, as shown by the 1.6 times lower average photon flux measured for CBG99 emission with D-Luc + CycLuc1 as compared to D-Luc alone.

Next, we investigated whether dual color imaging of TbiLuc*OT-I T cell activation could be performed using the two substrates, D-luciferin and CycLuc1. Addition of a single substrate per sample allowed efficient detection of the constitutive signal from CBG99 green luciferase by D-luciferin, and the activation signal from PpyRE9 red luciferase by CycLuc1 (**Figure 4A**). Unlike in naïve T cells, in activated T cells expressing both luciferases, simultaneous addition of the two substrates produces a spectrum with no isolated peaks of emission (**Figure 4B**). Therefore, separate addition of substrates is warranted for efficient separation of light signals in activated T cells. The validity of using CycLuc1 for specific visualization of activation-induced PpyRE9 luciferase was also found in CD4 and CD8 T cells from parental TbiLuc mice (data not shown).

Visualization of T cell localization and activation in vaccinated mice

We set out to investigate whether antigen-specific target recognition by T cells could be visualized in vivo, using an adoptive T cell transfer system. First, we visualized the fate of T cells after adoptive transfer. Intravenously injected TbiLuc*OT-I CD8 T cells homed efficiently to the lymphoid organs of recipient Albino B6 mice, and the number of transferred T cells correlated to the signal strength (**Supplemental Figure 3**). Next, mice were vaccinated subcutaneously in the tail-base with dendritic cells

(DCs) pre-loaded with OVA protein immune complexes, containing the specific T cell antigen recognized by OT-I T cells, while control mice received unloaded DCs. Based on previous in vitro results, we adopted an in vivo imaging protocol with separate administration of the two substrates with a time interval to allow clearance of the first substrate, measuring CBG99 luciferase activity using D-luciferin and measuring PpyRE9 luciferase activity using CycLuc1. Periodical bioluminescence imaging was then performed, focusing on the vaccine-draining inguinal lymph nodes, and the green and red light signals were quantified. In the first week after vaccination, OVA-vaccinated mice showed a sharp increase in both the constitutive green light signal and the activation-induced red light signal in the lymph nodes, peaking at day 8 after injection (**Figure 5A**).

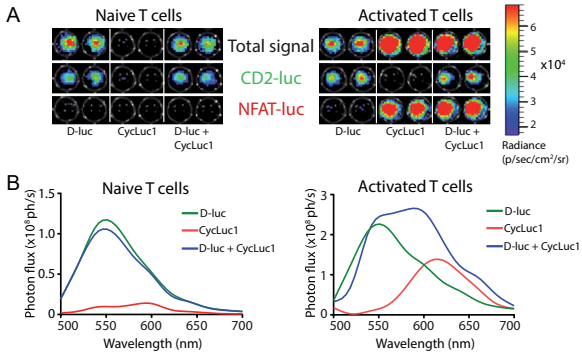

Figure 4. Efficient visualization of NFAT-induced PpyRE9 luciferase using the CycLuc1 substrate. (A) CD8 T cells from TbiLuc*OT-I mice left untreated ('Naive') or stimulated O/N with OVA immune complex-loaded dendritic cells ('Activated') were imaged using the substrate D-luciferin (D-luc), CycLuc1, or both. Total signal (top), the constitutive CD2-CBG99 green luciferase (middle) and the activation-induced NFAT-PpyRE9 red luciferase (bottom) are shown separately, on the same scale. **(B)** Emission spectra of naive and activated T cells (from Figure A) using different substrates, showing strong constitutive CBG99 signals using the D-luciferin substrate, and specific activation-induced PpyRE9 signals using CycLuc1.

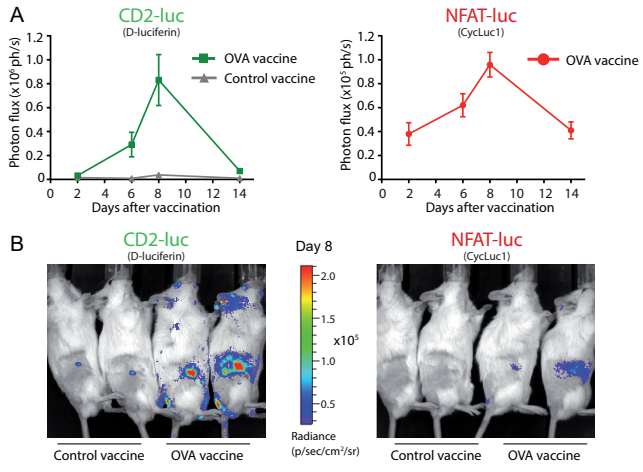

Figure 5. Visualization of T cell localization and activation in vaccinated mice. (A) Constitutive CD2-luciferase (left) and NFAT-luciferase (right) signals from vaccine-draining inguinal lymph nodes of vaccinated mice. On day 0, mice received adoptive transfer of TbiLuc*OT-I CD8+ T cells and were vaccinated with OVA immune complex-loaded dendritic cells or with unloaded control dendritic cells (n=4 mice per group). CD2-CBG99 and NFAT-PpyRE9 luciferases were imaged using the D-luciferin and CycLuc1 substrates, respectively. Mice receiving the control vaccine showed no detectable NFAT-luc signal. **(B)** Representative pictures of OVA-vaccinated and control-vaccinated mice on day 8, showing T cell proliferation (left) and activation (right) in OVA-vaccinated mice.

In contrast, control mice had a comparable constitutive green light signal on day 2 as OVA-vaccinated mice, but did not show a strong T cell expansion and had undetectable red light signal, suggesting that the DC-OVA vaccine specifically induced activation and expansion of TbiLuc*OT-I T cells. Two days after vaccination, T cell activation could be detected by means of PpyRE9 luciferase activity, while

T cell expansion as measured by CBG99 luciferase activity started later in time. The dramatic increase in luciferase activity in OVA-vaccinated mice, and the lack of activation-dependent red luciferase activity in control mice, can be seen in representative images from day 8 (**Figure 5B**).

Discussion

In this study, we report the design and development of a dual-luciferase T cell transgenic mouse, called TbiLuc, as a novel tool for non-invasive imaging of T cells. The dual-luciferase construct allows live visualization of both the location and the activation status of T cells, which we established in antigen-specific T cell activation studies both in vitro and in vivo. The TbiLuc mouse model has numerous applications both in fundamental T cell biology and in preclinical translational studies on the many diseases in which T cells play a role. For instance, since it has been established that T cells are crucial in the spontaneous or therapeutically-induced clearance of malignant cells, the TbiLuc mouse can be used to test the efficacy of cancer vaccines, immunomodulatory antibodies and other treatment modalities that depend on T cells. Disease models of viral infection and autoimmunity involving T cell effector cells are other possible applications of the TbiLuc mouse (17,18).

To introduce luciferase-encoding genes into cells, researchers commonly use retroviral transduction. However, naïve T cells cannot be efficiently transduced unless they are pre-treated by either TCR stimulation with cognate antigen or with cytokines such as IL-7, both of which trigger downstream signaling pathways in the T cells (6–9,19,20). This makes studies on truly naïve T cells impossible, although T cell 'rested' after activation and transduction are sometimes considered to represent naïve T cells; a perhaps more pragmatic rather than immunological interpretation. Instead, integration of a luciferase-encoding gene into murine oocytes, resulting in a luciferase-transgenic mouse strain, is a time-consuming but scientifically much more attractive alternative that allows the isolation of luciferase-expressing naïve T cells from the lymphoid organs of the mouse. Indeed, several groups have created luciferase reporter mice for T cell imaging and showed the potential of BLI for T cell tracking (10–12). However, these single-luciferase reporter mice only provide information on the location of T cells, without additional information on their activation state. The feasibility of creating dual-luciferase transgenic mice has been shown before, but never using cell type-specific expression (21,22). We describe the first dual-luciferase T cell transgenic mouse, which offers an important advantage in allowing simultaneous visualization of T cell location and activation.

Luciferase T cell imaging, and optical imaging in general, is especially well-suited for visualization of superficial light signals, as the signal from deeper locations in the body will be influenced by absorption and scattering of photons in the tissues. In this view, radio-imaging provides more accurate information on the location of T cells (23,24). However, optical imaging strategies avoid the undesired use of radioactive material, and BLI in particular allows the creation of reporter mice where luciferase expression can be restricted to the cell type of choice by choosing a cell-specific promoter. Our choice of the human CD2 minigene as the promoter driving the constitutively expressed CBG99 luciferase is based on earlier studies showing T cell-specific transgene expression (15,25). To our knowledge, we are the first to add a second luciferase in the creation of a T cell reporter mouse and to optimize an in vivo imaging protocol for measuring the activity of both luciferases. The NFAT response element driving PpyRE9 luciferase expression allows a straightforward readout of T cell activation, which is valuable extra information besides the location of the T cell. Our optimized in vivo imaging protocol involves separate injection of the two substrates such that the first substrate is cleared before the second substrate is administered, measuring CBG99 activity using D-luciferin and measuring PpyRE9 activity using CycLuc1. This setup provides the maximal light emission for each luciferase and avoids both biochemical interference from the other substrate and spectral interference from the other luciferase. An in vivo vaccination study visualized the expansion and activation of adoptively transferred T cells in vaccine-draining lymph nodes following typical kinetics of T cell responses upon vaccination (26–28). Finally, although a weak NFAT-driven luciferase activity was observed in NK cells after TCR independent PMA-ionomycin treatment, these cells can be distinguished from T cells because of the absence of green CD2-driven luciferase emission. Moreover, in models using adoptive T cell transfer, NK cells are efficiently excluded during the T cell isolation process.

Our data have shown that dual-luciferase reporter mice can be easily crossed to other (T cell-) transgenic mouse strains, which brings many possibilities to further fine-tune the reporter system for the biomedical experimental model of interest. Taken together, this proof-of-concept manuscript introduced the TbiLuc dual-luciferase T cell transgenic mouse that allows to track activation and expansion of T cell populations in naturally organized lymphoid tissue, with full retention of T cell naivety and antigen-specific functionality. Many biomedical research fields can potentially benefit from this advanced live T cell imaging model.

Acknowledgments

This work was supported by project grants from CTMM (Project 030-302), TI Pharma (Project D4-603) and European H2020 MSCA grant under proposal number 675743 (project acronym: ISPIC).

References

1. Contag CH, Bachmann MH. Advances in in vivo bioluminescence imaging of gene expression. Annu Rev Biomed Eng. 2002;4:235–60.
2. Kaijzel EL, van der Pluijm G, Löwik CWGM. Whole-body optical imaging in animal models to assess cancer development and progression. Clin Cancer Res. 2007;13:3490–7.
3. Coombe DR, Nakhoul AM, Stevenson SM, Peroni SE, Sanderson CJ. Expressed luciferase viability assay (ELVA) for the measurement of cell growth and viability. J Immunol Methods. 1998;215:145–50.
4. Karimi MA, Lee E, Bachmann MH, Salicioni AM, Behrens EM, Kambayashi T, et al. Measuring Cytotoxicity by Bioluminescence Imaging Outperforms the Standard Chromium-51 Release Assay. Amendola R, editor. PLoS One. 2014;9:e89357.
5. Na I-K, Markley JC, Tsai JJ, Yim NL, Beattie BJ, Klose AD, et al. Concurrent visualization of trafficking, expansion, and activation of T lymphocytes and T-cell precursors in vivo. Blood. 2010;116:e18-e25.
6. Kim D, Hung C-F, Wu T-C. Monitoring the Trafficking of Adoptively Transferred Antigen-Specific CD8-Positive T Cells *In Vivo* , Using Noninvasive Luminescence Imaging. Hum Gene Ther. 2007;18:575–88.
7. Rabinovich BA, Ye Y, Etto T, Chen JQ, Levitsky HI, Overwijk WW, et al. Visualizing fewer than 10 mouse T cells with an enhanced firefly luciferase in immunocompetent mouse models of cancer. Proc Natl Acad Sci U S A. 2008;105(38):14342-6.
8. Hailemichael Y, Dai Z, Jaffarzad N, Ye Y, Medina MA, Huang X-F, et al. Persistent antigen at vaccination sites induces tumor-specific CD8+ T cell sequestration, dysfunction and deletion. Nat Med. 2013;19:465–72.
9. Patel MR, Chang Y-F, Chen IY, Bachmann MH, Yan X, Contag CH, et al. Longitudinal, Noninvasive Imaging of T-Cell Effector Function and Proliferation in Living Subjects. Cancer Res. 2010;70:10141–9.
10. Chewning JH, Dugger KJ, Chaudhuri TR, Zinn KR, Weaver CT. Bioluminescence-based visualization of CD4 T cell dynamics using a T lineage-specific luciferase transgenic model. BMC Immunol. 2009;10:44.
11. Azadniv M, Dugger K, Bowers WJ, Weaver C, Crispe IN. Imaging CD8+ T cell dynamics in vivo using a transgenic luciferase reporter. Int Immunol. 2007;19:1165–73.
12. Charo J, Perez C, Buschow C, Jukica A, Czeh M, Blankenstein T. Visualizing the dynamic of adoptively transferred T cells during the rejection of large established tumors. Eur J Immunol. 2011;41:3187–97.
13. Mezzanotte L, Que I, Kaijzel E, Branchini B, Roda A, Löwik C. Sensitive Dual Color In Vivo Bioluminescence Imaging Using a New Red Codon Optimized Firefly Luciferase and a Green Click Beetle Luciferase. Herrera-Estrella A, editor. PLoS One. 2011;6:e19277.
14. Evans MS, Chaurette JP, Adams ST, Reddy GR, Paley MA, Aronin N, et al. A synthetic

luciferin improves bioluminescence imaging in live mice. Nat Methods. 2014;11:393–5.
15. Lang G, Wotton D, Owen MJ, Sewell WA, Brown MH, Mason DY, et al. The structure of the human CD2 gene and its expression in transgenic mice. EMBO J. 1988;7:1675–82.
16. Schuurhuis DH, Ioan-Facsinay A, Nagelkerken B, van Schip JJ, Sedlik C, Melief CJM, et al. Antigen-antibody immune complexes empower dendritic cells to efficiently prime specific CD8+ CTL responses in vivo. J Immunol. 2002;168:2240–6.
17. Hutchens M, Luker GD. Applications of bioluminescence imaging to the study of infectious diseases. Cell Microbiol. 2007;9:2315–22.
18. Luker KE, Luker GD. Bioluminescence imaging of reporter mice for studies of infection and inflammation. Antiviral Res. 2010;86:93–100.
19. Cavalieri S, Cazzaniga S, Geuna M, Magnani Z, Bordignon C, Naldini L, et al. Human T lymphocytes transduced by lentiviral vectors in the absence of TCR activation maintain an intact immune competence. Blood. 2003;102:497–505.
20. Takada K, Jameson SC. Naive T cell homeostasis: from awareness of space to a sense of place. Nat Rev Immunol. 2009;9:823–32.
21. Tehrani AM, Hwang S-K, Kim T-H, Cho C-S, Hua J, Nah W-S, et al. Aerosol delivery of Akt controls protein translation in the lungs of dual luciferase reporter mice. Gene Ther. 2007;14:451–8.
22. Noguchi T, Michihata T, Nakamura W, Takumi T, Shimizu R, Yamamoto M, et al. Dual-Color Luciferase Mouse Directly Demonstrates Coupled Expression of Two Clock Genes. Biochemistry. 2010;49:8053–61.
23. Tavare R, McCracken MN, Zettlitz KA, Knowles SM, Salazar FB, Olafsen T, et al. Engineered antibody fragments for immuno-PET imaging of endogenous CD8+ T cells in vivo. Proc Natl Acad Sci. 2014;111:1108–13.
24. Leech JM, Sharif-Paghaleh E, Maher J, Livieratos L, Lechler RI, Mullen GE, et al. Whole-body imaging of adoptively transferred T cells using magnetic resonance imaging, single photon emission computed tomography and positron emission tomography techniques, with a focus on regulatory T cells. Clin Exp Immunol. 2013;172:169–77.
25. Zhumabekov T, Corbella P, Tolaini M, Kioussis D. Improved version of a human CD2 minigene based vector for T cell-specific expression in transgenic mice. J Immunol Methods. 1995;185:133–40.
26. Knudsen ML, Ljungberg K, Kakoulidou M, Kostic L, Hallengärd D, García-Arriaza J, et al. Kinetic and phenotypic analysis of CD8+ T cell responses after priming with alphavirus replicons and homologous or heterologous booster immunizations. J Virol. 2014;88:12438–51.
27. Song X-T, Turnis ME, Zhou X, Zhu W, Hong B-X, Rollins L, et al. A Th1-inducing adenoviral vaccine for boosting adoptively transferred T cells. Mol Ther. 2011;19:211–7.
28. Blattman JN, Cheng LE, Greenberg PD. CD8+ T cell responses: it's all downhill after their prime ... Nat Immunol. 2002;3:601–2.
29. Branchini BR, Ablamsky DM, Davis AL, Southworth TL, Butler B, Fan F, et al. Red-emitting luciferases for bioluminescence reporter and imaging applications. Anal Biochem. 2010;396:290–7.
30. Winzler C, Rovere P, Rescigno M, Granucci F, Penna G, Adorini L, et al. Maturation Stages of Mouse Dendritic Cells in Growth Factor–dependent Long-Term Cultures. J Exp Med. 1997;185.
31. Karttunen J, Shastri N. Measurement of ligand-induced activation in single viable T cells

using the lacZ reporter gene. Proc Natl Acad Sci. 1991;88:3972–6.
32. Rahimian S, Kleinovink JW, Fransen MF, Mezzanotte L, Gold H, Wisse P, et al. Near-infrared labeled, ovalbumin loaded polymeric nanoparticles based on a hydrophilic polyester as model vaccine: Invivo tracking and evaluation of antigen-specific $CD8^+$ T cell immune response. Biomaterials. 2015;37.

Supplementary Information

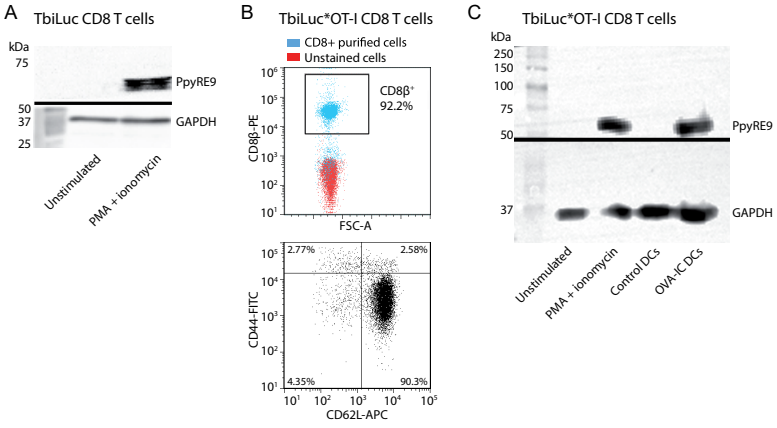

Supplementary Figure S1. (A) Western blot for the activation-induced PpyRE9 luciferase. CD8 T cells from TbiLuc mice stimulated with PMA+ionomycin, but not unstimulated cells, produce PpyRE9 luciferase protein. **(B)** Representative flow cytometry plots showing the efficient purification of CD8 T cells (top), which have a naïve phenotype (CD44lo, CD62Lhi, bottom) from TbiLuc*OT-I mice. **(C)** Western blot for the activation-induced PpyRE9 luciferase. CD8 T cells from TbiLuc*OT-I mice stimulated with PMA+ionomycin or OVA immune complex-loaded dendritic cells (OVA-IC DCs), but not unstimulated cells or control DC-stimulated cells, produce PpyRE9 luciferase protein.

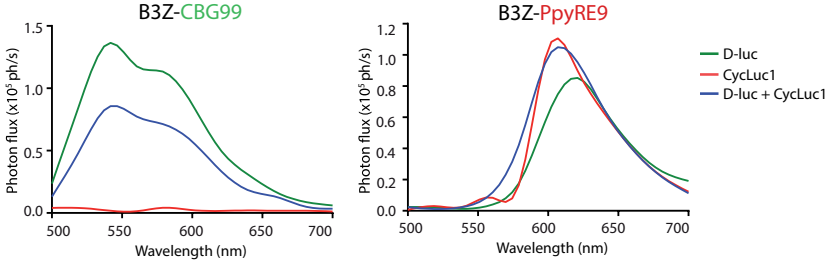

Supplementary Figure S2. Comparison of the efficacy of D-luciferin (D-luc), CycLuc1, or mixed substrates using B3Z T cell hybridoma cells transduced to constitutively express either green CBG99 (left) or red PpyRE9 (right) luciferases, as indicated. D-luciferin is the optimal substrate for CBG99, and CycLuc1 is the optimal substrate for PpyRE9, but mixing the two substrates reduces signal strength.

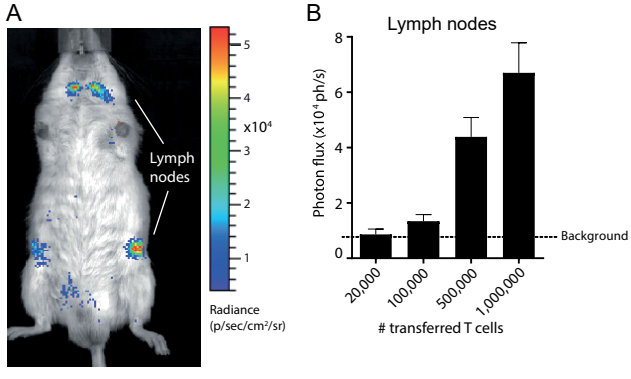

Supplementary Figure S3. Bioluminescence imaging of TbiLuc*OT-I CD8 T cells after adoptive transfer into recipient mice. **(A)** Adoptively transferred T cells home to the secondary lymphoid organs of recipient mice. Representative image, the cervical and inguinal lymph nodes are indicated. **(B)** Quantification of the signals in inguinal lymph nodes showing that signal strength correlates to the number of transferred T cells.

Chapter 7

Summary and General Discussion

The use of light in cancer immunotherapy

Decades of research have established the field of oncoimmunology and resulted in the new paradigm stating that tumors co-exist with the immune system throughout their life (1,2). Avoidance of immune clearance is now recognized as a major hallmark of cancer (3). As mutations may not only provide tumor cells their unique proliferative capacities but also introduce non-self characteristics, the immune system manages to eliminate many early developing tumors. This means that cancer cells that managed to progress to clinically apparent tumors either were not sufficiently recognizable by the immune system, or managed to actively suppress and evade immune attack. Cancer immunotherapy aims to facilitate immune attack by inducing new immune responses and/or boosting the efficacy of existing immune responses. Most forms of cancer immunotherapy are focused on T cells (4), as these are the most prominent immune cells capable of tumor cell killing based on their ability to recognize mutated self-proteins processed and presented in MHC molecules. Unfortunately, their efficacy in doing so can be heavily influenced by other immune and non-immune cells (5,6). While impressive clinical responses have been observed in some patients after cancer immunotherapy, many patients do not respond to therapy, which has raised the need to better understand immune evasion mechanisms and to develop superior (combination) therapies (7–9). This thesis shows several examples of how these two needs can be directly or indirectly addressed. Light plays a central role in all these examples, either as a diagnostic tool for live in vivo visualization of relevant cells and molecules during cancer immunotherapy, or therapeutically as an external energy source that triggers the ablation of tumors.

Immunogenic tumor ablation

Advanced cancer generally responds worse to therapy than early lesions. Advanced tumors are not only be bigger in size, but also have a longer evolutionary history of immune pressure and therefore had more time to develop immune suppression mechanisms. From this perspective, tumor ablation therapies that cause immunogenic cell death are attractive treatment options for advanced cancer, as they both reduce tumor burden and may induce or enhance anti-tumor immune responses. In comparison to other tumor mass-reducing protocols such as chemotherapy and radiotherapy, Photodynamic Therapy (PDT) is known for its high target-specific toxicity and limited side effects, and gaining recognition among surgeons for a tissue recovery with minimal scarring, when compared to surgery (10). PDT involves the administration of an inert photosensitizer which is then to be activated by exposure to light, using laser fibers or lamps as a light source. PDT

in clinical practice is therefore mostly applied to tumor types that are relatively accessible for the light source, such as skin lesions and tumors in the gastrointestinal and reproductive tract. However, many more cancer types can potentially be treated by PDT using interstitial fibers in a surgery setting. In this dissertation, we described two combination protocols of PDT and immunotherapy in preclinical models of advanced cancer. In chapter 2, combined treatment of tumor-bearing mice with PDT and therapeutic SLP vaccination could eradicate local (PDT-treated) and distant tumors, where either monotherapy showed limited efficacy. PDT induced and enhanced tumor antigen-specific CD8 T cell responses, which were necessary for the therapeutic effect (11). Chapter 3 described combination therapy of PDT and CTLA-4 immune checkpoint blockade in two highly mutated tumor models, and also showed superior efficacy of combination treatment in mice bearing two established tumors, fully dependent on the presence of CD8 T cells. Both studies emphasize the immunogenicity of tumor ablation by PDT, thereby functioning as an in situ vaccination, and suggest that this feature makes it an ideal combination partner for immunotherapy of large tumors.

The potential immunogenicity of PDT has been described before, most prominently by the group of Michael Hamblin, who urged collaborations between PDT experts and tumor immunologists in the search for combination treatments with immunotherapy (12). We believe that the combination regimens investigated in this thesis are good candidates for clinical application, as they combine PDT with clinically applied immunotherapeutics (7,13,14). Moreover, the two different combination protocols correspond to two different classes of human cancer. Tumors induced by oncogenic viruses can express known viral T cell antigens that are widely shared among patients, which allows antigen-specific immunotherapy. Our findings in chapter 2 indicate that if tumor antigens are known, combination treatment of PDT and SLP vaccination can provide a highly tumor-specific treatment. The enhanced clearance of distant secondary tumors suggests that spontaneous metastases, known or unknown, will also be attacked. Nonetheless, the majority of cancers arise not from oncoviruses but from familial or acquired mutations, in which case patients display a (mostly) unique tumor-antigenic profile. It is technically feasible to identify mutated T cell epitopes in every individual patient and produce personalized therapeutic peptide vaccines (15,16). However, alternative treatment strategies may be more appropriate, especially in those cancer types with a high mutational burden, which has been suggested to correlate to a higher neo-antigen load (17). The combination protocol described in chapter 3, using CTLA-4 immune checkpoint blockade, can be widely applied regardless of the tumor antigen makeup. The disadvantage of applying potent non-specific immunostimulatory treatments is the inevitable occurrence of off-target toxicity (18). Previous work in our group has

addressed this issue by supplying CTLA-4 blockers locally, strongly reducing toxicity while therapeutic efficacy is maintained (19).

Alternative ablation therapies have been shown to mediate comparable immunogenic effects as we describe here for PDT, and several preclinical studies have shown successful combinations with immune checkpoint blockade (20–23). Although several photosensitizers have been clinically approved, PDT has much fewer applications as a standard-of-care compared to other ablative therapies such as chemotherapy and radiotherapy. One might therefore argue that it is attractive to opt for combinations of chemotherapy or radiotherapy with immunotherapies to accelerate clinical translation. However, systemic immune stimulation by checkpoint inhibitors, as it is currently commonly applied, often already cause substantial side-effects. It may therefore be preferred to avoid increasing the therapeutic burden much further, as would happen considerably by radiotherapy and especially chemotherapy. From this perspective, the highly focused nature of PDT favors combinations of immunotherapy with PDT, which as a monotherapy is associated with only mild side-effects such as painful skin at the target site during treatment (24). Moreover, there are no indications that PDT treatment itself can be mutagenic, as is the case for both chemotherapy and radiotherapy. We believe that our studies have provided proof of concept of PDT-immunotherapy combinations, but additional preclinical and clinical studies are required to assess its broader clinical applicability.

Visualizing vaccines by optical imaging

Optical imaging of fluorescence or bioluminescence is a widely used technique to study biological or experimentally-induced processes in vitro and in vivo. Excellent technologies have been developed to visualize biomolecules, track cells, quantify bioactivities and study kinetics of physiological processes in vivo. Fluorescent dyes are usually coupled to the biomolecules of interest prior to administration, while bioluminescence is a feature of luciferase enzymes for which the coding gene can be introduced into the genome in order to visualize the cells of interest. Fluorescent dyes and bioluminescent enzymes therefore each have their own advantages and disadvantages and are applied accordingly (25). Compared to optical imaging, alternative techniques to visualize injected molecules offer some advantages, such as excellent spatial resolution in the case of MRI, and absolute quantification using nuclear imaging (26–28). Nonetheless, fluorescence imaging is often preferred and applied as it is non-invasive, fast and cost-effective (29,30). In particular, near-infrared (NIR) fluorescent dyes are preferred because light of NIR wavelength has superior tissue penetration compared to visible light, allowing the detection of signals from

deeper layers of the body or sample. Chapter 4 describes a feasibility study of SLP vaccine tracking using a conjugated NIR fluorescent dye. By live optical imaging, we visualized this NIR-SLP vaccine at the injection site and in vaccine-draining lymph nodes. The applicability of this vaccine imaging platform was assessed by formulating the NIR-SLP in several different pharmacological formulations, whose expected distinct kinetics were adequately identified by NIR fluorescence imaging. Similarly, chapter 5 describes the tracking of NIR-labeled protein vaccines encapsulated in biodegradable nanoparticles (NP), which were labeled which a different NIR dye to allow independent visualization of vaccine and carrier. Fluorescence imaging showed that encapsulated protein is retained longer at the injection site and accumulated more gradually in the draining lymph nodes, when compared to soluble protein in saline. NPs and protein had overlapping kinetics, suggesting that the vaccine is transported while still being encapsulated, rather than having been released at the injection site. Both studies showed that NIR-labeling of the vaccine does not affect its ability to achieve its ultimate functional purpose, the activation of CD8 T cells. These studies illustrate that NIR-labeling allows live vaccine visualization and quantification, which can be used as tool to address scientific research questions on vaccine functionality as the systemic localization and quantity of the vaccine may be determinants of its eventual therapeutic efficacy (31–33). Further studies using other NIR-labeled SLPs are required to determine whether our findings using a model SLP of chicken ovalbumin are generally applicable, or were instead partly or fully influenced by the specific characteristics of the chosen peptide (34). The safety and applicability of our NIR dye has been shown in a clinical study using a clinically applied and NIR-conjugated SLP vaccine, which could be visualized after administration and did not cause adverse effects. The experimental approach of vaccine delivery by nanoparticle carriers as applied in chapter 5 was chosen based on several potential advantages over soluble vaccine administration. For instance, non-adjuvanted soluble antigen is weakly immunogenic, which can be improved by carrier systems that can deliver antigen vaccines to antigen-presenting cells, and may also protect the protein from undesired degradation (35,36). Additional opportunities are co-encapsulation of adjuvants with the antigen and attaching targeting molecules on the surface (37,38). Moreover, unlike the widely used oil-in-water emulsions as alternative sustained-release formulations, nanoparticles can be labeled and imaged as we have described. To show the concept of dual color NP-vaccine imaging we made us of the model protein chicken ovalbumin for practical reasons regarding NIR labeling and encapsulation. As previous work in our group has shown that SLP vaccines are therapeutically superior to protein vaccines, it would be of interest to study NIR-labeled peptide vaccines encapsulated in nanoparticles and attempt to correlate kinetics to functionality (39).

Dual-color T cell imaging

Chapter 6 introduced the new T cell luciferase transgenic mouse termed TbiLuc, as a tool for bioluminescence imaging of T cell location and activation status using two separately controlled luciferases. T cells are involved in a wide variety of physiological and pathological conditions and are highly mobile due to their ability to differentially express homing ligands that determine their localization in the bloodstream or entry in peripheral lymphoid and non-lymphoid tissues (40,41). Therefore, there is substantial interest among researchers in being able to measure the presence of T cells throughout the body in time, which is conventionally solved by the laborious process of sacrificing experimental animals at different time points and analyzing T cell counts in different organs ex vivo. Our study is the first to address this issue by creating a T cell dual-luciferase transgenic mouse. Earlier attempts to apply bioluminescence imaging (BLI) for T cell tracking mostly used retroviral vectors carrying luciferase genes to transduce T cells, which requires T cell activation and is not very efficient (42–44). Several groups have solved this issue by creating T cell luciferase transgenic mice to supply a large pool of untouched luciferase-expressing T cells, but all used only one constitutively expressed luciferase (45–47). The basic concept of dual-luciferase T cell imaging was first shown by Na et al., who used an indirect approach of lentiviral transduction in bone marrow to create chimeric mice as a source of naïve T cells (48). We used a more straightforward approach to limit the constitutively expressed luciferase to T cells by coupling it to the human CD2 promoter, which in mice is specific to T cells (49). The two luciferases in the TbiLuc construct, termed CBG99 (click-beetle green) and PpyRE9 (a red mutant of the common firefly Photinus pyralis), both function with the common D-luciferin substrate. However, the considerably higher quantum yield of CBG99 proved problematic in simultaneous dual-color measurements in mice, as the emission of PpyRE9 could not be separated from the bulky CBG99 emission. Therefore, the novel cyclic substrate CycLuc1 was used (50,51), which produces a stronger PpyRE9 signal than D-luciferin, while the CBG99 signal was nearly absent. As simultaneous imaging using mixed substrates reduced the amount of signal, since substrates compete for the active sites of the luciferases, we used a sequential imaging setup and visualized T cell activation and expansion in an in vivo vaccination model. Although sequential imaging depicts the biological situation with a 3 hours difference due to the substrate washout time, which has to be taken into account when studying T cell processes with fast kinetics, the two relevant biological parameters of localization of T cells and their activation status can now be clearly distinguished. In conclusion, the TbiLuc transgenic mouse is a suitable model to visualize endogenous T cell responses, with possible applications in many fields such as vaccinology, cancer immunotherapy including T cell reinvigoration

by immune checkpoint blockade, auto-immune disease and transplantation. In addition, crossing TbiLuc to T cell receptor-transgenic mouse strains produces large numbers of light-producing cells of known antigen specificity, usually applied in adoptive T cell transfer models. This transgenic mouse model can be widely applied in immunology research, as T cells play a role in many physiological or pathological processes. One example is the field of cancer immunotherapy, due to the crucial role of T cells in the killing of malignant cells. The efficacy of cancer vaccines can be assessed by measuring T cell activation and expansion following vaccination. Similarly, reactivation of suppressed T cells in cancer models can be visualized upon treatment with immunomodulatory antibodies. Other applications lie in models of viral infection, transplantation and autoimmunity.

Concluding remarks

This manuscript has illustrated several applications of light in the field of cancer immunology and immunotherapy. The luciferase enzymes used in our studies are derived from animal species that naturally express them, which has sent researchers into the woods with a catching net searching for a new undiscovered enzyme. Visible light drives the physicochemical reaction underlying the therapeutic effect of PDT, whose potential was already observed by ancient civilizations. Given the vast amount of time that people have spent in the sun throughout human history, and nowadays would still like to, it is important to realize that light can have substantial effects on the human body. We should understand both its dangers and its benefits, and use this knowledge to our advantage.

References

1. Parish CR. Cancer immunotherapy: The past, the present and the future. Immunol Cell Biol. 2003;81:106–13.
2. Budhu S, Wolchok J, Merghoub T. The importance of animal models in tumor immunity and immunotherapy. Curr Opin Genet Dev. 2014;24:46–51.
3. Hanahan D, Weinberg RA. Hallmarks of cancer: the next generation. Cell. 2011;144:646–74.
4. Couzin-Frankel J. Cancer Immunotherapy. Science 2013;342.
5. Zarour HM. Reversing T-cell Dysfunction and Exhaustion in Cancer. Clin Cancer Res. 2016;22:1856–64.
6. Jiang Y, Li Y, Zhu B. T-cell exhaustion in the tumor microenvironment. Cell Death Dis. Nature Publishing Group; 2015;6:e1792.
7. Hodi FS, O'Day SJ, McDermott DF, Weber RW, Sosman JA, Haanen JB, et al. Improved survival with ipilimumab in patients with metastatic melanoma. N Engl J Med. 2010;363:711–23.
8. Topalian SL, Hodi FS, Brahmer JR, Gettinger SN, Smith DC, McDermott DF, et al. Safety, Activity, and Immune Correlates of Anti–PD-1 Antibody in Cancer. N Engl J Med. 2012;366:2443–54.
9. Callahan MK, Postow MA, Wolchok JD. CTLA-4 and PD-1 Pathway Blockade: Combinations in the Clinic. Front Oncol. Frontiers Media SA; 2014;4:385.

10. Dolmans DEJGJ, Fukumura D, Jain RK. TIMELINE: Photodynamic therapy for cancer. Nat Rev Cancer. 2003;3:380–7.
11. Kleinovink JW, Van Driel PB, Snoeks TJ, Prokopi N, Fransen MF, Cruz LJ, et al. Combination of photodynamic therapy and specific immunotherapy efficiently eradicates established tumors. Clin Cancer Res.2016;22:1459–68.
12. Reginato E, Mroz P, Chung H, Kawakubo M, Wolf P, Hamblin MR. Photodynamic therapy plus regulatory T-cell depletion produces immunity against a mouse tumour that expresses a self-antigen. Br J Cancer. 2013;109:2167–74.
13. Melief CJM, van der Burg SH. Immunotherapy of established (pre)malignant disease by synthetic long peptide vaccines. Nat Rev Cancer. 2008;8:351–60.
14. Grosso JF, Jure-Kunkel MN. CTLA-4 blockade in tumor models: an overview of preclinical and translational research. Cancer Immun. 2013;13:5.
15. Castle JC, Kreiter S, Diekmann J, Lower M, van de Roemer N, de Graaf J, et al. Exploiting the Mutanome for Tumor Vaccination. Cancer Res. 2012;72:1081–91.
16. Schumacher TN, Schreiber RD. Neoantigens in cancer immunotherapy. Science. 2015;348:69–74.
17. Rizvi NA, Hellmann MD, Snyder A, Kvistborg P, Makarov V, Havel JJ, et al. Mutational landscape determines sensitivity to PD-1 blockade in non-small cell lung cancer. Science. 2015;348:124–8.
18. Spain L, Diem S, Larkin J. Management of toxicities of immune checkpoint inhibitors. Cancer Treat Rev. 2016;44:51–60.
19. Fransen MF, van der Sluis TC, Ossendorp F, Arens R, Melief CJM. Controlled Local Delivery of CTLA-4 Blocking Antibody Induces CD8+ T-Cell-Dependent Tumor Eradication and Decreases Risk of Toxic Side Effects. Clin Cancer Res. 2013;19:5381–9.
20. Formenti SC, Demaria S. Systemic effects of local radiotherapy. Lancet Oncol. Elsevier; 2009;10:718–26.
21. Belcaid Z, Phallen JA, Zeng J, See AP, Mathios D, Gottschalk C, et al. Focal radiation therapy combined with 4-1BB activation and CTLA-4 blockade yields long-term survival and a protective antigen-specific memory response in a murine glioma model. PLoS One. 2014;9:1–9.
22. Sharabi AB, Nirschl CJ, Kochel CM, Nirschl TR, Francica BJ, Velarde E, et al. Stereotactic Radiation Therapy Augments Antigen-Specific PD-1-Mediated Antitumor Immune Responses via Cross-Presentation of Tumor Antigen. Cancer Immunol Res. 2015;3:345–55.
23. Drake CG. Combination immunotherapy approaches. Ann Oncol. 2012;23:viii41-viii46.
24. Ibbotson SH. Adverse effects of topical photodynamic therapy. Photodermatol Photoimmunol Photomed. 2011;27:116–30.
25. Weissleder R, Ntziachristos V. Shedding light onto live molecular targets. Nat Med. 2003;9:123–8.
26. Kherlopian AR, Song T, Duan Q, Neimark MA, Po MJ, Gohagan JK, et al. A review of imaging techniques for systems biology. BMC Syst Biol. 2008;2:74.
27. Penet M-F, Mikhaylova M, Li C, Krishnamachary B, Glunde K, Pathak AP, et al. Applications of molecular MRI and optical imaging in cancer. Future Med Chem. 2010;2:975–88.
28. Wu C, van der Have F, Vastenhouw B, Dierckx RAJO, Paans AMJ, Beekman FJ. Absolute quantitative total-body small-animal SPECT with focusing pinholes. Eur J Nucl Med Mol Imaging. 2010;37:2127–35.
29. Escobedo JO, Rusin O, Lim S, Strongin RM. NIR dyes for bioimaging applications. Curr Opin Chem Biol. 2010;14:64–70.
30. Frangioni J V. In vivo near-infrared fluorescence imaging. Curr Opin Chem Biol. 2003;7:626–34.
31. Johansen P, Storni T, Rettig L, Qiu Z, Der-Sarkissian A, Smith KA, et al. Antigen kinetics determines immune reactivity. Proc Natl Acad Sci U S A. National Academy of Sciences; 2008;105:5189–94.
32. Leggatt G, R. G. Peptide Dose and/or Structure in Vaccines as a Determinant of T Cell Responses. Vaccines. 2014;2:537–48.
33. Appay V, Douek DC, Price DA. CD8+ T cell efficacy in vaccination and disease. Nat Med. 2008;14:623–8.

34. Collawn JF, Bhayani H, Paterson Y. An analysis of the physical properties of peptides that influence the pigeon cytochrome c specific T lymphocyte response. Mol Immunol. 1989;26:1069–79.
35. Reddy ST, Swartz MA, Hubbell JA. Targeting dendritic cells with biomaterials: developing the next generation of vaccines. Trends Immunol. 2006;27:573–9.
36. Elamanchili P, Lutsiak CME, Hamdy S, Diwan M, Samuel J. ???Pathogen-Mimicking??? Nanoparticles for Vaccine Delivery to Dendritic Cells. J Immunother. 2007;30:378–95.
37. Rahimian S, Fransen MF, Kleinovink JW, Christensen JR, Amidi M, Hennink WE, et al. Polymeric nanoparticles for co-delivery of synthetic long peptide antigen and poly IC as therapeutic cancer vaccine formulation. J Control Release. 2015;203:16–22.
38. Rahimian S, Fransen MF, Kleinovink JW, Amidi M, Ossendorp F, Hennink WE. Particulate systems based on poly(Lactic-co-glycolic)acid (pLGA) for immunotherapy of cancer. Curr Pharm Des. 2015;21.
39. Rosalia RA, Quakkelaar ED, Redeker A, Khan S, Camps M, Drijfhout JW, et al. Dendritic cells process synthetic long peptides better than whole protein, improving antigen presentation and T-cell activation. Eur J Immunol. 2013;43:2554–65.
40. Masopust D, Schenkel JM. The integration of T cell migration, differentiation and function. Nat Rev Immunol.2013;13:309–20.
41. Brinkman CC, Peske JD, Engelhard VH. Peripheral tissue homing receptor control of naïve, effector, and memory CD8 T cell localization in lymphoid and non-lymphoid tissues. Front Immunol. 2013;4:241.
42. Kim D, Hung C-F, Wu T-C. Monitoring the Trafficking of Adoptively Transferred Antigen- Specific CD8-Positive T Cells *In Vivo* , Using Noninvasive Luminescence Imaging. Hum Gene Ther. 2007;18:575–88.
43. Rabinovich BA, Ye Y, Etto T, Chen JQ, Levitsky HI, Overwijk WW, et al. Visualizing fewer than 10 mouse T cells with an enhanced firefly luciferase in immunocompetent mouse models of cancer. Proc Natl Acad Sci U S A. 2008;105(38):14342-6.
44. Hailemichael Y, Dai Z, Jaffarzad N, Ye Y, Medina MA, Huang X-F, et al. Persistent antigen at vaccination sites induces tumor-specific CD8+ T cell sequestration, dysfunction and deletion. Nat Med. 2013;19:465–72.
45. Chewning JH, Dugger KJ, Chaudhuri TR, Zinn KR, Weaver CT. Bioluminescence-based visualization of CD4 T cell dynamics using a T lineage-specific luciferase transgenic model1. BMC Immunol. 2009;10:44.
46. Azadniv M, Dugger K, Bowers WJ, Weaver C, Crispe IN. Imaging CD8+ T cell dynamics in vivo using a transgenic luciferase reporter. Int Immunol. 2007;19:1165–73.
47. Charo J, Perez C, Buschow C, Jukica A, Czeh M, Blankenstein T. Visualizing the dynamic of adoptively transferred T cells during the rejection of large established tumors. Eur J Immunol. 2011;41:3187–97.
48. Na I-K, Markley JC, Tsai JJ, Yim NL, Beattie BJ, Klose AD, et al. Concurrent visualization of trafficking, expansion, and activation of T lymphocytes and T-cell precursors in vivo. Blood. 2010;116:e18-e25.
49. Lang G, Wotton D, Owen MJ, Sewell WA, Brown MH, Mason DY, et al. The structure of the human CD2 gene and its expression in transgenic mice. EMBO J. 1988;7:1675–82.
50. Reddy GR, Thompson WC, Miller SC. Robust Light Emission from Cyclic Alkylaminoluciferin Substrates for Firefly Luciferase. J Am Chem Soc. 2010;132:13586–7.
51. Evans MS, Chaurette JP, Adams ST, Reddy GR, Paley MA, Aronin N, et al. A synthetic luciferin improves bioluminescence imaging in live mice. Nat Methods. 2014;11:393–5.

Appendices

Nederlandse Samenvatting

Dankwoord

Curriculum Vitae

List of publications

Nederlandse samenvatting

De Nederlandse samenvatting van dit proefschrift is bewust geschreven voor leken, waarbij zo weinig mogelijk wetenschappelijke termen zijn gebruikt en er hier en daar wat is gegeneraliseerd of selectief benoemd om de boodschap goed over te brengen.

1. Over de strijd tussen kanker en het immuunsysteem

Wanneer er bij een patiënt een tumor wordt gevonden, heeft deze tumor al een lange geschiedenis achter de rug waarin het immuunsysteem in veel gevallen een rol heeft gespeeld. Anders gezegd: het feit dat een tumor zo ver is gekomen dat hij kan worden opgemerkt in scans en klachten geeft, betekent waarschijnlijk dat hij erin is geslaagd aan het immuunsysteem te ontsnappen. Dit immuunsysteem is namelijk uitstekend in staat om tumorcellen te herkennen en aan te vallen, op vergelijkbare wijze als het dat doet wanneer iemand een infectie heeft. Tumorcellen zijn namelijk anders dan onze eigen normale cellen, en het immuunsysteem heeft als taak om lichaamsvreemde dingen op te ruimen, zoals dat gebeurt bij afstoting van een donororgaan of bij het oplossen van een virusinfectie. De manier waarop tumorcellen lichaamsvreemd zijn, en als zodanig worden herkend door het immuunsysteem, laat zich het best uitleggen door te beginnen bij het vroegste begin van kanker.

De ontwikkeling van een tumorcel begint met mutaties in het DNA. DNA is de blauwdruk voor het maken van eiwitten: elk eiwit heeft zijn eigen stukje DNA (een gen) en mutaties in een gen kunnen leiden tot veranderingen in het betreffende eiwit. Mutaties vinden continu plaats bij celdeling van gezonde cellen, maar worden ook veroorzaakt door blootstelling aan bijvoorbeeld UV-licht of kankerverwekkende stoffen. In veruit de meeste gevallen worden de mutaties opgemerkt en gecorrigeerd door DNA-herstelmechanismes van de cel zelf. In sommige gevallen blijven de mutaties wel bestaan. Meestal hebben deze mutaties geen merkbaar effect op de cel omdat ze niet hebben geleid tot veranderingen in eiwitten, of omdat deze eiwitten niet zo belangrijk waren, maar in sommige gevallen raakt er wel een belangrijk eiwit in zijn functie verstoord. Vaak heeft de cel hier behoorlijk nadeel van en zal dit leiden tot de dood van deze cel, maar in sommige gevallen kan de verstoring leiden tot een voordeel in de groei of overleving van een cel. Voorbeelden van processen die vaak verstoord zijn in tumorcellen zijn het al eerder genoemde DNA-herstel en mechanismes die voorkomen dat een cel zich oneindig kan vermenigvuldigen en ervoor zorgen dat de cel op zijn natuurlijke plek in het weefsel blijft zitten. Kortom, mutaties meestal worden gecorrigeerd, en niet-gecorrigeerde mutaties hebben meestal een negatief of geen enkel effect. De kans is dus klein dat de verschillende

belangrijke processen die een cel in toom houden allemaal worden uitgeschakeld door toevallige mutaties. Dit kansspel met minieme kans op tumorcelvorming kan daarom tientallen jaren duren, zelfs in het geval van dagelijkse massale blootstelling aan kankerverwekkende stoffen zoals bij roken.

Zodra alle belemmeringen zijn verbroken en er toch een tumorcel is ontstaan, is de strijd nog lang niet gewonnen door de tumorcel: hij zal namelijk moeten zien te ontsnappen aan het immuunsysteem. Hoe herkent het immuunsysteem een tumorcel als lichaamsvreemd? Beter is het de omgekeerde vraag te stellen: hoe herkent het immuunsysteem onze gezonde eigen cellen als lichaamseigen? De cellen van ons lichaam laten continu hun inboedel zien aan het immuunsysteem, door de eiwitten van de cel in stukjes te knippen en aan het oppervlak tentoon te stellen. Immuuncellen scannen het oppervlak van alle cellen die ze tegenkomen, en hebben tijdens hun ontwikkeling geleerd om cellen met rust te laten wanneer er alleen lichaamseigen stukjes eiwit worden gevonden. Dit is de link tussen DNA-mutaties en het immuunsysteem: wanneer mutaties in genen leiden tot veranderingen in eiwitten, en een cel deze veranderde en dus lichaamsvreemde stukjes eiwit aan zijn oppervlak tentoonstelt, kan de cel worden herkend en aangevallen door het immuunsysteem. Ook dit is weer een kansproces: niet alle veranderde stukjes eiwit vormen een bruikbaar herkenningsteken voor het immuunsysteem. Wanneer er wel herkenning plaatsvindt, begint de evolutionaire strijd tussen tumorcellen en het immuunsysteem pas op volle toeren. Tumorcellen kunnen bijvoorbeeld hun ‘tentoonstellingsmechanisme’ uitschakelen, maar het immuunsysteem heeft dan weer speciale cellen die cellen aanvallen waarop niets tentoongesteld wordt. Een andere manier om te ontsnappen aan een aanval van het immuunsysteem is door de lokale omstandigheden in de tumor zo ongunstig mogelijk te maken voor immuuncellen. Ook kunnen tumorcellen misbruik maken van bepaalde remmingsmechanismes op immuuncellen, die bedoeld zijn om al te hevige immuunreacties zoals auto-immuunziektes te voorkomen. In deze strijd tussen tumor en immuunsysteem gelden de basisprincipes van evolutie: er is geen programma of bewuste sturing, tumoren ‘weten’ niet wat ze moeten doen, en tumorcellen gaan dan ook massaal ten onder aan immuun-aanvallen. Er is echter in tumoren een grote variëteit aan tumorcellen, onder andere omdat het DNA-herstel is uitgeschakeld en er daardoor een wildgroei aan DNA-mutaties optreedt en er een bonte verzameling veranderde eiwitten aanwezig is in de cellen. Verschillende tumorcellen in een tumor bevatten daarom doorgaans voor een deel dezelfde DNA-mutaties die nog stammen uit het vroegste begin, maar ook cel-eigen DNA-mutaties die later zijn ontstaan. Door deze variëteit zijn er van de duizenden of miljoenen tumorcellen in een tumor altijd wel een paar die bij toeval een ontsnappingsmechanisme hebben ingeschakeld. Deze cellen zullen als enige

overleven en zich vermenigvuldigen, zodat na enige tijd de tumor grotendeels bestaan uit deze cellen: de tumor is geüpgraded (zo schrijf je dat blijkbaar). Het feit dat een patiënt met een merkbare tumor bij de dokter komt, betekent dus vaak dat deze tumor gedurende zijn ontwikkeling succesvol aan het immuunsysteem is ontsnapt.

2. Immuuntherapie voor kanker

Nu u weet dat het immuunsysteem tumorcellen kan herkennen en opruimen, en dat tumoren op hun beurt ontsnappingsmechanismes hiertegen kunnen ontwikkelen, zal het u niet verbazen dat men volop probeert behandelingen te ontwikkelen die er specifiek op gericht zijn om het immuunsysteem tumoren op te laten ruimen. Immuuntherapie voor kanker beoogt immuunresponsen tegen tumorcellen op te wekken, of bestaande immuunresponsen te versterken, bijvoorbeeld door de immuun-remmingsmechanismes te blokkeren.

Het immuunsysteem kent vele verschillende types cellen en moleculen die betrokken zijn bij immuunresponsen. De immuuncellen die bij uitstek lichaamsvreemde stukjes eiwit herkennen en vervolgens de betreffende cel kunnen doden, heten T-cellen. De T staat voor de thymus, het orgaan waar de T-cellen 'geschoold' worden om lichaamsvreemd van lichaamseigen te onderscheiden. Van deze T-cellen hebben tumorcellen veel te duchten, en hun ontsnappingsmechanismes zijn voornamelijk op T-cellen gericht. Ook de meeste vormen van immuuntherapie voor kanker zijn op T-cellen gericht: vaccinaties om T-celresponsen op te wekken, antilichaam-behandelingen om T-celresponsen te versterken, of simpelweg injectie van grote aantallen anti-tumor T-cellen die in het laboratorium zijn geprepareerd. Immuuntherapie is de grootste recente doorbraak in de behandeling van kanker, maar helaas reageert maar een deel van de patiënten goed op deze therapie. Tumorcellen kunnen resistent zijn voor een bepaalde behandeling, maar ook resistent worden, bijvoorbeeld door over te schakelen naar een ander ontsnappingsmechanisme. Zelfs na medisch ingrijpen gaat de evolutionaire strijd tussen tumor en immuunsysteem dus nog door. Er zijn twee belangrijke manieren waarop wetenschappers proberen dit probleem aan te pakken. Ten eerste moeten we weten hoe immuuntherapie precies werkt, om erachter te kunnen komen waarom de therapie niet bij iedereen succesvol is. Daarnaast wordt er volop onderzoek gedaan naar combinatie-behandelingen van immuuntherapie plus een andere therapie, met het doel een sterkere immuunrespons te krijgen waartegen de tumor zich minder goed kan verweren. In dit proefschrift staan voorbeelden beschreven van beide strategieën, en licht speelt hierbij een centrale rol. De weinig creatieve titel van het proefschrift is dan ook:

3. Het gebruik van licht in kanker-immuuntherapie

Het proefschrift bestaat uit zeven hoofdstukken. Het eerste hoofdstuk is een algemene inleiding op de verschillende onderwerpen die in het proefschrift aan bod komen, met een overzicht van de wetenschappelijke vraagstellingen die in de verschillende hoofdstukken onderzocht worden. In het laatste hoofdstuk worden de bevindingen samengevat en bediscussieerd. De overige vijf hoofdstukken bevatten de resultaten van mijn promotieonderzoek.

Als eerste worden combinatiebehandelingen beschreven van immuuntherapie met een ander type behandeling genaamd FotoDynamische Therapie (Engelse afkorting: PDT). Bij PDT wordt een stof in het lichaam ingespoten die pas effect heeft na blootstelling aan licht. Deze stof verspreidt zich door het hele lichaam, maar door alleen de tumor te belichten wordt de stof alleen daar geactiveerd en richt het alleen daar schade aan. Op deze manier maakt PDT dus alleen in de tumor cellen dood, het heeft dan ook veel minder vervelende bijwerkingen dan bijvoorbeeld chemotherapie. Daarnaast veroorzaakt PDT in tegenstelling tot chemotherapie en radiotherapie geen nieuwe DNA-mutaties.

In **hoofdstuk 2** wordt PDT gecombineerd met peptide-vaccinatie, een type immuuntherapie waarbij kleine stukjes eiwit (peptides) worden ingespoten als vaccin tegen de tumor. Dit zijn dezelfde stukjes eiwit die leiden tot herkenning van lichaamsvreemde cellen door T-cellen. Het doel van peptide-vaccinatie is dan ook om een sterke T-celrespons te krijgen. Muizen met een tumor werden behandeld met PDT, waardoor een groot deel van de tumor doodging, maar later groeide de tumor toch weer verder. Door de muizen te vaccineren met stukjes lichaamsvreemd tumoreiwit werden T-cellen geactiveerd die specifiek de tumor herkennen. Bij deze combinatietherapie konden de tumoren volledig worden opgeruimd, en we hebben aangetoond dat het inderdaad de T-cellen zijn die de na PDT overgebleven tumorcellen opruimden. Nu is het voor peptide-vaccinatie nodig om te weten welke stukjes eiwit op de tumorcellen zitten en belangrijk zijn bij de herkenning door T-cellen. Wanneer dit niet bekend is, kunnen er andere soorten immuuntherapie gebruikt worden die niet tumor-specifiek zijn.

In **hoofdstuk 3** wordt een dergelijke immuuntherapie getest in combinatie met PDT. Deze immuuntherapie bestaat uit het toedienen van een antilichaam dat het molecuul CTLA-4 op T-cellen blokkeert en hiermee een bekend remmingsmechanisme van T-cellen opheft, wat leidt tot hogere activiteit van de T-cellen. We hebben deze combinatiebehandeling getest in muizen met een type tumor dat spontaan al wel herkend wordt door T-cellen, maar aan de aanval weet te ontsnappen. Ook in dit geval zien we een duidelijk verbeterd effect van combinatiebehandeling ten

opzichte van de beide individuele behandelingen, en wederom een cruciale rol voor T-cellen in het opruimen van de tumoren. Deze twee hoofdstukken tonen aan dat immuuntherapie goed gecombineerd kan worden met andere therapieën zoals PDT. Dit is relevante informatie, aangezien patiënten met gevorderde kanker niet goed reageren op peptide-vaccinatie en een aanzienlijk deel van de patiënten weinig baat heeft bij behandeling met het antilichaam tegen CTLA-4. PDT wordt al tientallen jaren toegepast bij kankerpatiënten, dus het is relatief eenvoudig om te onderzoeken of de combinatie met immuuntherapie ook in mensen beter werkt.

In de overige hoofdstukken hebben we licht niet gebruikt om een effect te veroorzaken in de muis, maar juist om te kunnen zien wat er gebeurt binnenin de muis, dus als beeldvormende techniek (in het Engels: imaging). Het doel van het project beschreven in **hoofdstuk 4** was om erachter te komen wat er gebeurt met een peptide-vaccin na toediening in het lichaam. Hiervoor hebben we een fluorescerende (lichtgevende) kleurstof aan het vaccin gekoppeld. Deze aanpak bleek succesvol: de fluorescentie kon duidelijk worden waargenomen op de plek van injectie, waarbij de hoeveelheid geleidelijk afnam in de tijd. Het vaccin wordt namelijk getransporteerd naar lymfeklieren, waar T-cellen en andere immuuncellen wachten om geactiveerd te worden (de gezwollen lymfeklieren tijdens een verkoudheid of andere infectie zijn deels het gevolg van grootschalige activatie en vermenigvuldiging van T-cellen). Het transport van het vaccin vanaf de injectieplek naar de lymfeklieren kon eenvoudig worden gevisualiseerd. We hebben verschillende toedieningsmethodes vergeleken die het vaccin langer of korter op de injectieplek zouden moeten vasthouden, en konden dit verschil inderdaad herkennen door de fluorescentie te meten.

In **hoofdstuk 5** hebben we deze fluorescentie-imaging getest bij een iets andere vaccinatiestrategie. Het vaccin werd wederom gelabeld met een fluorescerende stof, maar nu verpakt in een soort biologisch afbreekbaar bolletje. Het doel van de verpakking in bolletjes is om het vaccin beter te beschermen tegen afbraak door het lichaam en zo in totaal meer vaccin op de plek van bestemming te laten aankomen. Door de fluorescentie te meten op de injectieplek en de lymfeklieren konden we aantonen dat de bolletjes het vaccin langer op de plek van injectie hielden, waardoor er een geleidelijke maar uiteindelijk grotere hoeveelheid in de lymfeklieren aankwam.

In **hoofdstuk 6** tenslotte waren het juist de T-cellen zelf die we lichtgevend hebben gemaakt. Hiervoor gebruikten we geen fluorescerende stoffen, maar lichtgevende eiwitten die bekend zijn van bijvoorbeeld vuurvliegjes: luciferases. Zoals u inmiddels weet, worden eiwitten gemaakt vanuit een broncode in het DNA, en wetenschappers hebben de stukjes DNA met de code voor luciferases uit vuurvliegjes en andere

dieren kunnen isoleren. Dit stukje DNA hebben wij weer ingepast in het DNA van een muis, en wel op zo'n manier dat het alleen de T-cellen zijn waarbij de luciferases worden gemaakt. Sterker nog, we hebben twee luciferases met verschillende kleuren ingebouwd in de T-cellen: een groene die altijd actief is, en een rode die pas actief wordt als een T-cel zelf geactiveerd wordt. Kortom: een rustende T-cel geeft alleen groen licht, een geactiveerde T-cel geeft groen én rood licht. Door muizen te vaccineren en zo T-cellen te activeren, hebben we aangetoond dat deze twee-kleurenstrategie inderdaad werkt: de wachtende T-cellen in de lymfeklier waren groen, en pas na vaccinatie werden ze ook rood. De imaging-technieken beschreven in hoofdstuk 4 tot 6 kunnen gebruikt worden om te onderzoeken hoe immuuntherapie werkt, en waarom het in sommige gevallen niet werkt. Op basis van deze inzichten kan de behandelstrategie worden aangepast om een beter effect te krijgen, bijvoorbeeld door de timing, dosering of locatie van behandeling te veranderen of door de juiste combinatietherapie te kiezen.

Samengevat heeft het onderzoek beschreven in dit proefschrift op twee manieren geprobeerd een oplossing te vinden voor het beperkte succes van immuuntherapie bij gevorderde kanker: door combinatie-behandelingen toe te passen en door methodes te ontwikkelen die het inzicht in immuunresponsen tegen kanker kunnen vergroten.

Dankwoord

Ferry, je wist me vanaf het eerste sollicitatiegesprek enthousiast te maken voor het project, en ik hoefde niet na te denken toen je me uitnodigde om de baan aan te nemen. Je vertrouwen heeft mij enorm gemotiveerd. Clemens, bedankt voor je creativiteit die vele goede ideeën heeft opgeleverd die ook terug te vinden zijn in dit proefschrift. Marieke, we werkten vanaf het begin samen en je was zeer betrokken bij mijn onderzoek, wat ook officieel werd door je co-promotorschap. Dankjewel!

Laura, as two persons who are always fashionably late, we never had to wait for each other. I enjoyed our collaboration a lot and I'm glad you are still around occasionally. Sima, we have not reported it as an official Milestone of the CTMM project but for me our friendship was the most significant result! It was great doing experiments together. Thank you both for teaching me a lot about scientific disciplines that are not my own – I hope I learned enough to survive the defense! Natasa, I was lucky to have a student like you. You enthusiastically accepted a tricky project and soon it was already obvious that you would make a great PhD student, and indeed you have. Thanks to you and Christine for being my paranymphs! Thomas, Pieter, Maryam, Henrik, Charlotte, bedankt voor de goede samenwerking. De steun van wijlen Harrie Vink voor de PDT-projecten heeft de voortzetting van ons onderzoek mogelijk gemaakt en indirect ook geleid tot het absolute hoogtepunt van onze carrière: een publicatie in het Leidsch Dagblad.

De volgende zin zal menigeen bekend voorkomen vanwege eerdere proefschriften uit de groep: ik heb mij vanaf de eerste dag thuis gevoeld bij de Tumorimmunologie. Bedankt dat jullie allemaal een beetje raar zijn, waardoor ik er perfect tussen paste. Dank aan alle overige IHB'ers voor de nuttige meetings en de leuke borrels en buitendagen. ONCO'ers, eind 2010 lukte het me nog net even niet, maar tegenwoordig zijn we alsnog collega's. Dankjulliewel voor vele leerzame meetings en memorabele labuitjes.

Aangezien dit het dankwoord is voor mijn promotieonderzoek, niet voor mijn leven in het algemeen, heb ik het beperkt tot bij het promotieonderzoek betrokken personen en de verdere werkomgeving. Anderen voor wie ik grote dank of waardering heb, weten dit bovendien al lang. Teleurgestelde lezers die toch op een vermelding in het dankwoord hadden gehoopt, moeten het maar doen met: alle anderen ook bedankt hoor.

Curriculum Vitae

Jan Willem Kleinovink was born on the 29th of December 1986 in Den Ham, the Netherlands. In 2004 he obtained the VWO diploma at CSG Het Noordik in Almelo. At Radboud University Nijmegen, Jan Willem initially studied Medicine but switched to Biomedical Sciences in 2006. He completed the Bachelor program of Biomedical Sciences in June 2009, which included an internship in the group of dr. Leo Joosten at the Experimental Rheumatology lab at Radboud University, studying the possible synergy between IL-17 and TLR ligands, supervised by dr. Marije Koenders. In the Master's program of Biomedical Sciences, he did a minor internship in the laboratory of Pediatrics and Neurology, Radboud University, studying the deposition of heparan sulphate proteoglycans in amyloid plaques in a mouse model of Alzheimer's disease, supervised by dr. Nienke Timmer. Jan Willem did his major internship in the Department of Cellular and Molecular Medicine at the Centro de Investigaciones Biológicas in Madrid, Spain, studying the possible anti-metastatic role of the Rho GTPase inhibitor p190RhoGAP, supervised by dr. Rubén Bartolomé Conde and dr. Joaquín Teixidó. He obtained his Master's degree in Biomedical Sciences in November 2010. In February 2011, he started working on the PhD project described in this thesis in the Tumor Immunology group of the department of Immunohematology and Blood Transfusion at Leiden University Medical Center, supervised by Dr. Marieke Fransen and Prof. Dr. Ferry Ossendorp, in collaboration with Prof. dr. Clemens Löwik of the department of Radiology (now at Erasmus Medical Center in Rotterdam). Jan Willem currently works as a post-doc in the department of Medical Oncology at Leiden University Medical Center with dr. Thorbald van Hall and Prof. dr. Sjoerd van der Burg on the characterization and modulation of myeloid cells in the tumor microenvironment.

List of publications

- **Kleinovink JW**, Fransen MF, Löwik CW, Ossendorp F. Photodynamic-Immune Checkpoint Therapy Eradicates Local and Distant Tumors by CD8+ T Cells. *Cancer Immunol Res. 2017 Oct;5(10):832-838.*

- **Kleinovink JW**, van Hall T, Ossendorp F, Fransen MF. PD-L1 immune suppression in cancer: Tumor cells or host cells? *Oncoimmunology. 2017 May 12;6(7):e1325982.*

- **Kleinovink JW**, Marijt KA, Schoonderwoerd MJA, van Hall T, Ossendorp F, Fransen MF. PD-L1 expression on malignant cells is no prerequisite for checkpoint therapy. *Oncoimmunology. 2017 Feb 21;6(4):e1294299.*

- **Kleinovink JW**, van Driel PB, Snoeks TJ, Prokopi N, Fransen MF, Cruz LJ, Mezzanotte L, Chan A, Löwik CW, Ossendorp F. Combination of Photodynamic Therapy and Specific Immunotherapy Efficiently Eradicates Established Tumors. *Clin Cancer Res. 2016 Mar 15;22(6):1459-68.*

- Rahimian S, Fransen MF, **Kleinovink JW**, Amidi M, Ossendorp F, Hennink WE. Particulate Systems Based on Poly(Lactic-co-Glycolic)Acid (pLGA) for Immunotherapy of Cancer. *Curr Pharm Des. 2015;21(29):4201-16. Review.*

- Rahimian S, Fransen MF, **Kleinovink JW**, Amidi M, Ossendorp F, Hennink WE. Polymeric microparticles for sustained and local delivery of antiCD40 and antiCTLA-4 in immunotherapy of cancer. *Biomaterials. 2015 Aug;61:33-40.*

- Rahimian S, Fransen MF, **Kleinovink JW**, Christensen JR, Amidi M, Hennink WE, Ossendorp F. Polymeric nanoparticles for co-delivery of synthetic long peptide antigen and poly IC as therapeutic cancer vaccine formulation. *J Control Release. 2015 Apr 10;203:16-22.*

- Rahimian S*, **Kleinovink JW***, Fransen MF, Mezzanotte L, Gold H, Wisse P, Overkleeft H, Amidi M, Jiskoot W, Löwik CW, Ossendorp F, Hennink WE. Near-infrared labeled, ovalbumin loaded polymeric nanoparticles based on a hydrophilic polyester as model vaccine: In vivo tracking and evaluation of antigen-specific CD8(+) T cell immune response. *Biomaterials. 2015 Jan;37:469-77.* *shared first authorship

- Cruz LJ, Rosalia RA, **Kleinovink JW**, Rueda F, Löwik CW, Ossendorp F. Targeting nanoparticles to CD40, DEC-205 or CD11c molecules on dendritic cells for efficient CD8(+) T cell response: a comparative study. *J Control Release. 2014 Oct 28;192:209-18.*

- Bartolomé RA, Díaz-Martínez M, Coló GP, Arellano-Sánchez N, Torres-Ayuso P, **Kleinovink JW**, Mérida I, Teixidó. A Blk-p190RhoGAP signaling module downstream of activated Gα13 functionally opposes CXCL12-stimulated RhoA activation and cell invasion. *J. Cell Signal. 2014 Nov;26(11):2551-61.*

- Timmer NM, Herbert MK, **Kleinovink JW**, Kiliaan AJ, De Waal RM, Verbeek MM. Limited expression of heparan sulphate proteoglycans associated with Aβ deposits in the APPswe/PS1dE9 mouse model for Alzheimer's disease. *Neuropathol Appl Neurobiol. 2010 Oct;36(6):478-86.*